DOE/LC/10886-1556
(DE84003087)

FOSSIL ENERGY

A COMPUTATIONAL METHOD FOR THERMOVISCOELASTICITY WITH APPLICATION TO ROCK MECHANICS

By
S. C. Lee

January 1984

Work Performed Under Contract No.: DE-AS20-82LC10886

For
U. S. Department of Energy
Office of Fossil Energy
Morgantown Energy Technology Center
Laramie Project Office
Laramie, Wyoming

By
Ohio State University
Columbus, Ohio

Technical Information Center
Office of Scientific and Technical Information
United States Department of Energy

DISCLAIMER

DISCLAIMER

This report has been reproduced directly from the best available copy.

Available from the National Technical Information Service, U. S. Department of Commerce, Springfield, Virginia 22161.

Price: Printed Copy A09
Microfiche A01

Codes are used for pricing all publications. The code is determined by the number of pages in the publication. Information pertaining to the pricing codes can be found in the current issues of the following publications, which are generally available in most libraries: *Energy Research Abstracts (ERA); Government Reports Announcements* and Index (*GRA* and I); *Scientific and Technical Abstract Reports (STAR);* and publication NTIS-PR-360 available from NTIS at the above address.

DOE/LC/10886-1556
(DE84003087)
Distribution Category UC-90c

A COMPUTATIONAL METHOD FOR THERMOVISCOELASTICITY WITH APPLICATION TO ROCK MECHANICS

By
S. C. Lee

January 1984

Work Performed Under Contract No.: DE-AS20-82LC10886

For
U. S. Department of Energy
Office of Fossil Energy
Morgantown Energy Technology Center
Laramie Project Office
Laramie, Wyoming 82071

By
Ohio State University
Columbus, Ohio 43210

THIS PAGE

WAS INTENTIONALLY

LEFT BLANK

TABLE OF CONTENTS

LIST OF FIGURES

LIST OF TABLES

NOMENCLATURE

Alaphabetic Symbols

A	Helemholtz free energy
A_o	Mean free energy
a	A halt crack length
a_T	Temperature shift factor
$\mathbf{B}$	Matrix related to derivatives of shape functions
$\mathbf{b}$	Body force
$\mathbf{C}$	Heat capacity matrix
c	Heat capacity
$D_{ij}(0)$	Initial stress functional
$\mathbf{D}_e$	Elasticity material matrix
$\bar{\mathbf{D}}$	Matrix related to creep strains
E	Elastic modulus
$E(t)$	Strain functional
e_{ij}	Deviatoric strains
$\mathbf{F}, f_i$	Load vector in stiffness equation
$\bar{\mathbf{F}}$	Forcing vector in heat conduction equation
$f(T)$	Function related to time-temperature shift
$F(\xi), F(\eta)$	Function related with upwinding weight functions
g	Gravitational acceleration

G	Shear modulus
G_{ijkl}	Matrix related to free energy functional
G_1	Bulk relaxation modulus
G_2	Shear relaxation modulus
h_T	Heat transfer coefficient
H_i, H_j	Gaussian weights
$H(x,t)$	Heat source/sink term
$[J]$	Jacobian matrix
J_1	Compressive creep compliance
J_2	Shear creep compliance
$\bar{J}$	Uniaxial creep compliance
$\mathbf{K}$	Heat conductivity matrix
$\bar{\mathbf{K}}$	Stiffness matrix
$K_{I,II}$	Stress intensity factors
K^*	Material constant related to stress intensity factor expressions
k_{ij}	Thermal conductivity
$\mathbf{L}$	Functional operator
L	Element length
L_i	Function related to upwinding weight functions
$\mathbf{N}, N$	Shape functions
$m(t-\tau)$	Material constant related to free energy functional
$\mathbf{P}_c$	Concentrated force
$\bar{\mathbf{P}}$	Distributed force
P	Internal pressure

Q	Heat flux vector
$\Delta \mathbf{R}_n$	Force increment for incremental stiffness equation
$S_C(T), S_C$	Tensile strength
$S_T(T), S_T$	Compressive strength
$\bar{S}_{max}$	Maximum differential surface subsidence
S_o	Uniform reference surface subsidence
S_{ij}	Deviatoric stresses
S	Entropy
s	Variable related to temperature shift function
$\bar{T}, T, T(t)$	Temperature
T_c	Cavity/chamber boundary temperature
t_n	Time at transient step n
Δt	Time increment at transient step n
$\mathbf{U}, U$	Displacement
X_i, x, y, z	Cartesian coordinate
r, θ, z	Cylindrical coordinate
V_i	Gas velocity
$\bar{V}_i$	Lumped convection coefficient
W	Work done by external loads
W_i	Weight functions

Greek Alphabetic Symbols

α	Coefficient of linear thermal expansion
$\bar{\alpha}_i$	Upwinding control parameter
$\beta(t-\tau)$	Material property related to free energy functional
$\bar{\beta}_i$	Upwinding control parameter
γ_{ij}	Engineering shear strains
γ	Heat supply function
$\overset{\infty}{\underset{s=0}{T}}$	Linear functional operator related to stresses
γ	Angle of convection flow direction (Sec. 4.2.1)
$\Delta\sigma, \Delta\varepsilon, \Delta F$	Increment of stress, strain, and force
δ	Kronecker delta
$\varepsilon_{ij}, \varepsilon$	Strains
ξ_i, η_i	Gaussian quadrature points
ξ, η	Coordinate on parent plane
ξ	Reduced time scales
θ	Pseudo-temperature (Sec. 2.1.3)
$\bar{\theta}$	Control parameter in two-point recurrence scheme for heat conduction equation (Sec. 3.1)
θ	Control parameter in implicit time stepping scheme for stiffness equation (Sec. 3.3.3)
Λ	Strain energy
μ_f	Coefficient of internal friction
υ	Poisson's ratio
Π	Total potential energy

ρ	Mass density
σ	Stresses
τ	Control parameter for time step size selection
τ_{ij}	Shear stresses
$\chi(T)$	Temperature shift function
Ψ_{ij}	Matrix related to free energy functional
ψ	Relative temperature ($\psi = T - T_0$)
$\bar{\Psi}$	Incremental loads due to temperature and creep
Ω	Domain
Γ	Boundary

Subscripts

i,j,k,l,α,β	Running indces
c	Variable related to creep
e	Variable related to elasticity
M	Variable related to mechanical responses
n	Transient step counter
o	Reference state
T	Variable related to temperature

Superscripts

b	Variable related to body force
e	Element basis
E	Variable related to elasticity
T	Transpose of matrix
V	Variable related to viscoelasticity

A COMPUTATIONAL METHOD OF THERMOVISCOELASTICITY WITH APPLICATIONS TO ROCK MECHANICS

by

Seong Chul Lee, Ph.D.
The Ohio State University, 1983

The effects of temperature on a viscoelastic medium are important in considering the long-term design of a structure. Large-scale numerical computations associated with rock mechanics problems have required efficient and economical models for predicting temperature, stress, failure, and deformed structural configuration under various loading conditions. To meet this requirement, the complex dependence of the properties of geological materials on the time and temperature is modified to yield a reduced time scale as a function of time and temperature under the thermorheologically simple material (TSM) postulate. The thermorheologically linear concept is adopted in the finite element formulation by uncoupling thermal and mechanical responses.

The thermal responses, based on transient heat conduction or convective-diffusion, are formulated by using the two-point recurrence scheme and the upwinding scheme, respectively. An incremental solution procedure with the implicit time stepping scheme is proposed for the solution of the thermoviscoelastic response. The proposed thermoviscoelastic solution algorithm is based on the uniaxial creep experimental data and the corresponding temperature shift functions, and is intended to minimize computational efforts by allowing the large time step size with sta-

ble solutions. A thermoelastic fracture formulation is also presented by introducing the degenerate quadratic isoparametric singular element for the thermally-induced line crack problems. The stress intensity factors are computed by use of the displacement method.

Efficiency of the presented formulation and solution algorithm is initially demonstrated by comparison with other available solutions for a variety of problems. Subsequent field applications are made to simulate the post-burn and post-repose phases of an underground coal conversion (UCC) experiment and an in-situ nuclear waste disposal management problems. Time- and space-dependent temperature boundary conditions are used to simulate the chamber and radioactive heat source temperatures. The UCC chamber configuration is predicted by use of two-dimensional failure criteria using temperature-dependent mechanical properties of coal and overburden. A UCC fracture model is also evaluated by considering a thermoelastic elliptic cavity model with a linking channel demonstrating a possible channel closure in the active-burn stage. The presented FEM model simulations illustrate the feasibility of the developed formulations and numerical investigations in predicting the post-burn/post-repose temperature, displacement and stress responses. Recommendations for additional work on thermo-mechanical response formulation and associated computational technique are provided.

Chapter I

INTRODUCTION

Thermomechanics is concerned in general with the interrelations between the forces acting on a continuum and the resulting time and temperature dependent kinematical deformations. For thermoelastic materials, the deformation response is fully recoverable on release of forces and temperatures. In the deformation of ideally viscous and plastic materials, the release of the forces is not accompanied by the recovery of the expended energy, and the strain caused by the forces is nonrecoverable. The behavior of real materials is composed of the above deformational responses in varying proportion, depending on the nature of the material and conditions under which the forces are applied.

There are many reasons why the influence of temperature on the mechanical response of a viscoelastic material is of great interest. As a purely practical nature, many engineering materials such as polymers, composites, and geological materials, etc are subjected to a wide range of environmental and loading conditions, and a complete specification of the mechanical properties of these materials can not be restricted to room temperature nor a narrow range of temperatures. Another important reason is that by use of the temperature dependence in the viscoelastic response, a more comprehensive analysis can be conducted by extending experimental results to define the response of the material at variable temperatures as well as extending the test results to portions of the physical time scale normally inaccessible by conventional methods.

The thermally-sensitive viscoelastic behavior is described by two classes of materials, namely, "thermorheologically simple materials (TSM)" and "thermorheologically complex materials (TCM)". The thermorheologically simple material exhibits a thermal trend similar to the one with time, while the thermorheologically complex material reveals an independent thermal trend. These material classifications are mainly based on the experimental data, namely, the creep or relaxation tests at elevated temperatures. In particular, three characteristic regions of viscoelastic behavior for thermally-sensitive materials are observed. At reference temperature, a glassy region is observed in which the magnitude of the creep modulus, $E_c(t)$, defined as the constant stress divided by the time dependent strain, is quite high and the loading time effects are not pronounced. A transition region for viscoelastic response in which the modulus varies rapidly with time and temperature is observed at more elevated temperatures. At still higher temperatures, the response of the material is in the flow region and the modulus changes very rapidly with time from a small finite value to a value which approaches zero. In studying the responses of thermoviscoelastic materials, the factors of time and temperature must therefore be taken into account.

1.1 NUMERICAL MODELING

The purpose of "modeling" material and structural responses is to establish "a hypothetical or stylized representation" of a certain prototype. Many different types of modeling activities may be categorized as conceptual, physical, analytical, and numerical. Conceptual, analytical, and numerical modeling activities rely on the selection of an adequate

model of the proptotype. Indeed, a major objective of such activities may be improvement of the conceptual model which provides a framework of investigation. For large-scale modeling studies, qualitative physical models are mainly restricted by the size effect and the complex nonlinear behavior of the prototype while closed-form solutions of analytical models are often impossible to derive. These restrictions, coupled with the high cost and inflexibilities associated with experimental testing, have led to an increasing emphasis on numerical models. The typical numerical modeling activities include i) selection of a conceptual model, ii) development of an appropriate numerical procedure or computer code, iii) construction of numerical model, iv) verification of cases against known solutions, and iv) their subsequent applications to the solution of the problem.

Long-term analysis of large-scale problems require efficient and economical numerical modeling coupled with necessary modifications for the field process mechanisms and the host environment. In addition, problems of scaling laboratory-test results to actual problems must be investigated by using comprehensive computer models. For these applications, finite element computer models are often developed due to their varsatility and commensurate growth in computational technology. A typical FEM modeling sequence proceeds in the following manner;

a) Problem definition: Problem type, model size, selection of proper conceptual model, and estimate of required capacity of computer resource.

b) Model data preparation: Model geometry, material data, constraint conditions, and initial conditions.

c) Computational procedure: Application of appropriate solution algorithms and presentation of solutions.

In the above modeling sequence, model validation and refinement are prerequisites to achieving meaningful results for the simulation of large-scale field problems.

1.2 LITERATURE REVIEW

The importance, in thermal stress problems, of responses which stem from the temperature effects of the viscoelastic properties was first emphasized by Freudenthal [37] and Hilton [53] in the early 1950's. Christensen and Naghdi [22], Schapery [95], and Biot [16] developed the constitutive relations for linear thermoviscoelasticity based on the thermodynamical postulates. The uniqueness of the solution in the isothermal linear theory of viscoelasticity for the thermorheologically simple ablating solids was established by Sternberg and Curtin [105] based on Volterra's uniqueness theorem. Under the assumptions of infinitesimal deformation and positive-definite and continuous relaxation/creep functions, Lubliner and Sackman [78] generalized the uniqueness theory for anisotropic, non-homogeneous and time-variable viscoelastic medium by use of the Laplace transformation and asymtotic methods.

Morland and Lee [84] introduced linear thermoviscoelastic analysis with temperature-dependent characteristics on the basis of the time and temperature correspondence hypothesis originally proposed by Leaderman [72] and Ferry [33]. In this hypothesis, the relaxation moduli and creep compliances are affected by a constant temperature change only

within a corresponding uniform shift of the logarithmic time scale. A material exihibiting such behavior was termed a "thermorheologically simple material (TSM)" by Schawarzl and Staverman [96]. A few analytical solutions have been obtained for simple boundary-value problems and have been mainly approached by using the integral transform techniques (cf. ref. [23,24,84,85]). These analytical solutions have been faced with complexibilities in the evaluation of integro-differential equations and inflexibilities in the boundary conditions. This has motivated the development of numerical approaches including the finite difference and finite element methods. In this chapter, only the finite element approaches are reviewed with emphasis on the thermorheological FEM models and the FEM solution procedures. The FEM formulations of the transient heat conduction and convective-diffusion equations are also briefly reviewed.

1.2.1 THERMORHEOLOGICAL MODELS

An incremental FEM approach to linear viscoelastic analysis was introduced by King [64]. The creep phenomenon was viewed as a sequence of stress relaxation at a constant displacement over a short time interval followed by sudden release of constraints to satisfy the overall equilibrium. The stress change in any time interval was expressed in terms of the stress changes in the previous time interval replacing integrals by rectangular sums. This approach was further extended to two- and three-dimensional stress states by Sandhu, Wilson, and Raphael [94] with the uniaxial creep compliance represented by exponential functions. Based on the above incremental concept, the rheological behaviors of viscoelastic

media have been represented by several forms of viscoelastic constitutive laws classified as differential, integral, and empirical (cf. ref. [45,90,130,132]).

Zienkiewicz Watson and King [136] adopted a differential operator for a series of Kelvin models and proposed the use of temperature-dependent elastic and viscous components and thermal strains due to the thermal expansion. This model requires characterizations of each rheological component as a function of the temperature, and poses difficulties in obtaining such information from experimental data.

Taylor and Chang [110] initiated the hereditary integral approach with the TSM postulate. The temperature effect was incorporated in the integral equations by replacing the physical time by the reduced time determined from the temperature shift function. This was further extended to the problem of the variable temperature state by Taylor, Pister, and Goudreau [111]. The heat conduction equation was assumed to be unaffected by the deformation and was solved separately, but simultaneously, with the mechanical responses. They used an explicit exponential expression for the relaxation moduli associated with the generalized Maxwell model, and the reduced time expressed in the form of integral of the temperature shift function for the non-isothermal application. A similar approach, with an alternative form of equilibrium equations, can also be found in Srinatha and Lewis [104]. The temperature responses for the coupled system with an internal dissipation function was studied by Cost [27] with emphasis on the influence of thermorheological simple material behavior on the heat generation phenomenon. Batra et al [14] and

Batra [15] adopted the TSM postulate for the semi-coupled system where the coupling effect is considered only in the energy equation. Based on the integral constitutive law, the thermorheological behavior is assumed to be characterized by a single relaxation time so that only the relaxation time is replaced by the reduced time computed from the temperature shift function expressed in the form of the WLF equation (cf. ref. [34,98]). The WLF equation, named after William, Landel and Ferry, represents a logarithmic shift of relaxation/creep functions in terms of the universal gas constant and the temperature increment referenced to the glassy transition temperature.

The most popular representation of the rheological behavior has been an empirical creep expression, since it simplifies the numerical modeling procedure and can be easily obtained from the experimental data. Greenbaum and Rubinstein [41] proposed an empirical creep function composed of effective stress, strain, temperature, and time. This was later adopted in the finite element code developed by Sutherland [108] with the general functional form of the creep strain rate dependent on stress, strain, temperature, and time. Cyr and Teter [29] and Zudans et al [137] used the steady creep flow law of Soderberg (Norton's law) for the elastic-plastic-creep analysis with temperature-dependent material properties. Similar creep laws have been adopted by Anderson [8], Anderson and Bridwell [7], and Liu and Hsu [76] with applications to a spherical cavity, layered geological structures, and a frozen foundation in cold region engineering, respectively. The above creep laws are often called "power creep laws", and the thermal behavior is expressed by an exponetial function associated with the universal gas constant, activa-

tion energy, and temperature. Although these expressions are compact and convenient for computer implementation, they are based on the crude approximation of the thermal behavior compared to the one based on the TSM postulate. Recently, Morjaria and Mukherjee [83] have adopted Hart's model with a rate formulation. This model combines plastic and creep strains into a single non-elastic strain where the thermorheological behavior is represented by a simple power expression similar to Norton's law. A similar constitutive model, a combination of Hooke-Kelvin-Bingham-Newton models, can be found in Duddeck and Nipp [32] adopting temperature-dependent elastic moduli, transient and stationary creep with the analogy of von Mises yield criteria while the temperature dependence of rheological components is represented by a simple power expression.

In summary, most of the rigorous thermorheological models have been presented in the form of hereditary integrals under the time and temperature correspondence concept (TSM postulate), while empirical creep laws (power creep laws) have been adopted mainly in the phenomenological approaches. In addition, the uniaxial creep data has been extended to the multi-axial case under the assumption of volumetric behavior being elastic, which enables one to keep the Poisson's ratio constant. It is also found that the bulk relaxation modulus remains constant while only the shear relaxation modulus represents the time-temperature effect for most thermorheologically simple materials (cf. ref. [14,15,77,104,111]).

1.2.2 FEM SOLUTION ALGORITHMS

The general FEM solution algorithms for nonlinear problems have been based on the incremental formulation of the governing equations. Early solution algorithms for the viscoelastic problems used a simple step-forward procedure requiring a small time step size to obtain stable solutions (cf. ref. [41,64,94,108,136]). This forward time step procedure has been further modified to include an iterative process in each increment by Dong, Pister, and Dunham [30], Nayak and Zienkiewicz [87], and Zudans et al [137]. Since the incremental iterative solution procedure requires considerable computational effort and complex formulations, Zienkiewicz and Cormeau [133] and Cormeau [26] used a simple incremental procedure, the "initial strain method", for viscoplastic problems with emphasis on the practical implementation of the program and proposed an empirical rule for the selection of the time step size. This rule limits the maximum increment of the viscoplastic strain to a certain fraction of the total accumulated strain to control the solution stability To enhance the stability and accuracy of solution, Cyr and Teter [29] used an equilibrium correction in a simple step-forward procedure. The unbalanced force, the "pseudo incremental force", is treated as the "driving force" contributing the load terms on the right hand side of the equilibrium equation. In this manner, the unbalanced forces in the previous step are corrected during the next increment. Hughes and Taylor [55] proposed an implicit time stepping scheme to overcome the stability restriction on the size of the time step. For the appropriate values of the scheme parameter, the method has appeared to be unconditionally stable under the incremental iterative procedure. This

implicit time stepping scheme along with the equilibrium correction have been adopted in various inelastic problems and relevant references can be found in Owen and Hinton [90] and Zienkiewicz [130]. Reviews of the nonlinear FEM solution algorithms associated with the inelastic rate processes are also found in Willam [125] and Argyris et al [9].

The fore-mentioned literature for the FEM solution algorithms for nonlinear problems has been focussed on viscoelasticity and viscoplasticity with the empirical constitutive laws. In the hereditary integral method for solving uncoupled thermoviscoelastic problems, a time step-forward procedure has been adopted with the integrals expressed as rectangular summations (cf. ref. [110,111]). Unlike the conventional procedure with empirical creep laws, the solution procedure for the integral approach is rather unique since a set of the Volterra type integral equations is explicitly evaluated in terms of summations of finite series. Batra et al [14] and Batra [15] adopted the above approximation scheme for the mechanical response, while the finite difference method has been used for the semi-coupled energy equation. Recently, Srinatha and Lewis [104] presented an alternative set of equilibrium equations based on the above approximation. The equilibrium equations, expressed in a recurrence form, are solved by using an iterative technique.

In summary, the conventional FEM solutions for nonlinear problems have been obtained by the incremental iterative procedure with empirical constitutive laws. As a practical implementation of the program, the incremental procedure with the implicit time stepping scheme appears to be the most efficient algorithm. For thermoviscoelastic problems, the con-

ventional incremental solutions have been used only for the phenomenological formulation. (empirical creep law) In the case of the integral formulation using the TSM postulate, a set of the Volterra type integral equations obtained from the series approximation has been solved in the context of finite element theory.

1.2.3 THERMAL RESPONSE

The thermal response is based on the transient heat conduction and convective-diffusion energy equations. The transient heat conduction equation has been well discussed and established in the finite element context by several authors (cf. ref. [13,97,130,132]). For discretization in the time domain, a variational functional has been adopted by Wilson and Nickell [126], Fried [38], and Argyris and Scharpf [10]. Such variational principles have been known to be equivalent to the weak formulation using the Galerkin procedure and yield no new alternative numerical schemes. Zienkiewicz and Parkesh [135] introduced wighted residual forms in time, which have led to the analogy with the finite difference formulae such as forward, mid, and backward difference equations depending on the scheme parameter associated with weight functions. A stability criterion for the two-point recurrence scheme based on the eigenvalue problem has been reported by Irons [59]. It shows that the highest system eigenvalue must always be less than the highest eigenvalues of the individual elements. Multipoint recurrence schemes are due to Lees [74] and Bonacina et al [19] for the three-point scheme, and Zienkiewicz [131] for the four-point scheme. These multipoint recurrence schemes have been adopted in various field problems such as

phase change, ground seepage, and welding applications (cf. ref. [25,36,52]).

For the convective-diffusion equation, the finite element discretization with the Galerkin method has encountered serious difficulties in situations where the convective terms (first derivative terms) are significant. The numerical oscillations occuring in non-self-adjoint operators have only been removed by severe mesh refinements, which undermine the practical utility of the Galerkin method (cf. ref. [24,134]). The weighted residual formulation for one-dimensional problems has been proposed by Christie et al [24] adopting the "upwinding scheme". Heinrich et al [46], Heinrich and Zienkiewicz [47], and Barrett and Demunshi [11] have proposed various weight functions for two-dimensional problems. The above upwinding schemes have been competitive with the finite difference methods in regards to stability, and indeed the solution accuracy has been improved by varying the necessary upwinding from element to element. Hughes [57] has proposed numerical quadrature techniques with the Galerkin method to avoid complicated weight functions and their expensive evaluations with higher-order quadrature rules. The one-point quadrature rule on the convective term has appeared to reduce numerical oscillations although excessive "cross-wind diffusion" has been noticed for certain cases. Brooks and Hughes [20] and Hughes and Brooks [56] have recently proposed the streamline upwinding scheme along with the quadrature technique to overcome the cross-wind diffusion. The streamline upwinding scheme, employing an artificial diffusivity acting only in the direction of the flow and associated weight functions, has provided less cross-wind diffusion than the case of the simple quadrature technique.

1.3 RESEARCH OBJECTIVES

The overall objective of this research is to establish a comprehensive FEM model focussing on the simulation of the thermal and mechanical responses associated with the large-scale continuum mechanics problems with applications to rock mechanics. The schematic representation of the coupled system and associated engineering fields are illustrated in Figure 1. Specific rock mechanics areas such as underground coal combustion (UCC) and in-situ waste disposal are considered here with emphasis on innovative thermorheological model formulations.

The FEM formulations for the thermoviscoelastic responses can be divided into two main categories; namely, the treatment of the thermorheological properties and the FEM solution algorithms. The thermorheological properties incorporated in the FEM formulations have been represented by either temperature-dependent rheological components or modified time scales adopting the time and temperature correspondence concept. The presented approach is focussed on the use of the time and temperature correspondence concept with the creep compliances, since geological materials appear to be thermorheologically simple materials and their rheological properties are currently available only from the creep tests at elevated temperatures. An appropriate FEM solution algorithm using the implicit time stepping scheme is proposed by using the strain rate expression. The governing field equations include i) the transient heat conduction equation, ii) the convection-diffusion equation, iii) the elastic and viscoelastic constitutive equations, and iv) the equilibrium equations. Specific objectives of the research include:

a) Formulation of the uncoupled thermoviscoelastic boundary-value problems by use of the time and temperature correspondence concept.

b) Selection of appropriate FEM solution schemes for the transient heat conduction and convective-diffusion equations.

c) Development of an initial strain type incremental solution algorithm using the strain rate expression with the uniaxial creep compliance for the four parameter fluid model.

d) Incorporation of failure criteria and crack tip singular element along with the computation of the stress intensity factors for the thermoelastic line crack problems.

e) Model validation and comparisons with currently available analytical and numerical solutions.

f) Thermoviscoelastic FEM model simulation of large scale rock mechanics field problems (UCC post-burn, elliptic cavity with a linking channel, and salt-dome waste disposal).

The developed crack tip singularity element and the computation of the thermally-induced stress intensity factors are presented in Appendix A and B, respectively. A finite element computer code TMFC is developed by the author and is used to solve all the models in this study. The structure and capabilities of the developed computer code are briefly summarized in Appendix D.

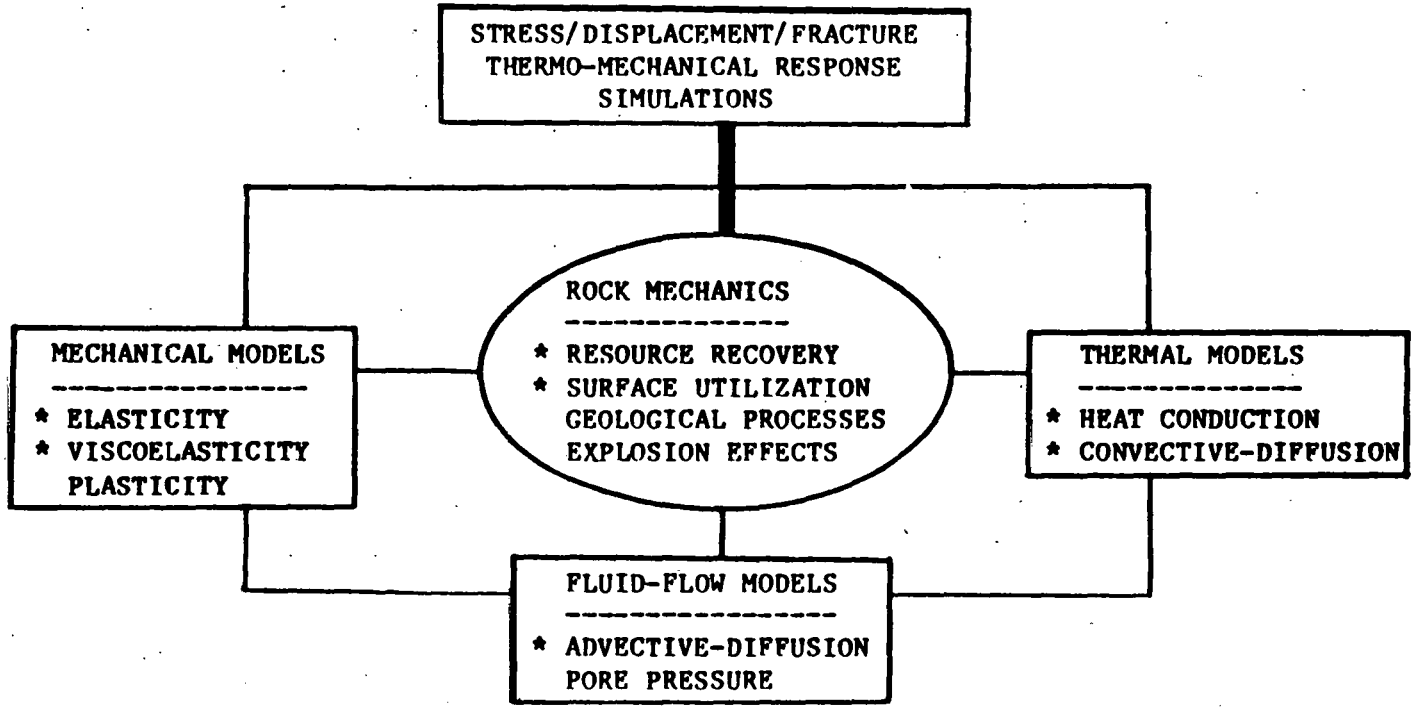

Note: * designates the areas investigated in the dissertation

Figure 1: Some Interactions for Coupled Systems in Rock Mechanics

Chapter II

GOVERNING EQUATIONS AND FORMULATIONS

In this chapter, the thermodynamical theory of thermoviscoelasticity is presented. The mechanical responses of materials are considered in terms of temperature dependent thermal and mechanical properties representing the material nonlinearity. The transient heat conduction and convective-diffusion responses are formulated separately in the uncoupled thermoviscoelastic theory. Considerations for the analysis of thermoelastic line crack problems are reported in Appendix A. The equations and formulations of boundary-value problems presented here are used in the finite element formulations developed in Chapter III.

2.1 THERMODYNAMICAL BACKGROUND OF THERMOVISCOELASTICITY

The linear theory of thermoviscoelasticity is based upon two fundamental postulates, the balance of energy and the entropy production inequality. Christensen and Naghdi [22], Schapery [95] and Biot [16] have developed governing equations incorporating constitutive assumptions for the irreversible thermodynamical conditions. The isothermal theory has been further extended to special types of non-isothermal cases by use of the thermorheologically simple material(TSM) postulate presented by Leaderman [72] and Ferry [34]. The uncoupled theory, neglecting the coupled terms in the heat conduction equation, enables one to separate the stress field from the temperature field. Here, derivations of the coupled first order theory associated with the TSM postulate are presented.

2.1.1 CONSTITUTIVE EQUATIONS OF COUPLED THEORY

The local energy balance equation using infinitesimal theory is

$$\rho\gamma - \rho(\dot{A} + \dot{T}S + T\dot{S}) + \sigma_{ij}\,\dot{\varepsilon}_{ij} - Q_{i,i} = 0 \tag{2.1}$$

where ρ is the mass density, γ is the heat supply function per unit mass, A is the Helemholtz free energy per unit mass, T is the absolute temperature, S is the entropy per unit mass, Q_i are the Cartesian components of the heat flux vector measured per unit area, and a superimposed dot designates a time derivative.

The related local entropy production inequality is given by

$$\rho T\dot{S} - \rho\gamma + Q_{i,i} - Q_i(T_{,i}/T) \geq 0 \tag{2.2}$$

and is often referred to as the Clausius-Duhem inequality.

Under the basic constitutive assumptions that the free energy functional is a linear functional and the real continuous functional of history-dependent strain and temperature may be approximated by a polynomial with the Stieltjes integral, the free energy functional is represented by the following polynomial expression with the leading error term of order 3 [23],

$$\rho A = \rho A_0 + \int_{-\infty}^{t} D_{ij}(t-\tau)\frac{\partial \varepsilon_{ij}}{\partial \tau}\,d\tau - \int_{-\infty}^{t} \beta(t-\tau)\frac{\partial \psi}{\partial \tau}\,d\tau$$

$$+ \frac{1}{2}\int_{-\infty}^{t}\int_{-\infty}^{t} G_{ijkl}(t-\tau,\, t-\eta)\frac{\partial \varepsilon_{ij}}{\partial \tau}\frac{\partial \varepsilon_{kl}}{\partial \eta}\,d\tau d\eta$$

$$- \int_{-\infty}^{t} \int_{-\infty}^{t} \Psi_{ij}(t-\tau,\, t-\eta)\, \frac{\partial \varepsilon_{ij}}{\partial \tau}\, \frac{\partial \psi}{\partial \eta}\, d\tau d\eta$$

$$- \frac{1}{2} \int_{-\infty}^{t} \int_{-\infty}^{t} m(t-\tau,\, t-\eta)\, \frac{\partial \psi}{\partial \tau}\, \frac{\partial \psi}{\partial \eta}\, d\tau d\eta + O(\varepsilon^3) \tag{2.3}$$

where A_0 is the mean free energy, ψ is the infinitesimal temperature deviation from the base temperature T_0, and the mechanical properties are assumed to be continuous for $\tau_i > 0$ and are assumed to vanish identical for $\tau_i < 0$; i.e.,

$$\beta(\tau_1) = 0, \quad D_{ij}(\tau_1) = 0, \quad G_{ijkl}(\tau_1, \tau_2) = 0,$$
$$\Psi_{ij}(\tau_1, \tau_2) = 0, \quad m(\tau_1, \tau_2) = 0 \text{ for } \tau_1 < 0,\ \tau_2 < 0 \tag{2.4}$$

The heat supply function γ is eliminated between eqns.(2.1) and (2.2) to yield

$$- \rho S \dot{\psi} - \rho A + \sigma_{ij} \dot{\varepsilon}_{ij} - Q_i(\psi_{,i}/T_0) \geq 0 \tag{2.5}$$

Substitution of eqn.(2.3) into eqn.(2.5) and differentiation with respect to t, using Leibnitz's rule, leads us to a new inequality which must hold for all arbitrary value of $\dot{\varepsilon}_{ij}$ and $\dot{\psi}(t)$. By manipulating the terms associated with $\dot{\varepsilon}_{ij}$ and $\dot{\psi}(t)$ with the symmetry of $G_{ijkl}(\tau_1, \tau_2)$ and $m(\tau_1, \tau_2)$ and letting them vanish the following relations are obtained;

$$\sigma_{ij} = D_{ij}(0) + \int_0^t G_{ijkl}(t-\tau, 0)\, \frac{\partial \varepsilon_{kl}}{\partial \tau}\, d\tau - \int_0^t \Psi_{ij}(0, t-\tau)\, \frac{\partial \psi}{\partial \tau}\, d\tau \tag{2.6}$$

$$\rho S = \beta(0) + \int_0^t \Psi_{ij}(t-\tau, 0)\, \frac{\partial \varepsilon_{ij}}{\partial \tau}\, d\tau + \int_0^t m(t-\tau, 0)\, \frac{\partial \psi}{\partial \tau}\, d\tau \tag{2.7}$$

and

$$-\int_0^t \frac{\partial}{\partial t} D_{ij}(t-\tau) \frac{\partial \varepsilon_{ij}}{\partial \tau} d\tau + \int_0^t \frac{\partial}{\partial t} \beta(t-\tau) \frac{\partial \psi}{\partial \tau} d\tau + \Lambda - Q_i \frac{\psi,_i}{T_o} > 0 \qquad (2.8)$$

In eqns.(2.6) and (2.7), it is clear that $D_{ij}(o)$ is the initial stress and $\beta(o)$ is the initial entropy, ρS_o . It is also noted that if G_{ijkl} is considered as a surface in (τ , η) space, then the relaxation functions involved in eqns.(2.6) and (2.7) are curves on this surface [23]. If Ψ_{ij} in eqn.(2.3) is symmetric with respect to τ_1 and τ_2 , then the corresponding generating functions in eqns.(2.6) and (2.7) are identical representing a symmetric coupling.

The first two terms in eqn.(2.8) are of the first order, whereas the last two terms are of the second order, assuming Q_i is of the first order. Hence, to satisfy the Clausius-Duhem inequality for all processes, it is necessary that

$$\frac{\partial D_{ij}}{\partial t} = 0, \quad \frac{\partial \beta(t)}{\partial t} = 0 \qquad (2.9)$$

as well as

$$\Lambda - Q_i(\psi,_i/T_o) > 0 \qquad (2.10)$$

By assuming a particular process such that $\psi,_i = 0$ (i.e., a uniform temperature field), we come up with the dissipation inequality

$$\Lambda > 0 \qquad (2.11)$$

where A is the rate of energy dissipation. By using eqn.(2.11), it is sufficient that eqn.(2.10) be satisfied by requiring

$$Q_i(\psi_{,i}/T_o) < 0 \tag{2.12}$$

The constitutive relation for the heat flux vector Q_i is assumed in the form

$$Q_i = -\int_{-\infty}^{t} k_{ij}(t-\tau) \frac{\partial \psi_{,j}}{\partial \tau} \partial\tau \tag{2.13}$$

Combination of eqns.(2.12) and (2.13) gives

$$\psi_{,i} \int_{-\infty}^{t} k_{ij}(t-\tau) \frac{\partial \psi_{,j}}{\partial \tau} \partial\tau > 0 \tag{2.14}$$

Further, for a fixed time and with the tensor k_{ij} being positive definite and constant with respect to time, the temperature gradient $\psi_{,i}$ and the integral in eqn.(2.14) have the same sign. Therefore, eqn.(2.13) reduces to

$$Q_i = - k_{ij}\psi_{,j} \tag{2.15}$$

For the development of the first order theory the energy eqn.(2.1) is rewritten using eqns.(2.3), (2.7), and (2.15) by neglecting the second order term A, i.e.

$$\rho\gamma - \frac{\partial}{\partial t} \int_{-\infty}^{t} \Psi_{ij}(t-\tau,0) \frac{\partial \varepsilon_{ij}}{\partial \tau} d\tau + \int_{-\infty}^{t} m(t-\tau,0) \frac{\partial \psi}{\partial \tau} \partial\tau + (k_{ij}\psi_{,j})_{,i} = 0 \tag{2.16}$$

The integral involving strain history in eqn.(2.16) gives rise to a coupling between thermal and mechanical effects. Without this term, eqn.(2.16) is the uncoupled equation governing heat conduction.

The above completes the development of the coupled linear theory of thermoviscoelasticity according to Christensen [23], and these relations are adopted in Section 2.1.3 in regard to the uncoupled formulation of the boundary-value problems.

2.1.2 THERMORHEOLOGICALLY SIMPLE MATERIAL(TSM) POSTULATE

There is a special type of thermorheological property which is applied to a wide variety of materials by use of a certain analytical description. This property exihibits a variation of relaxation/creep functions with temperature similar to the variation of the same function with time. Thus, it is found more convenient to study the effects between the behavior with time and temperature simultaneously by use of reduced variables [23,34,98].

The method of reduced variable provides a simple phenomenological function by reducing two main variables of time and temperature to a new reduced variable. The application of this method requires the transformation of a function $G(\ln t,T)$ depending upon the time and temperature into a function $G(x)$ where $x = \ln t+f(T)$ and $f(T)$ is a function of temperature alone. A material whose viscoelastic behavior with both time and temperature lends itself to the above reduction scheme is called a thermorheologically simple material(TSM).

To this end, we designate the relaxation functions at the base temperature T_0 for the constant temperature state by

$$G(t,T_0) \equiv L(\ln t) \tag{2.17}$$

The TSM postulate then takes the form

$$G(t,T) \equiv L\{\ln t + f(T)\} \tag{2.18}$$

where the shift function f(T) obeys

$$f(T_0) = 0, \quad \frac{\partial f}{\partial T} > 0 \tag{2.19}$$

Eqn.(2.18) states that the change in temperature cause the relaxation function to be shifted to the right or left when plotted against lnt, as the abscissa. Introducing a change of variable by setting

$$f(T) = \ln \chi(T) \tag{2.20}$$

eqn.(2.19) now implies that

$$\chi(T_0) = 1, \quad \frac{\partial \chi}{\partial T} > 0 \tag{2.21}$$

and is thus a positive monotone-increasing function of T throughout the range of eqn.(2.20). Also, eqn.(2.17), by virtue of eqn.(2.20), yields

$$G(t,T) = G(\xi) \tag{2.22}$$

provided that the reduced time ξ is defined by

$$\xi = t\chi(T) \tag{2.23}$$

Thus, the relaxation function $G(t,T)$ at any temperature can directly be obtained from the relaxation function $G(t)$ at the base temperature by replacing t with ξ from eqn.(2.23). Similar derivations can be formulated for creep functions.

For a continuum under the influence of a variable temperature field or non-constant temperature state, the constitutive equations require a modification such that the reduced time must be generalized consistent with the postulated temperature-time equivalence for non-isothermal conditions. Under the assumption that the non-isothermal stress constitutive relation is determined by the corresponding isothermal functional and with the modified time scale to account for the history of temperature, the isothermal functional expressing the non-isothermal functional is written as

$$\sum(t) = \overset{\infty}{\underset{s=0}{T}} [\{E(t-\xi_s) - \alpha(t-\xi_s)\}, \; E(t) - \alpha(t)] \tag{2.24}$$

where $\sum(t)$, $\overset{\infty}{\underset{s=0}{T}}$ and $E(t)$ denote the appropriate definition of stress, a linear functional operator, and strains. The modified time scale, ξ_s, which depends upon the history of temperature is defined by

$$\xi_s = \overset{\infty}{\underset{\lambda=0}{T}} [T(t-\lambda),s] \tag{2.25}$$

with the property

$$\xi_s \Big|_{s=0} = 0, \quad \frac{\partial \xi_s}{\partial s} > 0 \tag{2.26}$$

and

$$\xi_s \Big|_{T=T_0} = s \tag{2.27}$$

Here, $\alpha(t) = E(t)\Big|_{\Sigma=0}$ represents the volume change due to the temperature change under the stress free condition.

For the infinitesimal theory, eqn.(2.24) can be written as

$$\sigma_{ij}(t) = G_{ijkl}(0)\,[\varepsilon_{kl}(t) - \alpha_{kl}(t)] + \int_0^t [\varepsilon_{kl}(t-\xi_s) - \alpha_{kl}(t-\xi_s)]\,\frac{\partial G_{ijkl}}{\partial s}\,ds \tag{2.28}$$

Eqn.(2.28) is the desired constitutive relation for infinitesimal definition with the general nonlinear temperature dependence. Integrating eqn.(2.28) by parts and using the change of variable $t - \xi_s = \tau$ gives

$$\sigma_{ij}(t) = \int_{-\infty}^{t} G_{ijkl}(s)\,\frac{\partial}{\partial \tau}\,[\varepsilon_{kl}(\tau) - \alpha_{kl}(\tau)]\,d\tau \tag{2.29}$$

where

$$s = \int_0^{\xi_s} \chi[T(t-\lambda)]\,d\lambda \tag{2.30}$$

with $\chi(T)$ being the shift function such that

$$\chi(T_0) = 1, \quad \frac{\partial \chi(T)}{\partial T} > 0 \tag{2.31}$$

Using the change of variable $\xi_s = t - \tau$, eqn.(2.30) yields

$$S = \int_0^t \chi[T(\eta)]d\eta - \int_0^\tau \chi[T(\eta)]\, d\eta \tag{2.32}$$

Eqn.(2.29) can be rewritten with the use of eqn.(2.32) in the form

$$\sigma_{ij}(t) = \int_{-\infty}^t G_{ijkl}\,(\xi - \xi')\, \frac{\partial}{\partial \tau}\,[\epsilon_{kl}(\tau) - \alpha_{kl}(\tau)]\, d\tau \tag{2.33}$$

where

$$\xi = \int_0^t \chi[T(\eta)]\, d\eta, \quad \xi' = \int_0^\tau \chi\,[T(\eta)]\, d\eta \tag{2.34}$$

Here, we can identify the shift function in eqn.(2.34) with that in eqn.(2.23) for a constant temperature state. In fact, eqn.(2.34) reduces to eqn.(2.23) under a constant temperature state. Since the reduced time is computed explicitly from the given temperature at the corresponding physical time, the notations of the relevant quantities are maintained in the present text. The reduced variable scheme for creep compliance function is illustrated in Figure 2 and the corresponding shift function is shown in Figure 3.

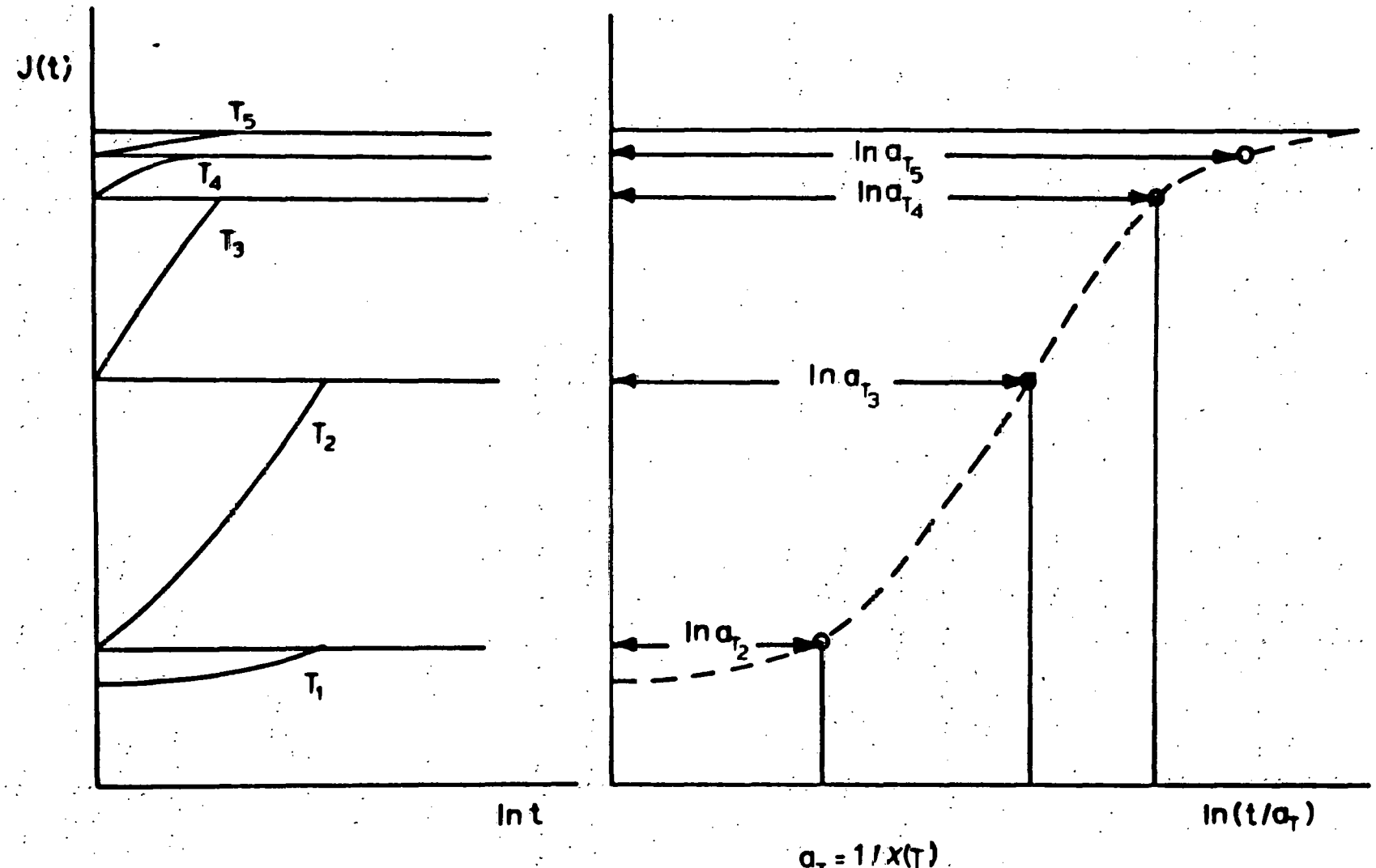

Figure 2: Time-Temperature Shift of Creep Curve

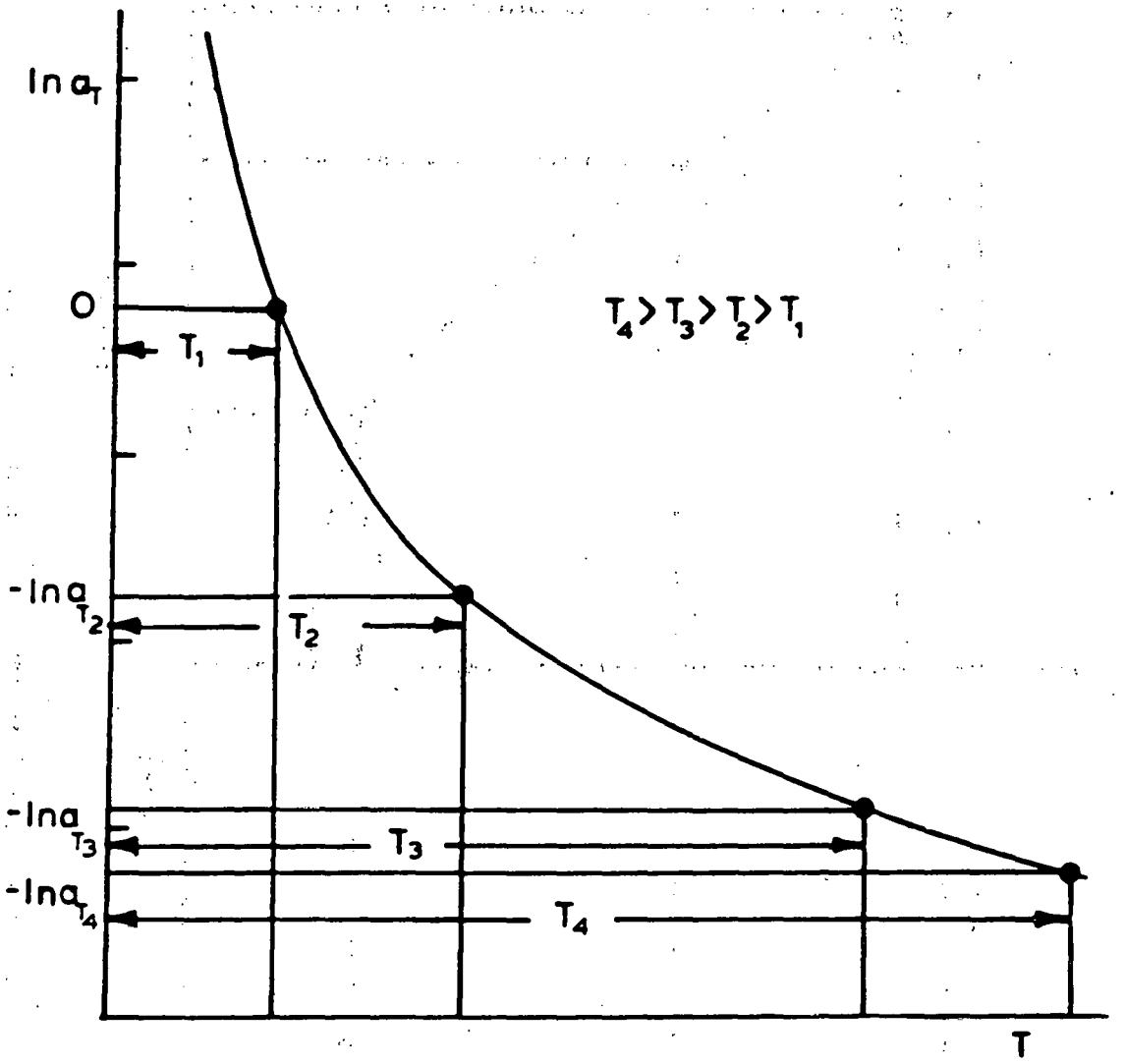

Figure 3: Variation of Shift Function with Temperature

2.1.3 FORMULATION OF BOUNDARY VALUE PROBLEMS

The relevant linear equations which govern the coupled thermoviscoelasticity theory are reviewed. The equations of quasi-static equilibrium, the strain displacement relations and the stress strain relations are

$$\sigma_{ij,j} + f_i = 0 \tag{2.35}$$

$$\epsilon_{ij} = \frac{1}{2}(U_{i,j} + U_{j,i}) \tag{2.36}$$

$$\sigma_{ij} = \int_0^t G_{ijkl}(\xi-\xi') \frac{\partial \epsilon_{kl}}{\partial \tau} d\tau - \int_0^t \Psi_{ij}(\xi-\xi') \frac{\partial \psi}{\partial \tau} d\tau \tag{2.37}$$

The heat transfer equation is given by

$$(k_{ij}\psi_{,j})_{,i} = \frac{\partial}{\partial t}\int_0^t m(\xi-\xi') \frac{\partial \psi}{\partial \tau} d\tau + \frac{\partial}{\partial t}\int_0^t \Psi_{ij}(\xi-\xi') \frac{\partial \epsilon_{ij}}{\partial \tau} d\tau \tag{2.38}$$

For the uncoupled linear theory of an isotropic viscoelastic medium, eqns.(2.37) and (2.38) can be further simplified in the form

$$S_{ij} = \int_0^t G_1(\xi-\xi') \frac{\partial}{\partial \tau} e_{ij} d\tau$$

$$\sigma_{kk} = \int_0^t G_2(\xi-\xi') \frac{\partial}{\partial \tau}[\epsilon_{kk} - 3\alpha_0\theta] d\tau \tag{2.39}$$

and

$$(k_{ij}T_{,j})_{,i} = \rho c \frac{\partial T}{\partial t} + \bar{Q} \tag{2.40}$$

where S_{ij} and e_{ij} are deviatoric stresses and strains, G_1 and G_2 are shear and bulk relaxation moduli, and k_{ij}, ρ, c and $\bar{Q}$ are heat conductivity, mass density, heat capacity and lumped heat supply function, respectively. The infinitesimal temperature ϕ is replaced by the absolute temperature T since the temperature response is separately obtained in the present linear uncoupled formulation. The pseudo-temperature, θ, is defined by

$$\theta = \frac{1}{\alpha_0} \int_{T_0}^{T} \alpha(T')\, dT' \tag{2.41}$$

and the mechanical response is posed separately after obtaining the temperature distribution from eqn.(2 40). Analogous considerations apply to the generalization of the creep law under non-isothermal conditions, which assumes the form of

$$e_{ij} = \int_0^t J_1(\xi-\xi') \frac{\partial}{\partial\tau} S_{ij}\, d\tau$$

$$e_{kk} = \int^t J_2(\zeta-\zeta') \frac{\partial}{\partial\tau} v_{kk}\, d\tau + 3\alpha_0\theta \tag{2.42}$$

where J_1 and J_2 are the shear and compressive creep compliances.

In the absence of thermo-mechanical coupling effects, the governing thermal system is separated from the mechanical system as described above. The general heat transfer equation may include the convective heat transfer term for the heat supply function as well as the conduction term under the interaction between the fluid and solid phase, which are represented by two heat balance equations [101,113],

solid:

$$\rho_s C_s \frac{\partial T_s}{\partial t} = (k_{ij} T_{s,j})_{,i} + h_T (T_f - f_s) \tag{2.43}$$

fluid:

$$\rho_f C_f \frac{\partial T_f}{\partial t} = - \rho_f C_f (V_i T_{f,i}) + h_T (T_s - T_f) \tag{2.44}$$

where h_T is the heat transfer coefficient and V_i is the fluid velocity, and subscripts s and f denote the solid and fluid phases, respectively. Under the assumption that the solid and fluid phases are at the temperature, the above equations reduce to

$$(\rho_s C_s + \rho_f C_f) \frac{\partial T}{\partial t} = (k_{ij} T_{,j})_{,i} - \rho_f C_f V_i T_{,i} \tag{2.45}$$

An equation of this type is known as a convective-diffusion equation in heat transfer. In fluid mechanics, the normalized form of eqn.(2.45) represents the advection-diffusion equation for the viscous boundary layer problems where the coefficient related to the first derivative term forms the Peclet number and the fluid velocity. The quasi-static version of eqn.(2.45) is also applied to the thermodynamic line drive model with the moving coordinate system [67,75].

The initial conditions are taken as

$$U_i(t) = \sigma_{ij}(t) = 0$$
$$T(t) = T_0 \qquad \text{at } t = 0 \tag{2.46}$$

For $t > 0$, the boundary conditions are

$$\begin{aligned} \sigma_{ij} n_j &= \bar{T}_i \ (x_i,t) \quad \text{on } \Gamma_\sigma \\ U_i &= \bar{U} \ (x_i,t) \quad \text{on } \Gamma_u \\ T &= \bar{T} \ (x_i,t) \quad \text{on } \Gamma_T \end{aligned} \tag{2.47}$$

and

$$k_{ij} T_{,i} n_j = \lambda \quad \text{on } \Gamma_\lambda \tag{2.48}$$

where Γ_T is the part of boundary on which the temperature is prescribed and Γ_λ is the complimentary part of the boundary over which the heat flux is prescribed. The above boundary conditions are illustrated in Figure 4.

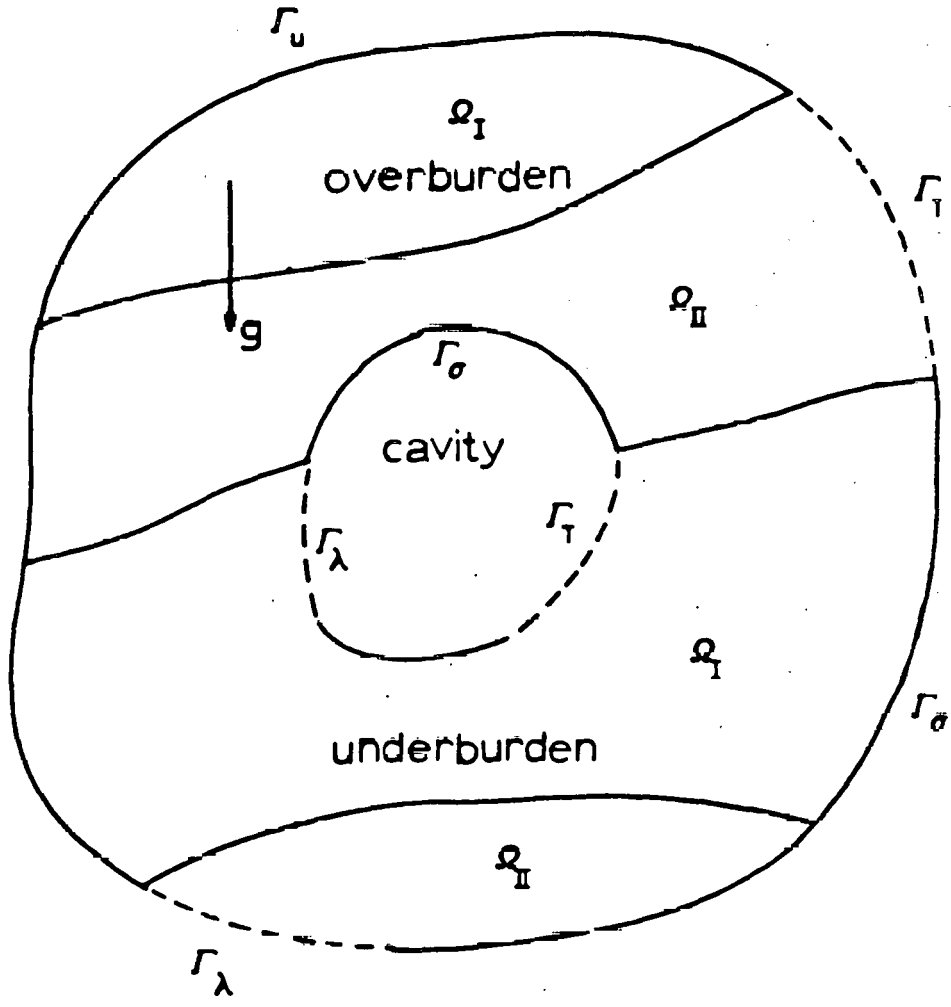

Figure 4: Boundary Conditions and a Domain of Interest

Chapter III

FINITE ELEMENT DISCRETIZATION AND SOLUTION METHODOLOGY

The fundamental concept of finite element methods is that any continuum variables, such as temperature, pressure, or displacements, can be approximated by a discrete model composed of a set of piecewise continuous functions defined over a finite number of subdomains. The general theoretical basis of FEM discretization includes the variational approach and the weighted residual procedure such as Galerkin method or the least square approach. The basic mathematical details and computer implementations can be found in many references [13,90,97,130,132].

The objective of this chapter is to discuss and present the finite element formulations pertaining to the solution of thermoviscoelastic boundary-value problems; namely, effects of heat transfer, two-dimensional elasticity, approximation of the integral creep constitutive law and the incremental solution procedure. The isoparametric singular element with the displacement method for computing stress intensity factors are also studied for the thermally-induced line crack problems in Appendix B.

3.1 ENERGY EQUATIONS

Finite element formulations for two special cases of energy equations, namely, the convective-diffusion equation and the transient heat conduction equation, are considered here.

Finite element solutions of the quasi-static convective-diffusion equation have encountered serious difficulties in situations where the convective/first derivative terms are significant. These difficulties stem from a combination of the essentially elliptic and parabolic nature of two terms and manifest themselves in an oscillatory nature of the solution. Whenever the mesh size exceeds a certain critical value, and with large convection coefficients, acceptable solutions can only be obtained by an excessive reduction in the element size and the use of an equivalent 'Upwind Difference' scheme [134]. These upwinding schemes for one- and two-dimensional cases have been studied by several authors (cf. ref. [24,47,48,56,57]).

The quasi-static version of eqn.(2.45) is written as

$$(k_{ij}\, T_{,j})_{,j} + \bar{V}_i T_{,i} = 0 \tag{3.1}$$

where $\bar{V}_i$ denotes the lumped convection coefficient. The weighted residual formulation of eqn.(3.1) with the weight function W_k is expressed as

$$\int_{\Omega} W_k \left[(k_{ij}\, T_{,j})_{,i} + \bar{V}_i\, T_{,i}\right] d\Omega = 0 \tag{3.2}$$

Using Green's theorem, eqn.(3.2) can be rewritten in the form

$$\int_{\Omega} (W_{k,i})\, k_{ij}\, T_{,j}\, d\Omega - \int_{\Omega} W_k\, \bar{V}_i\, T_{,i}\, d\Omega = \int_{\Gamma} W_k\, k_{ij}\, T_{,j}\, n_i\, d\Gamma \qquad (3.3)$$

Inserting $T = N_i T_i$ into eqn.(3.3) with suitable weighting functions $W_k(x,y)$ produces the classical system of discretized equation

$$\mathbf{H}\mathbf{T} = \mathbf{F} \qquad (3.4)$$

where some values of the unknown vector $\mathbf{T}$ are specified on boundaries and,

$$H_{ij} = \int_{\Omega} (W_{i,k})\, k_{kl}\, N_{l,j}\, d\Omega - \int_{\Omega} W_i\, \bar{V}_k\, N_{j,k} d\Omega \qquad (3.5)$$

with

$f_i = 0$ for Dirichlet conditions

$f_i = \int_{\Gamma} W_i\, k_{kl}\, T_{,l}\, n_k\, d\Gamma$ for Neuman conditions

In the conventional Galerkin formulations, we take $W_i = N_i$. Clearly other selection of weighting functions can be made.

The one-dimensional problem with the basis functions shown in Figure 5 is first considered with the weighting function

$$W_i = N_i \pm \bar{\alpha} F(x) \qquad (3.6)$$

where

$$F(x) = 3x(x-L)/L^2$$
$$N_i = 1 - x/L$$
$$N_{i+1} = X/L$$
$$\text{sgn } \bar{\alpha} = \text{sgn } \bar{V}_i \tag{3.7}$$

and L is the element length. Heinrich et al [46,47] have indicated that this scheme is unconditionally stable for $\bar{\alpha} = 1$ (full upwinding) and effectively eliminates the oscillation caused by high convection coefficients.

For two-dimensional isoparametric bilinear elements, the weighting functions can be analogously constructed in terms of products of one-dimensional functions similar to the formation of Lagrangian shape functions [39,46]. By defining

$$L_1(\xi) = (1 - \xi)/2$$
$$L_2(\xi) = (1 + \xi)/2$$
$$F(\xi) = -3\,(1 - \xi)\,(1 + \xi)/4 \tag{3.8}$$

where ξ is the transformed coordinate. The weighting functions for the four-noded isoparametric elements are

$$W_1(\xi,\eta) = [L_1(\xi) + \bar{\alpha}_1 F(\xi)]\,[L_1(\eta) + \bar{\beta}_1 F(\eta)]$$
$$W_2(\xi,\eta) = [L_2(\xi) - \bar{\alpha}_1 F(\xi)]\,[L_1(\eta) + \bar{\beta}_2 F(\eta)]$$
$$W_3(\xi,\eta) = [L_2(\xi) - \bar{\alpha}_2 F(\xi)]\,[L_2(\eta) - \bar{\beta}_2 F(\eta)]$$
$$W_4(\xi,\eta) = [L_1(\xi) + \bar{\alpha}_2 F(\xi)]\,[L_2(\eta) - \bar{\beta}_1 F(\eta)] \tag{3.9}$$

and Figure 6 illustrates variations of the above weigting fuctions. For quadratic elements, similar weight functions can be obtained from references [39,47,48].

The standard finite element discretization of the transient heat conduction equation has been well established (cf. ref. [54, 97,128,130]). The finite element discretization of eqn.(2.45), neglecting variables related to the fluid phase, can be expressed as a sum of element quantities as

$$\sum_{e=1}^{N} \left(\mathbf{C}^e \dot{\mathbf{T}} + \mathbf{K}^e \mathbf{T} + \mathbf{F}^e \right) = 0 \tag{3.10}$$

where N denotes the number of element, and the capacity matrix $\mathbf{C}^e$, the conduction matrix $\mathbf{K}^e$ and the force term $\mathbf{F}^e$ due to the heat source/sink term $H(\underline{x},t)$ are defined by

$$\mathbf{C}^e = \int_{\Omega^e} N_\alpha \rho C N_\beta \, d\Omega^e \tag{3.11}$$

$$\mathbf{K}^e = \int_{\Omega^e} N_{\alpha,i} \, k_{ij} \, N_{\beta,i} \, d\Omega^e \tag{3.12}$$

$$\mathbf{F}^e = \int_{\Omega^e} H(\underline{x},t) \, N_i \, d\Omega^e \tag{3.13}$$

Considering a typical time element of length Δt for the transient term, the two points recurrence formula widely adopted in the transient formulation yields the following general expression.

$$(\mathbf{C}/\Delta t + \mathbf{K}\bar{\theta})\,\mathbf{T}_{n+1} + [\mathbf{K}(1-\bar{\theta}) - \mathbf{C}/\Delta t]\,\mathbf{T}_n + \mathbf{F} = 0 \tag{3.14}$$

where

$$\mathbf{F} = \mathbf{F}_{n+1}\bar{\theta} + \mathbf{F}_n(1-\bar{\theta})$$

and $\bar{\theta}$ is the scheme control parameter with $0 \leq \bar{\theta} \leq 1$.

The above two-point recurrence scheme is accompanied by a restriction which requires the time step size within a certain magnitude. Here, the time step size is selected by the following rule of thumb

$$\Delta t \leq \frac{1}{2}\frac{\rho C}{k}(h)^2 \tag{3.15}$$

where h is the shortest element length. The above rule, stemmed from the eigenvalue problem for one-dimensional case, is adopted for two-dimensional case by choosing the minimum time step size.

The heat capacity matrix $\mathbf{C}$ is often diagonalized by adding the coefficient of each low and placing the sum on diagonal. Although this lumped heat capacity matrix requires less number of numerical operations, it results in a loss of accuracy in solutions when compared to the case of distributed heat capacity matrix [126]. Here, the computations are carried out with the distributed matrix, and detailed procedures of the time discretization and the characteristics of the scheme for different $\bar{\theta}$ can be found from a text book such as [130].

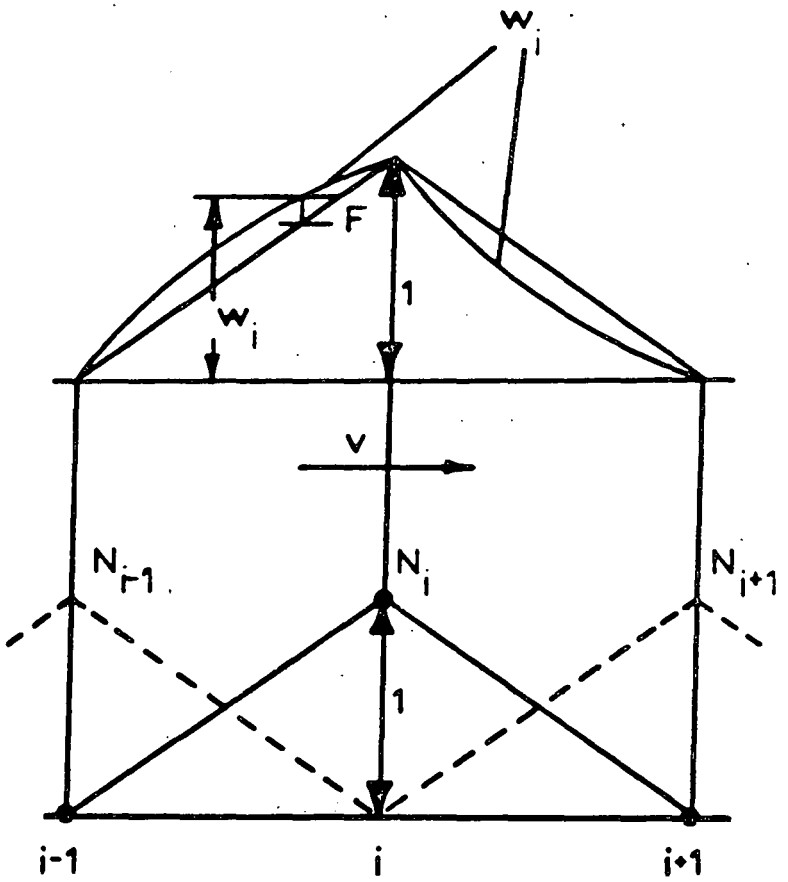

Figure 5: Shape and Weight Functions for One-Dimensional Convection Problem

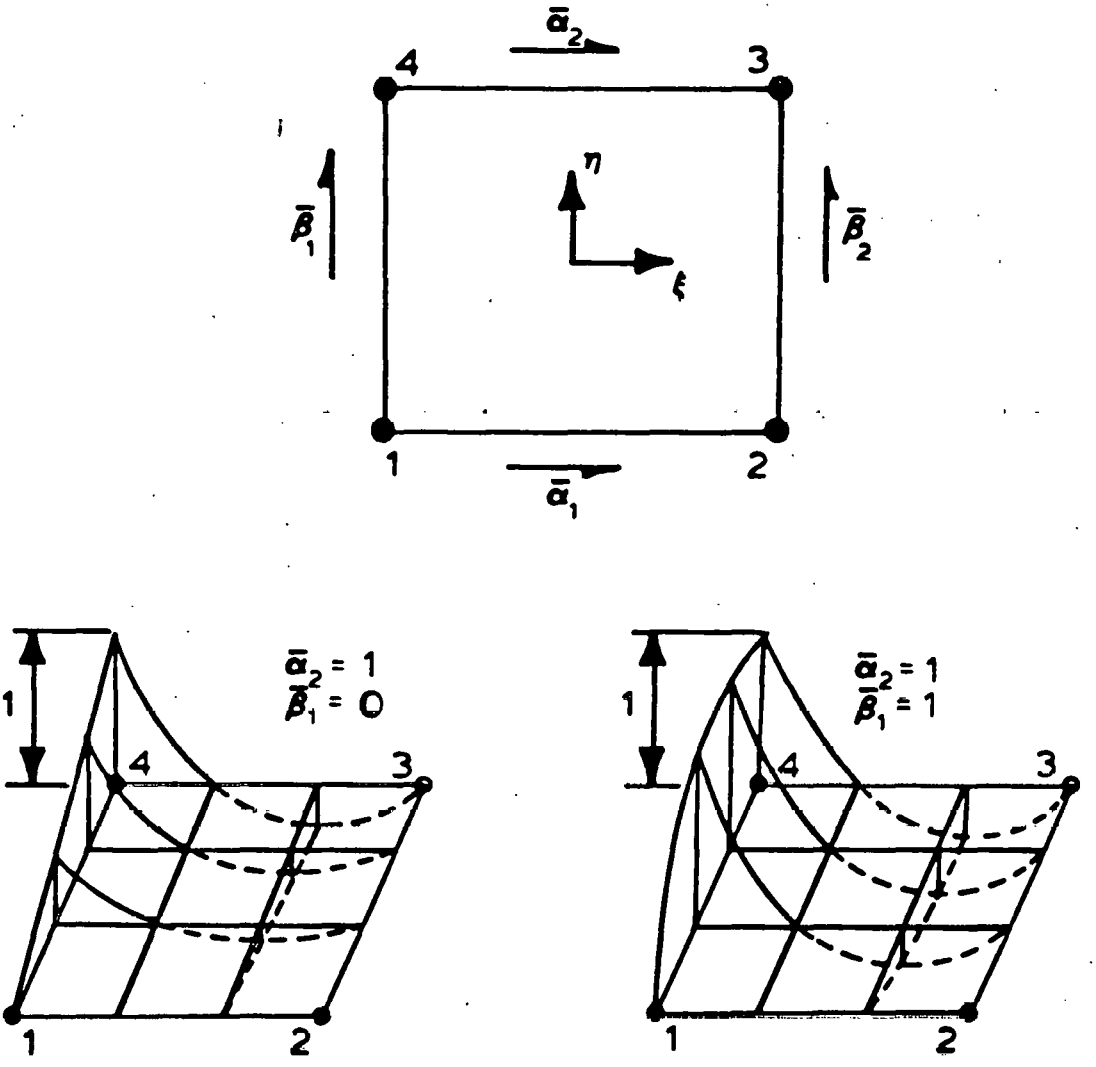

Figure 6: Weight Functions for Two-Dimensional Convection Problem

3.2 THERMOELASTIC FORMULATION

For an isotropic, homogeneous elastic medium under a uniform temperature change ΔT, the stress-strain relationship is given by

$$\sigma_{ij} = \lambda \varepsilon_{kk} \delta_{ij} + 2G \varepsilon_{ij} - \beta \delta_{ij} \Delta T \tag{3.16}$$

where

$$\lambda = E\nu/(1 + \nu)(1 - 2\nu)$$
$$G = E/2(1 + \nu)$$
$$\beta = E\alpha/(1 - 2\nu)$$

in which E is the elastic modulus, ν is Poisson's ratio, and α is the coefficient of thermal expansion. The constitutive law can be expressed in the matrix form as

$$\sigma = \mathbf{D}_e (\varepsilon - \varepsilon_0) \tag{3.17}$$

where $\mathbf{D}_e$ is the matrix of elastic constants and ε_0 is the initial strain. Here, the thermoelastic formulation is briefly summarized and further details can be found from a standard text such as [97,130] and Appendix C.

The formulation entails the selection of a kinematically admissible displacement field and subsequent minimization of the potential energy to obtain the nodal values of the displacements [97,130,132]. The total potential energy of the elastic system can be separated into two components; a component resulting from the strain energy in the body and a component related to the potential energy of the external loads.

$$\pi = \sum_{e=1}^{N} (\Lambda^e - W^e) \tag{3.18}$$

where Λ^e is the strain energy, W^e is the work done by the external loads, N is the number of element and the superscript e designates the element base. The strain energy for an element of volume V is given by

$$\Lambda^e = \int_{\Omega^e} \left(\frac{1}{2} \varepsilon \sigma - \varepsilon_T \sigma \right) d\Omega^e \tag{3.19}$$

where ε and σ are column vectors for the strains and stresses and ε_T are the thermal strains treated as the initial strains. The generalized Hooke's law, strain-displacement relationship, and displacement components in terms of nodal values, are expressed by

$$\sigma = \mathbf{D}_e (\varepsilon - \varepsilon_T) \tag{3.20}$$

$$\varepsilon = \mathbf{B} \mathbf{U} \tag{3.21}$$

$$U = \mathbf{N} \mathbf{U} \tag{3.22}$$

The work done by the external loads can be separated into three distinct parts;

1. Work done by concentrated forces.

$$W_c^e = \mathbf{U}^T \mathbf{P}_c \tag{3.23}$$

2. Work done by the body forces.

$$W_b^e = \int_{\Omega^e} \mathbf{U}^T \mathbf{N}^T \mathbf{b}\, d\Omega^e \tag{3.24}$$

3. Work done by the distributed loads on the surface.

$$W_p^e = \int_{\Gamma} \mathbf{U}^T \mathbf{N}^T \bar{\mathbf{P}}\, d\Gamma \tag{3.25}$$

Minimization of the potential yields

$$\sum_{e=1}^{N} \Big[\int_{\Omega^e} \mathbf{B}^T \mathbf{D} \mathbf{B}\, d\Omega^e \mathbf{U} - \int_{\Omega^e} \mathbf{B}^T \mathbf{D} \varepsilon_T\, d\Omega^e - \int_{\Omega^e} \mathbf{N}^T \mathbf{b}\, d\Omega^e - \int_{\Gamma} \mathbf{N}^T \bar{\mathbf{P}}\, d\Gamma - \mathbf{P}_c \Big] = 0 \tag{3.26}$$

or simply

$$\bar{\mathbf{K}}\mathbf{U} = \mathbf{F} \tag{3.27}$$

where the term associated with the initial strain is incorporated in the right hand side as an equivalent body force.

3.3 THERMOVISCOELASTICITY THEORY FORMULATION

Since the ealier finite element application to the creep problems initiated by King [64], many papers and reports on viscoelastic models and solution algorithms have been published, as reviewed in Section 1.2. For thermal creep problems, the common representation of the creep behavior is the empirical creep law under a constant temperature state as proposed in Greenbaum and Rubinstein [41] and Sutherland [108]. This approach with modifications in the solution algorithm is still adopted in current applications [7,76]. Meanwhile, Taylor and Chang [110] initiated a more rigorous approach by using the integral creep law under the isothermal condition with the TSM postulate. This approach has been further extended under the nonisothermal condition by Taylor et al [111], Cost [27] and Batra et al [14]. These FEM formulations require the solution of the set of Volterra type integral equations and rather unique solution procedure compared to the conventional structural formulation.

The present finite element approach is focussed on the adaptability of the standard linear viscoelastic formulation to the thermoviscoelastic problems by using the strain rate expressions. The FEM formulation includes the numerical approximation of the integral creep constitutive law with variable temperature fields and the incremental solution procedure. In addition, the mechanical model approach with the TSM postulate is adopted. This allows the incorporation of both time and temperature dependent viscoelasticity.

3.3.1 MODELING OF CREEP BEHAVIOR

It is known that the material constants or parameters pertinent to the model can be assesed more directly by a creep test rather than a relaxation test. In general, various creep models differ significantly in their mathematical form and physical basis; some are purely phenomenological approaches [8,76,108,129,133] while others are based on the viscoelastic and hereditary integral methods [27,110,111]. Here, the conventional model adopted is essentially the generalized Voigt type (Figure 7). Extensive references for modeling creep behavior are provided in reviews by Haisler and Sanders [45], Zienkiewicz [130] and Owen and Hinton [90].

The most widely used means of describing creep behavior in the finite element formulation is the strain rate expression

$$\dot{\varepsilon}_c = f(\sigma, T, t) \tag{3.28}$$

with the total strain given by

$$\varepsilon = \varepsilon_e + \varepsilon_c + \varepsilon_T \tag{3.29}$$

where the subscript e, c and T denote the elastic, creep and thermal terms. The common expression for eqn.(3.28) for the isothermal case takes the form of the differential operator [133] or empirical functions such as Norton's law [91,108]. For the non-isothermal case with the TSM postulate, the integral constitutive creep law is used to include the variable temperature history.

The general multi-axial relationship with creep compliances are expressed by eqn.(2.42). However, in most polymeric and porous materials, it has been known from experimental evidence that Poisson's ratio for creep strains remains constant approximately at the same value associated with elastic deformation [6]. This enables the uniaxial creep data to be applied to the multi-axial stress-strain relationships under the following conditions [41,108,132,136];

1. The volume of the body is assumed to remain constant during creep deformations.
2. A superimposed hydrostatic state of stress should not give rise to any change in the creep rate.
3. For an isotropic medium, the principal directions of strain and stress tensors should coincide during the time interval.

Therefore, the stress-strain law for the viscoelastic creep can be written in the form of standard elastic equations replacing the elastic compliance 1/E by the integral operators defined by replaced by

$$\bar{C} = \int_0^t J(t-\tau)\frac{\partial}{\partial\tau}\,d\tau \tag{3.30}$$

where J is a creep function for a constant uniaxial unit stress and the medium is assumed to be undisturbed prior to t = 0. In general, the strain is written as

$$\varepsilon = D_e^{-1}\sigma = \bar{C}\,D_0^{-1}\sigma \tag{3.31}$$

where $\mathbf{D}_e$ is the elasticity matrix and $\mathbf{D}_o^{-1}$ has the same form as an elasticity matrix with the constant Poisson's ratio as defined in Appendix C. Now, the strains are expressed as

$$\varepsilon = \mathbf{D}_o^{-1} \int_0^t J(t - \tau) \frac{\partial \sigma}{\partial \tau} d\tau \tag{3.32}$$

where $\mathbf{D}_o^{-1}$ incorporates the incompressible effect ($\nu = 1/2$) in which no viscoelastic creep develops due to the hydrostatic stress but a large amount of creep occurs due to the deviatoric stress components [41,132,136]. Here, the four parameter fluid model (Burger's model), which fits the experimental creep curves relatively well for the geological materials [75], is adopted (cf. Figure 7). Since coal and rock mass are found to be thermorheologically simple materials [99,40], they are assumed to adopt typical TSM behaviors so that the above assumptions can be applied to the present FEM model simulations. The creep compliance for the four parameter fluid model with the reduced time is expressed by

$$J(\xi) = \frac{\xi}{\eta_0} + \frac{1}{E_0} + \frac{1}{E_1} [1 - EXP(-\xi/\lambda)] \tag{3.33}$$

with

$$\xi = \int_0^t \chi[T(\underline{x}, \eta)] \, d\eta$$
$$\lambda = \eta_1/E_1 \tag{3.34}$$

and η_0 , E_0 and E_1 are material constants as shown in Figure 7. The temperature shift function $\chi(T)$ takes the form

$$x(T) = \tilde{a}\ \mathrm{EXP}\ (\tilde{b}T + \tilde{c}T^2) \tag{3.35}$$

where $\tilde{a}$, $\tilde{b}$ and $\tilde{c}$ are constants. In the present study, the constants of eqn.(3.33) are lumped so that the expression of the creep compliance is further simplified by

$$\bar{J}(\xi) = \bar{a} + \bar{b}\xi + \bar{c}\ \mathrm{EXP}(\bar{d}\xi) \tag{3.36}$$

where $\bar{a}$, $\bar{b}$, $\bar{c}$ and $\bar{d}$ are lumped constants. Discussions of the creep curves for the geological materials are presented in Chapter V.

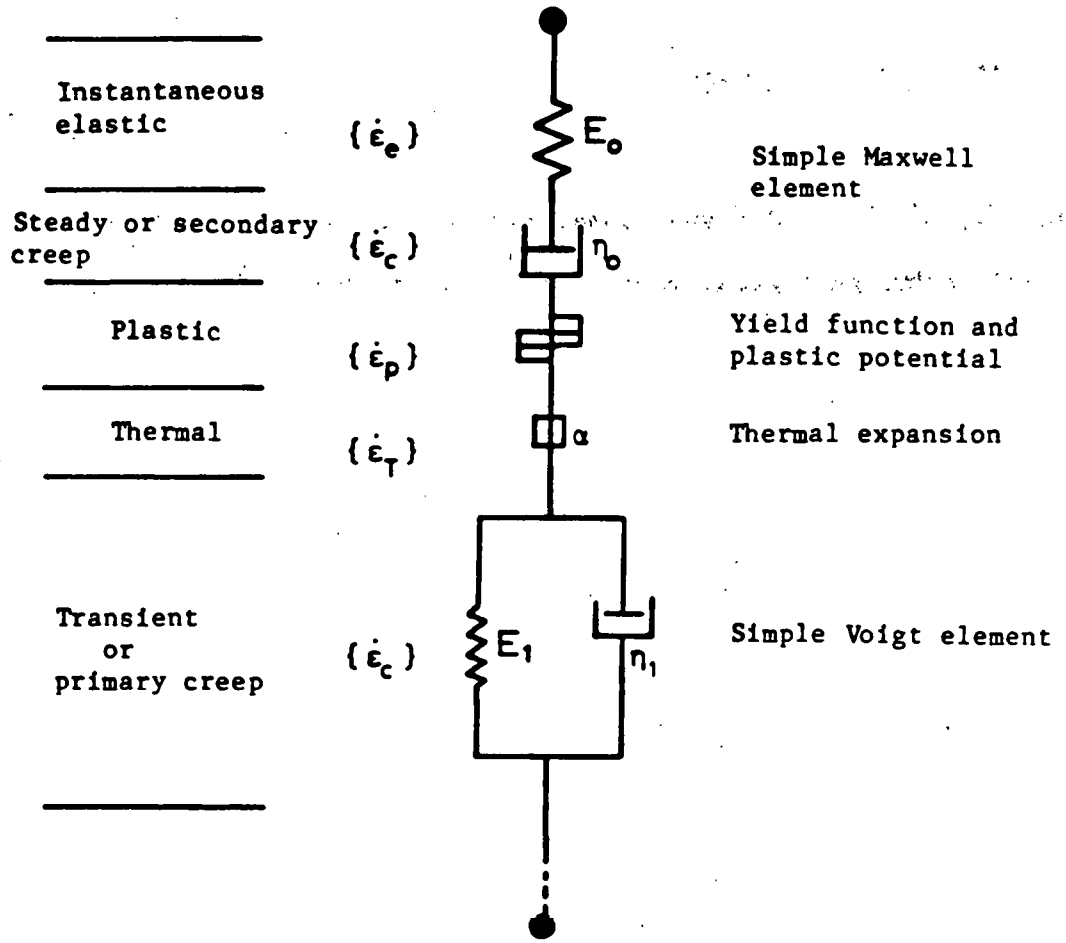

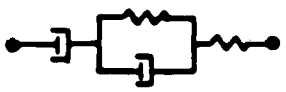

Four parameter fluid model (Burger's model)

Figure 7: Typical Generalized Voigt Model and Four Parameter Fluid Model

3.3.2 NUMERICAL APPROXIMATION OF CREEP STRAIN RATE

The constitutive creep law is usually of a form wherein the rate of creep strain is defined as a certain function of stresses and strains. In the incremental solution procedure, the state of stresses at each time step is updated by the incremental components which represent the time and temperature effects at each particular time. These incremental components are obtained by solving the incremental equilibrium equations with the updated creep strain rate and changes in thermal loads.

For the incremental creep strain, eqn.(3.32) is rewritten in terms of the reduced variables

$$\varepsilon_c = D_o^{-1} \int_0^t J(\xi - \xi') \frac{\partial \sigma}{\partial \tau} d\tau \tag{3.37}$$

and the the creep strain rate with respect to ξ with the application of the Leibnitz rule is expressed by

$$\dot{\varepsilon}_c = D_o^{-1} \int_0^t \frac{\partial}{\partial \xi} J(\xi - \xi') \frac{\partial \sigma}{\partial \tau} d\tau \tag{3.38}$$

Evaluating eqn.(3.38) in the form of summations by using the increment computed in the previous time interval, the approximated form of the creep strain rate is written as

$$\dot{\varepsilon}_{c,n+1} = D_o^{-1} \sum_{k=1}^{n+1} \frac{\partial}{\partial \xi} J(\xi - \xi') \Big|_{\substack{\xi = \xi_{n+1} \\ \xi' = \xi_k}} \Delta\sigma_{k-1} \tag{3.39}$$

The reduced time is evaluated by the summation

$$\xi_{n+1} = \sum_{k=1}^{n} \Delta\xi_k \tag{3.40}$$

where

$$\Delta\xi_k = \chi[T(t_k)]\Delta t_k \tag{3.41}$$

and $\dot{\varepsilon}_{c,n+1}$ is the creep strain rate at ξ_{n+1} and $\Delta\xi_k$ is the increment of the reduced time in the time interval Δt_k . This notation will also be applied to the strain and the stress increment in the present formulation.

In this study, the kernel function $J(\xi - \xi')$ is assumed to be exponential functions as in eqn.(3.36) so that the $\frac{\partial J}{\partial \xi}$ evaluated at $\xi = \xi_n$ and $\xi' = \xi_k$ can take the form

$$\frac{\partial}{\partial \xi} J(\xi - \xi') = a + b\ \mathrm{EXP}[c(\xi_n - \xi_k)] \tag{3.42}$$

where a, b and c are material constants associated with parameters of the mechanical model, and ξ_n and ξ_k are the reduced times at t_n and t_k respectively. In this manner, eqn.(3.39) can be evaluated explicitly according to the expression

$$\dot{\varepsilon}_{c,n+1} = \mathbf{D}_0^{-1} \{b\ \mathrm{EXP}(c\xi_{n+1}) \sum_{k=1}^{n+1} \mathrm{EXP}(-c\xi_k)\ \Delta\sigma_{k-1} + a\sigma_{n+1}\} \tag{3.43}$$

and eqn.(3.43) is further simplified by the following recurrence relationship

$$\dot{\varepsilon}_{c,n+1} = \dot{\varepsilon}_{c,n}\ \mathrm{EXP}(c\Delta\xi_n) + \mathbf{D}_0^{-1} \{(a + b)\ \Delta\sigma_n + a\sigma_n\ (1 - \mathrm{EXP}(c\Delta\xi_n))\} \tag{3.44}$$

This approach appears to be new and essentially allows us to employ the traditional incremental solution technique without any iteration, in which the time step coincides with the increment, which will be be discussed further in detail in the sequel.

3.3.3 STRAIN AND STRESS INCREMENT

Using the strain rate as exprcsscd by eqn.(3.44), the creep strain increment is defined by using an implicit time stepping scheme i.e.

$$\Delta \varepsilon_{c,n} = \Delta\xi_n \left[(1 - \theta)\, \dot{\varepsilon}_{c,n} + \theta\, \dot{\varepsilon}_{c,n+1}\right] \tag{3.45}$$

where $0 < \theta < 1$. The forward Euler, Crank-Nicholson, and fully implicit type of scheme can be obtained by setting $\theta = 0$, $1/2$, and 1, respectively.

Substitution of eqn.(3.44) into (3.45) yields the following explicit form of the creep strain increment

$$\Delta \varepsilon_{c,n} = \Delta\xi_n \left[(1 - \theta + \theta\, \mathrm{EXP}(c\Delta\xi_n))\, \dot{\varepsilon}_{c,n} + \mathbf{S}\, \Delta\sigma_n + \theta\, \mathbf{D}_0^{-1}\, a\, \sigma_n (1 - \mathrm{EXP}(c\Delta\xi_n))\right] \tag{3.46}$$

where

$$\mathbf{S} = \theta\, (a + b)\, \mathbf{D}_0^{-1} \tag{3.47}$$

The stress increments, in terms of the elastic portion of strain increment, are expressed by

$$\Delta\sigma_n = \mathbf{D}_e \, \Delta\varepsilon_{e,n} = \mathbf{D}_e \, (\Delta\varepsilon_n - \Delta\varepsilon_{c,n} - \Delta\varepsilon_{T,n}) \tag{3.48}$$

and the total strain increments can be written in terms of the nodal displacement increments

$$\Delta\varepsilon_n = \mathbf{B}\Delta\mathbf{U}_n \tag{3.49}$$

Substituting for $\Delta\varepsilon_{c,n}$ from eqn.(3.46), eqn.(3.48) then becomes

$$\Delta\sigma_n = \bar{\mathbf{D}}_{n+1} \, (\mathbf{B}\Delta\mathbf{U}_n - \bar{\Psi}_n) \tag{3.50}$$

where

$$\bar{\Psi}_n = \Delta\varepsilon_{T,n} + \Delta\xi_n \, [(1 - \theta + \theta \, \mathrm{EXP}(c\Delta\xi_n)) \, \dot{\varepsilon}_{c,n}]$$
$$+ \Delta\xi_n \theta \, a[1 - \mathrm{EXP}(c\Delta\xi_n)]\mathbf{D}_o^{-1} \, \sigma_n$$

In eqn.(3.50),

$$\bar{\mathbf{D}}_{n+1} = \{\mathbf{D}_e^{-1} + \theta\Delta\xi_n \, (a + b) \, \mathbf{D}_o^{-1}\}^{-1} \tag{3.51}$$

It is noted that the material propertiy matrix $\bar{\mathbf{D}}$ remains constant within an increment but requires inversion if $\theta \neq 0$. The selection of the parameter θ is discussed in section 3.3.5 along with the selection of the time step size. Another important aspect of eqn.(3.50) is that the primary dependent variable associated with the current increment ($\Delta\mathbf{U}_n$) is clearly distinguished from the ones computed at the last increment. This fact together with the constant material property matrix within an increment naturally lead us to employ the incremental solution technique without any iteration.

3.3.4 INCREMENTAL SOLUTION ALGORITHM

The discrete equilibrium equations at any time $t = t_{n+1}$ can be written as

$$\int_{\Omega} \mathbf{B}^T \boldsymbol{\sigma}_{n+1} \, d\Omega = \mathbf{F}_{n+1} \tag{3.52}$$

where $\mathbf{F}_{n+1}$ is the vector of equivalent nodal loads due to applied surface traction and gravitational force. The incremental form of eqn.(3.52) is given by

$$\int_{\Omega} \mathbf{B}^T \Delta\boldsymbol{\sigma}_n \, d\Omega = \Delta\mathbf{F}_n \tag{3.53}$$

where

$$\Delta\mathbf{F}_n = \Delta\mathbf{F}_n^T + \Delta\mathbf{F}_n^b \tag{3.54}$$

in which $\Delta\mathbf{F}_n^T$ and $\Delta\mathbf{F}_n^b$ represent the loads due to the increment of applied load and gravitational force during the time interval Δt_n. These load increments are caused by the discrete load increment $\bar{\mathbf{P}}$ and the mass density $\rho(T)$ under the temperature change at each time step. They are expressed by

$$\Delta\mathbf{F}_n^T = \int_{\Gamma} \mathbf{N}^T \bar{\mathbf{P}} \, d\Gamma \tag{3.55}$$

and

$$\Delta \mathbf{F}_n^b = \int_\Omega \mathbf{N}^T (\mathbf{b}_{n+1} - \mathbf{b}_n)\, d\Omega \tag{3.56}$$

where

$$\mathbf{b}_n = \mathbf{g}\,\rho(T_n) \tag{3.57}$$

Upon substitution of eqn.(3.50) into eqn.(3.53), we obtain

$$\bar{\mathbf{K}}_{n+1}\, \Delta \mathbf{U}_n = \Delta \mathbf{R}_n \tag{3.58}$$

where

$$\bar{\mathbf{K}}_{n+1} = \int_\Omega \mathbf{B}^T \bar{\mathbf{D}}_{n+1} \mathbf{B}\, d\Omega \tag{3.59}$$

$$\Delta \mathbf{R}_n = \int_\Omega \mathbf{B}^T \bar{\mathbf{D}}_{n+1} \Psi_n\, d\Omega + \Delta \mathbf{F}_n \tag{3.60}$$

The nodal displacements and stresses at the current increment can be found from, as usual,

$$\mathbf{U}_{n+1} = \mathbf{U}_n + \Delta \mathbf{U}_n \tag{3.61}$$

$$\sigma_{n+1} = \sigma_n + \Delta \sigma_n \tag{3.62}$$

where the incremental stress is computed according to eqn.(3.50).

The above algorithm becomes identical to the initial strain method [27,130,133] if $\theta = 0$. Here, by using an implicit scheme ($\theta \neq 0$) with the updated $\bar{D}_{n+1}$ matrix at each time step, the above algorithm is intended to allow a relatively large time step size within reasonable solution accuracy without requiring excessive computational efforts.

3.3.5 SELECTION OF TIME STEP SIZE

Hughes [54] has shown that the time integration scheme represented by eqn.(3.45) is unconditionally stable when $\theta \geq 0.5$ for nonlinear heat conduction problems. However, this does not guarantee sufficient accuracy of the solution at any stage and in practice a limit of the time step size is placed to achieve a reasonable solution. For $\theta < 0.5$, the integration process is only conditionally stable and Δt should be less than some critical value. The case $\theta = 0$ represents the forward Euler scheme and suffers from a numerical instability unless Δt is small enough. Depending on the problem characteristics, when the transient state is of interest for the short time interval, the forward scheme is often efficient since it requires easy computer implementation. Further studies and comparisons of several other algorithms can be found in references [9,68,125].

A simple and efficient rule for choosing appropriate time step can be found in Zienkiewicz and Cormeau [133]. In the variable time stepping scheme, the magnitude of the time step is controlled by a factor τ which limits the effective creep strain increment as a fraction of the total effective strain, i.e.,

$$\Delta\bar{\varepsilon}_{c,n} = \left(\frac{2}{3}\dot{\varepsilon}_{c,n}\,\dot{\varepsilon}_{c,n}\right)^{1/2}\Delta\xi_n = \bar{\dot{\varepsilon}}_{c,n}\,\Delta\xi_n < \bar{\varepsilon}_n\,\tau \tag{3.63}$$

where $\bar{\varepsilon}_n$ and $\bar{\dot{\varepsilon}}_{c,n}$ are the total effective strain and the effective creep strain rate respectively, and Δt_n is chosen by

$$\Delta t_n < \min.\{\tau[\bar{\varepsilon}_n/\bar{\dot{\varepsilon}}_{c,n}]/\chi(T_n)\} \tag{3.64}$$

The effective strain and strain rate are computed on element basis along with the temperature shift function at the centroid of each element. The minimum value of time step size computed for each element is selected for the next time step size and the change in the time step length between any two intervals is limited according to the empirical rule of thumb

$$\Delta t_n < 1.5\,\Delta t_{n-1} \tag{3.65}$$

The range of the factor τ is empirically selected to be $.01 < \tau < .1$ for the forward scheme ($\theta = 0$) and up to 10 for the implicit scheme ($\theta = 1$) although the accuracy subsequently deteriorates as τ increases.

3.3.6 COMPUTATIONAL PROCEDURE

The main step in the solution process is summarized here. The solution to the problem begins with the entire transient temperature distribution solved separately and the known initial conditions at t = 0, which repersents the instantaneous responses obtained by using elastic

constants. At this stage T_o, U_o, F_o, ε_o, σ_o are known and $\varepsilon_{c.n} = 0$. The solution sequence adopted is as follows:

(a) At $t = t_n$, the quantities ΔT_n, U_n, σ_n, ε_n, $\varepsilon_{c.n}$ and F_n are known for an equilibrium state. The following quantities are then assembled: $\bar{D}_n$, $\bar{K}_n$, $\Delta\xi_n$, ΔR_n.

(b) We now compute the displacement increment according to eqn.(3.58) and the stress increment from eqn.(3.50) and update the total displacements and stresses from eqns.(3.61) and (3.62).

(c) The time step increment Δt_{n+1} is selected by eqn.(3.64) and checked against eqn.(3.65) with a specified τ. When the time increment for the stress field does not match with the one for the temperature field solved, the linear interpolation of the temperature is carried out.

(d) The reduced time and the creep strain rate are calculated by eqns.(3.40) and (3.44) and the load increment ΔR_{n+1} for the next time interval Δt_{n+1} is formed according to eqn.(3.60).

The solution sequence (a)-(d) is repeated until the prescribed time is reached. The algorithm adopted above is general enough to include plastic strains and large deformations if iterations are allowed within an increment. The flow chart of the above solution procedure is shown in figure 8.

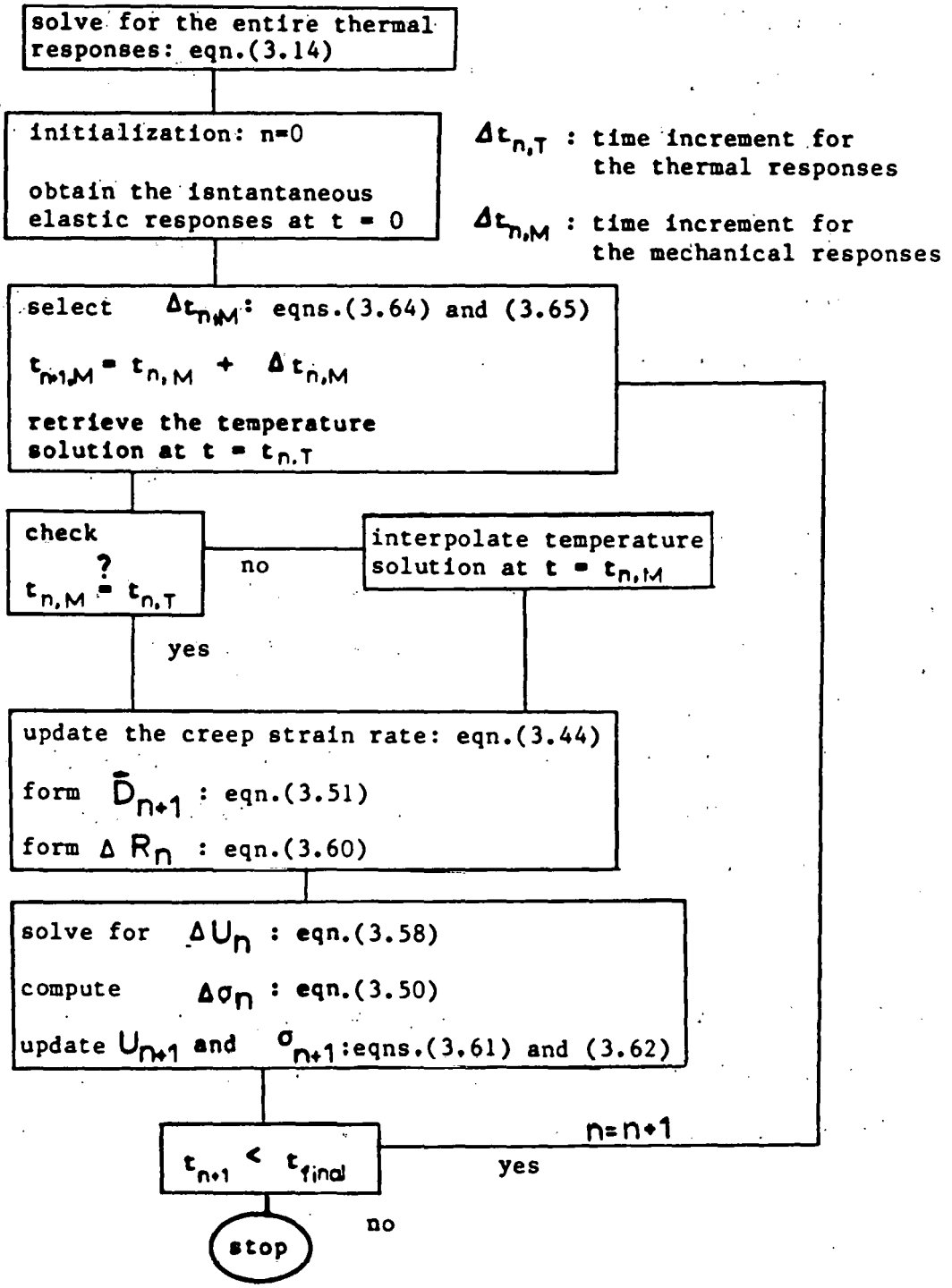

Figure 8: Flow Chart of Incremental Solution Procedure for Thermoviscoelastic Problem

Chapter IV

COMPUTATIONAL EXPERIMENTS

Prior to use of the developed code TMFC for field applications, code validation and model calibrations are essential requirements. In this chapter, FEM formulations associated with the uncoupled thermoviscoelastic analysis presented in Chapter III are validated. Since the thermal responses, separated from the mechanical responses, are affected by characteristics of the problem i.e., convective-diffusion, line crack etc, the temperature responses are independently obtained by using FEM and can then be used for the corresponding thermoelastic or thermoviscoelastic responses. Test numerical models include i) a thermoviscoelstic model, ii) a convective-diffusion model, iii) a transient heat conduction model, and iv) a thermoelastic line crack model. The effects of time step and scheme control parameters in the implicit incremental procedure are demonstrated for the thermoviscoelastic model. Comparisons with available analytical and numerical results are also presented. All calculations in this study are carried out on Amdahl 470/V8 using the implicit double precision.

4.1 THERMOVISCOELASTIC RESPONSES

In this section, the thermoviscoelastic formulation presented in Section 3.3 is validated. The effects of time step size and the implicit scheme control parameters are examined by comparing FEM solutions with the finite difference solutions obtained by Lockett and Morland [77]. The FEM results include the cases of the mechanical and thermal loads. The results from the presented FEM formulations are also compared with the ones given by Taylor et al [111] and analytical solutions obtained by Muki and Sternberg [85].

4.1.1 THERMORHEOLOGICAL PROPERTIES

The thermorheologically simple material characteristics of Polymethylmethacrylate are considered for the presented model. These properties have been adopted in several numerical models by Muki and Sternberg [85], Lockett and Morland [77] and Taylor et al [111]. For the temperature range from 80°C to 110°C with the base temperature T_o = 80°C, the normalized TSM properties are as follows (cf. ref. [77,111]).

1. The temperature shift function is expressed by

$$\chi(\bar{T}) = 3.98\times10^{3}\ \mathrm{EXP}[-6.127(1-\bar{T})\ (1.333 + \bar{T} + 1.095\bar{T}^{2})] \qquad (4.1)$$

where

$$\bar{T} = (T - T_o)/30. \quad (^{\circ}C) \qquad (4.2)$$

The strong dependence on temperature of the shift fuction is shown in Figure 9.a.

2. The relaxation moduli are

$$G_1 = 0.75\times10^{7} + 8.297\times10^{9}\ \mathrm{EXP}(-\xi)$$
$$G_2 = 2.5\times10^{10}$$

(dyne/cm^2) (4.3)

and the equivalent creep compliance is approximated by

$$\bar{J}(\xi) = (3G_2 + G_1)/(9G_1G_2) = (1 + G_1/3G_2)/3G_1$$
$$\approx 4.444458\times10^{-8} - 4.44\times10^{-8}\ \mathrm{EXP}(-9.036\times10^{-4}\xi)$$

(cm^2/dyne) (4.4)

Figure 9.b illustrates the creep compliance with respect to the reduced time.

3. Instantaneous elastic constants are obtained by setting $\xi = 0$ in eqn.(4.3), i.e.

$$\nu_o = (3G_2 - 2G_1)/(6G_2 + 2G_1)\Big|_{\xi=0} = 0.3504$$

$$E_o = (9G_1G_2)/(3G_2 + G_1)\Big|_{\xi=0} = 2.243\times10^{10}$$

(dyne/cm^2) (4.5)

and the temperature solutions are separately provided by a given functional form

$$\bar{T}(\bar{r},\bar{t}) = (1 - \bar{r})\ [1 - \mathrm{EXP}(-2\bar{t})]$$

(°C) (4.6)

where

$$\bar{r} = (r - r_{outer})/(r_{outer} - r_{inner})$$

$$\bar{t} = t/\tau_0 \qquad (4.7)$$

in which $\bar{r}$ and $\bar{t}$ are non-dimensionalized radial distance and time, τ_0 is the relaxation time at the base temperature T_0. The axisymmetric FEM model and the specified transient temperature profiles are shown in Figure 10. It is noted that the temperature reaches the quasi-steady-state at about $\bar{t} = 1.5$ while the inside boundary temperature is dependent on time.

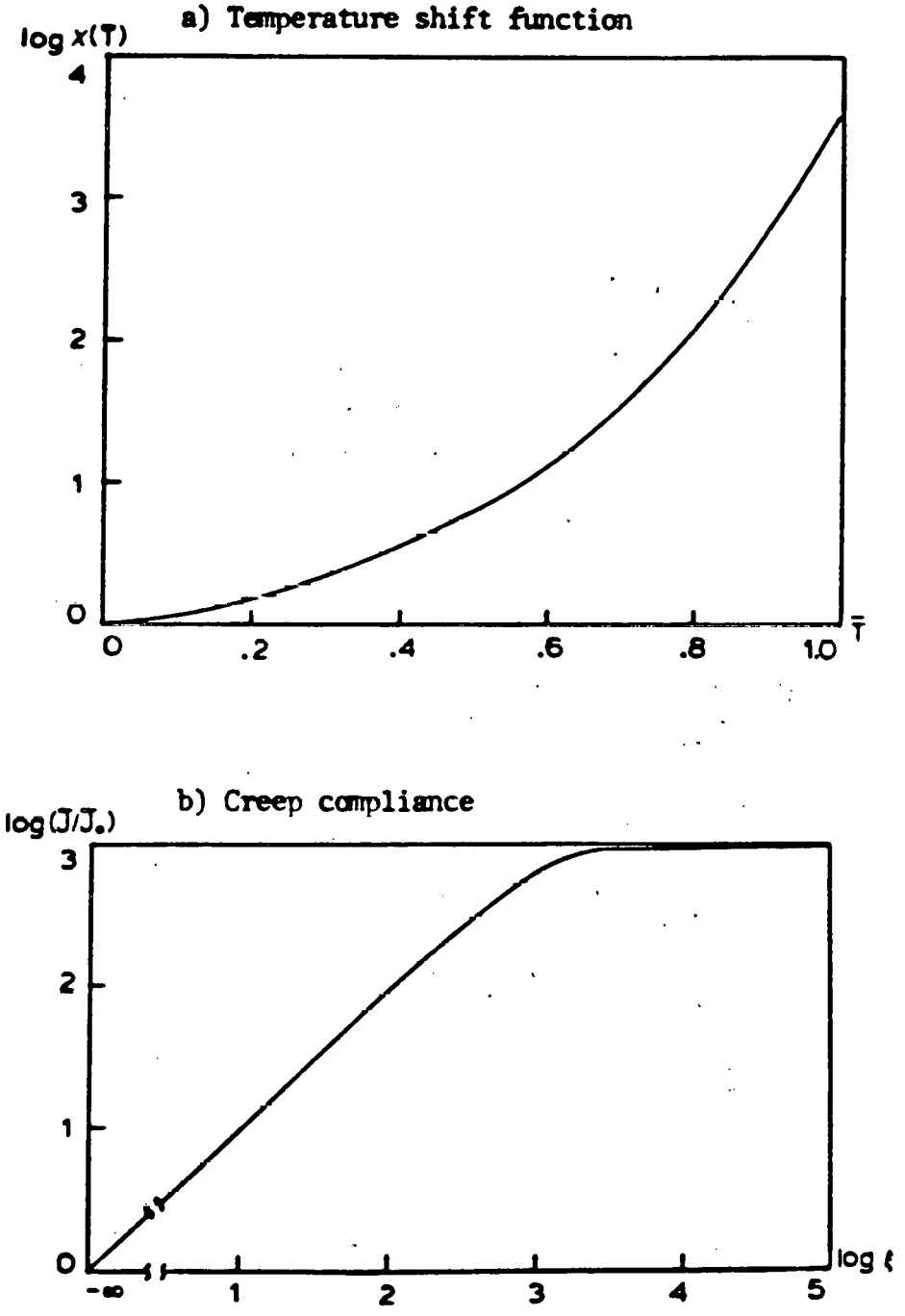

Figure 9: Temperature Shift Function and Creep Compliance for Thermoviscoelastic Test Model

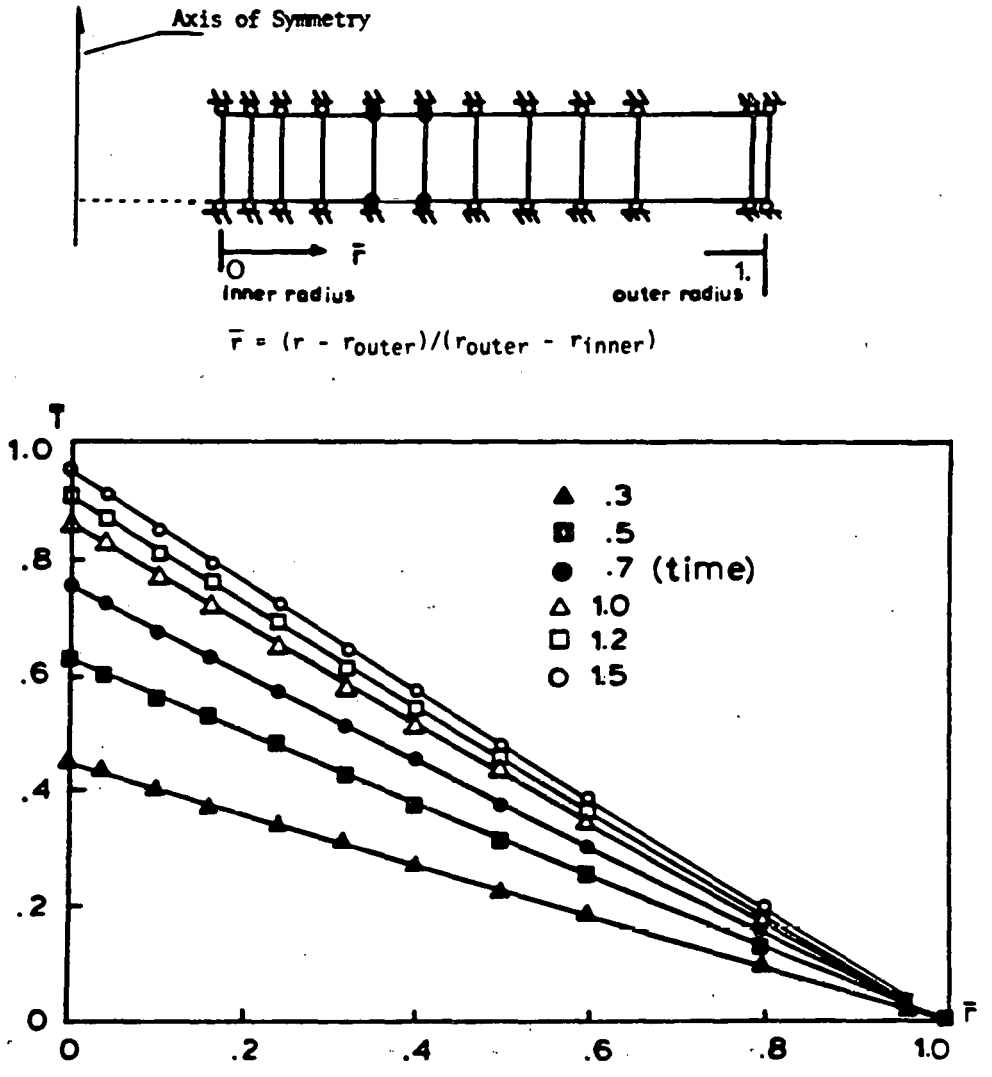

Figure 10: Axisymmetric FEM Model and Temperature Profiles for Thermoviscoelastic Test Problem

4.1.2 THERMOVISCOELASTIC RESPONSES WITH INTERNAL PRESSURE

Elastic solutions are obtained by applying a constant pressure on the inner boundary with instantaneous elastic constants. The uniform elastic solutions adopted from Lockett and Morland [77] are

$$\bar{\sigma}_{rr} = -0.278, \quad \bar{\sigma}_{\theta\theta} = 1.39$$
$$\bar{\sigma}_{zz} = 0.695, \quad \bar{\sigma}_{rz} = 0.0 \tag{4.8}$$

The FEM hoop stress results, excluding the thermal expansion term ($\alpha(T) = 0$ in eqn.(2.41)), are compared with the finite difference solutions. Several cases with different time step sizes and the implicit scheme control parameters are examined to investigate their effect on the solution.

For the forward scheme ($\theta = 0$), the FEM results for the hoop stresses are presented in Figure 11 and are compared with the finite difference solutions. In the forward scheme, the time step size is kept small enough to avoid unstable solutions. The hoop stresses for both FEM and the finite difference solutions compare well except in the region near the inside boundary after $\bar{t} \approx 0.7$. A similar discrepancy was noted in the solution with thermal expansion effects by Taylor et al [111]. The results from the presented formulation, including the thermal expansion effects, are presented in Section 4.1.3. The appropriate time step and scheme control parameters are selected on the basis of preliminary parameter sensitivity studies. Here the results from the implicit schemes are compared with the one from the forward scheme. As shown in

Table 1, the case $\theta = 0.5$ and $\tau = 0.1$ yields the best results. However, as time increases, the case $\theta = 0.5$ suffers from the numerical oscillations and subsequent degraded accuracy. Figure 12 illustrates the oscillations occuring at $\bar{r} = 0.05$ when τ increases up to 0.5. It shows that the solution is oscillatory but stable and converges to the expected solution for the case $\tau = 0.1$. On the other hand, the fully implicit scheme shows no oscillations and requires less computational time as the time step size increases. In addition, the solution accuracy does not deteriorate as quickly as the case $\theta = 0.5$ does.

As time increases with $\tau = 0.1$, compatible results are obtained for both the $\theta = 0.5$ and 1.0 cases (Figure 13). As shown in Figure 12 and 13, the material near the inner surface of the tube is weakened by the increase in temperature in that region. This results in a lower stress being induced in the inner region and a higher stress in the outer region. At subsequent times, the inner region with approximately uniform stress expands out toward the outer region.

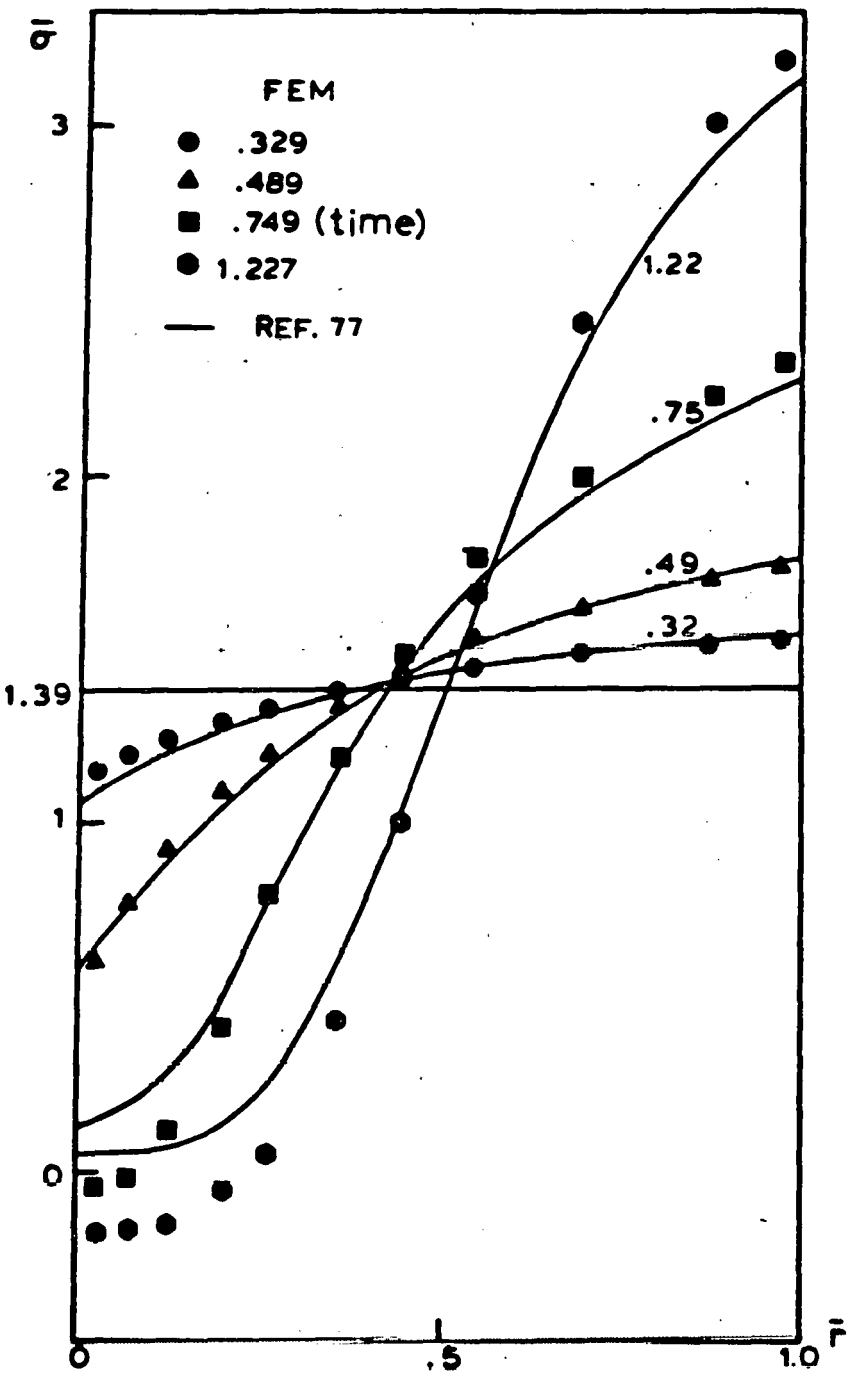

Figure 11: Hoop Stresses with Internal Pressure for Thermoviscoelastic Test Model

	$\theta = 0.5$			$\theta = 1.0$		
case	OSC/stability	error (%)	CPU (sec)	OSC/stability	error (%)	CPU (sec)
$\tau = .1$	no OSC stable	.34 t=1.35	18.67 55 cy.	no OSC stable	1.5 t=1.34	16.91 47 cy.
$\tau = .5$	OSC stable	38. t=1.4	18.42 58 cy.	no OSC stable	8.8 t=1.38	9.02 22 cy.
$\tau = 1.$	OSC stable	60. t=1.42	10.26 48 cy.	no OSC stable	14.1 t=1.17	8.69 21 cy.

* Error was computed with respect to the solution of the forward scheme ($\theta = 0$)

Table 1

Effects of Time Step Size and Implicit Solution Scheme

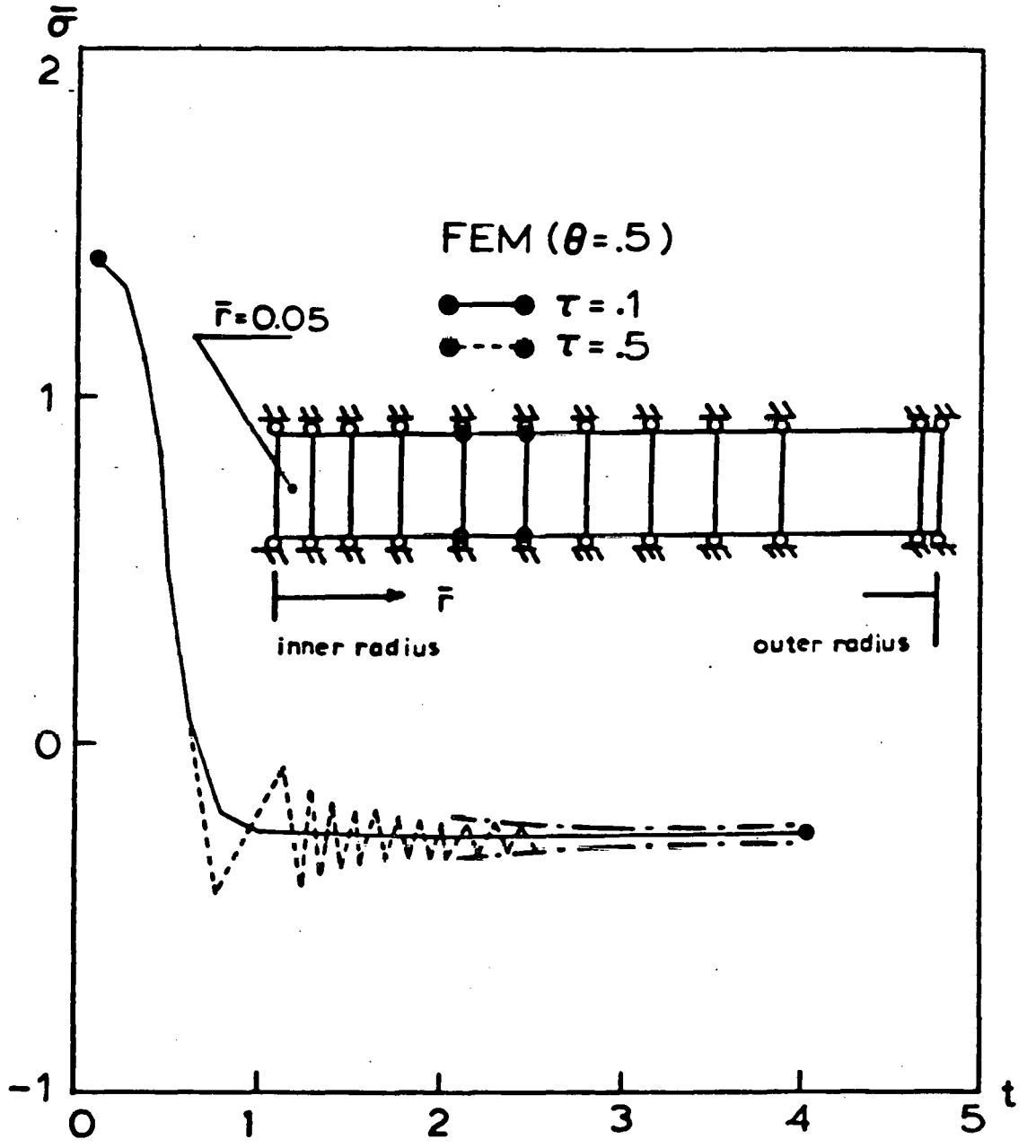

Figure 12: Oscillatory Results with θ= 0.5, τ= 0.5 at $\bar{r}$ = 0.05

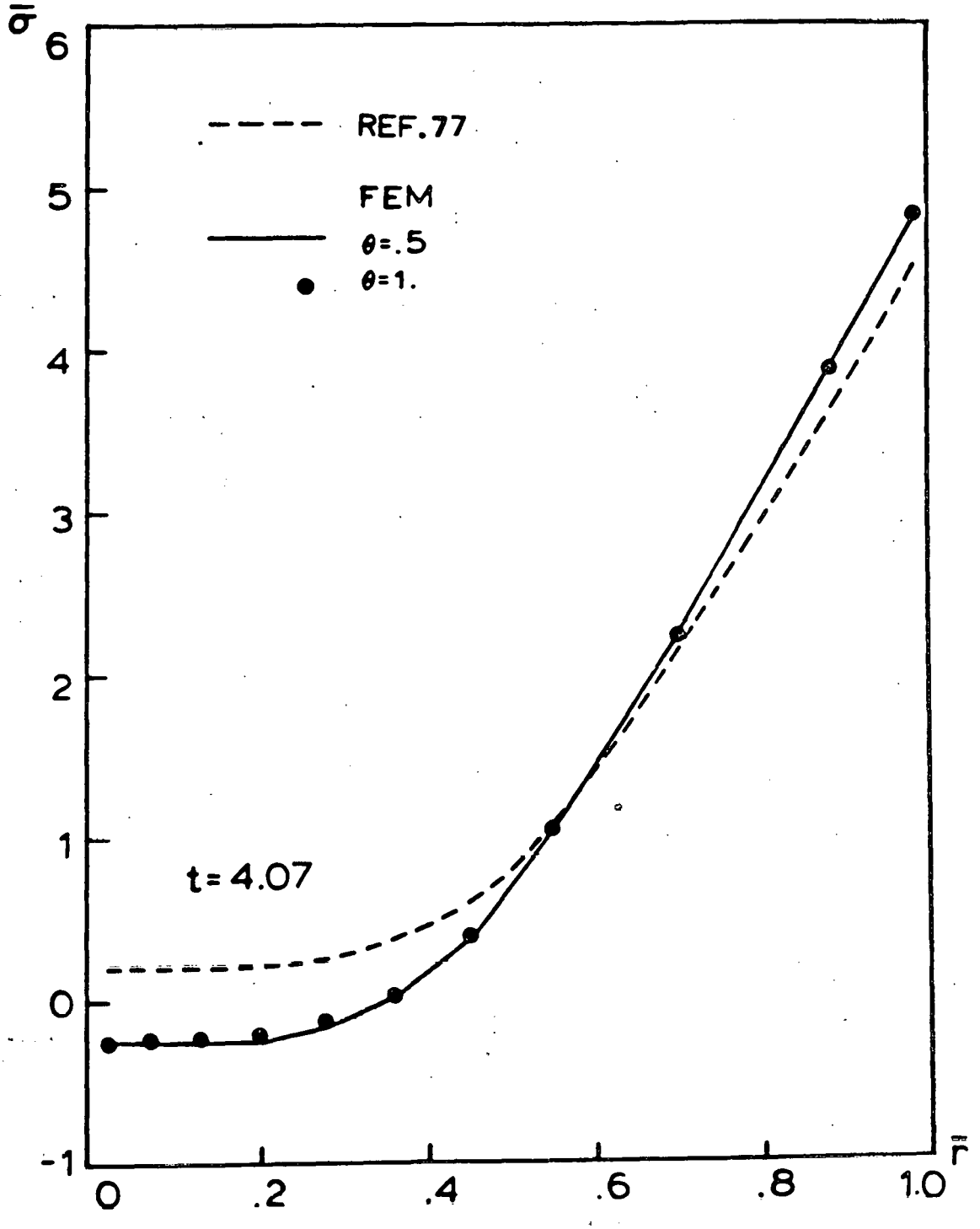

Figure 13: Hoop Stresses at t = 4.07 for Thermoviscoelastic Test Model with Internal Pressure

4.1.3 THERMOVISCOELASTIC RESPONSES WITH THERMAL EXPANSION

Based on the previous numerical experiments for the time step and scheme control parameters, the presented FEM solutions for $\theta = 1.0$ and 0.5 with $\tau = 0.1$ are compared with the finite difference and FEM solutions obtained by Lockett and Morland [77] and Taylor et al [111], respectively. The coefficient of thermal expansion is assumed to be independent of temperature and the normalized hoop stresses are: [85,77]

$$\bar{\alpha} = 2.666 \times 10^{-5}$$

$$\bar{\sigma} = \bar{\sigma}_{\theta\theta}/(3\bar{\alpha} G_0) \tag{4.9}$$

Figure 14 illustrates the effects of high temperature softening of the inner tube region so that a greater load is transferred to the outer region. Across this region, the stress varies from a tensile value at the outer region to a significant compressive stress at the inner region. It is again noticed that the presented FEM and the finite difference solutions do not agree at the inner boundary region at $\bar{t} = 0.32$ and 1.26. However, the solutions obtained by Taylor et al and the presented FEM formulations show a good agreement at $\bar{t} = 1.26$. The finite difference solutions in the inner region is apparently in error as reported in Taylor et al [111].

It can also be noted that the finite difference solutions were obtained by using 40 spatial points and 100 time points while Taylor's FEM solutions used 12 elements and 40 time cycles. In the FEM formulations

presented here, compatible solutions are obtained by using 12 elements and 27 time cycles, which illustrates a superior time discretization. In particular, the presented variable time interval scheme requires proper selection of the initial time step size, which must be chosen carefully according to the temperature solution and its effect on the temperature shift function by avoiding a abrupt change in the computed reduced time. For the presented test problem, the time step size increases with time and temperature, and its maximum value reaches 0.141 approximately 70 times the initial time step size (0.002) at the final time step. This corresponds to a normalized temperature of about 0.874 and a reduced time increment of about 360 times the real time increment. It is also recommended to keep a constant time step size during the early several steps to obtain stable and accurate solutions.

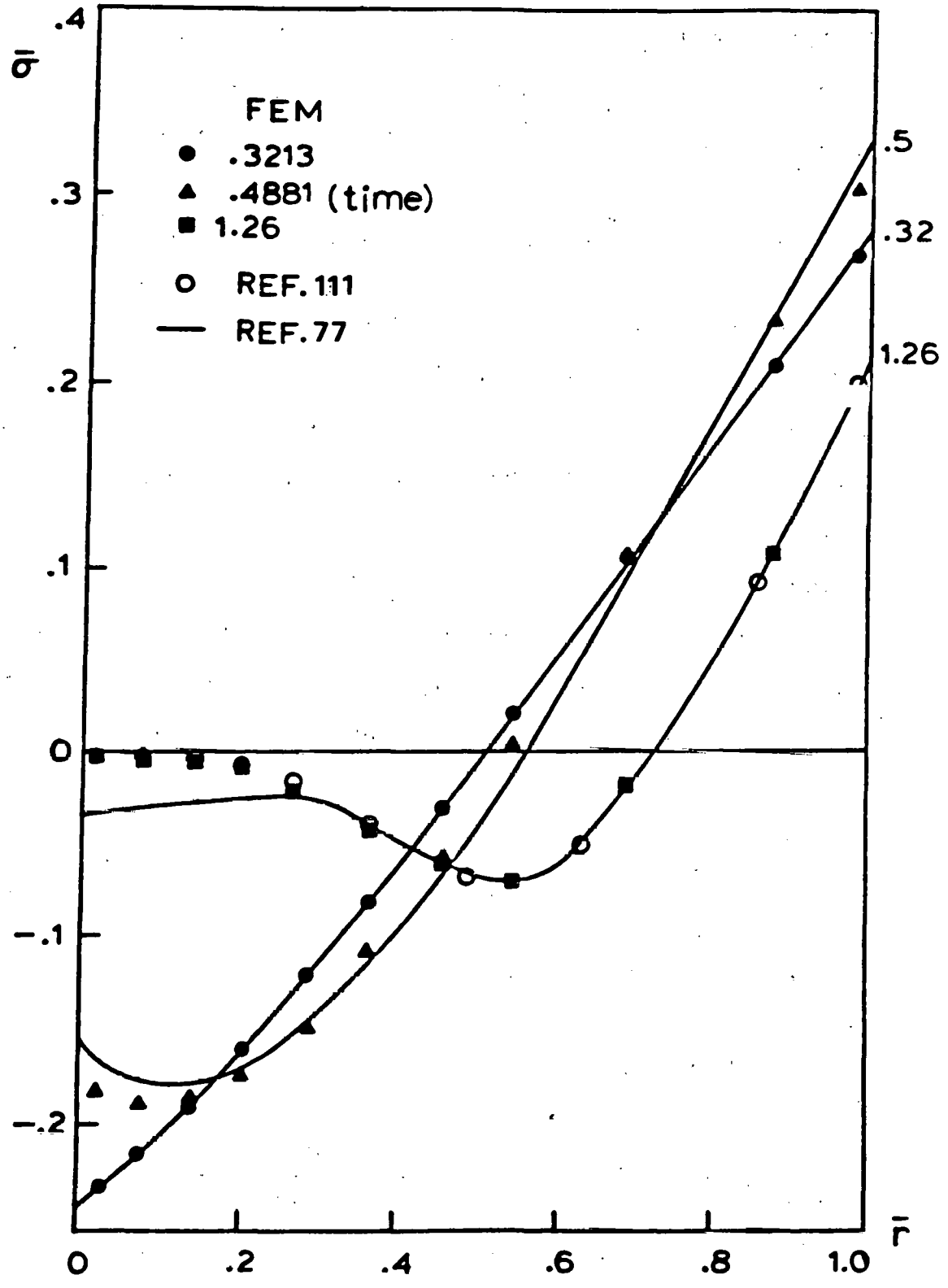

Figure 14: Hoop Stresses for Thermoviscoelastic Test Model with Thermal Expansion (θ=1.0, τ= 0.1)

4.1.4 THERMOVISCOELASTIC RESPONSES OF A SLAB PROBLEM

The presented FEM formulation is applied to evaluate the thermoviscoelastic responses of a slab. This problem has been solved analytically by Muki and Sternberg [85]. A slab of infinite extent with finite thickness 2a is bounded by planes z=±a under the influence of a transient temperature field (Figure 15). The slab displacements are governed by

$$U_x = U_y = 0, \quad U_z = U_z(z,t) \tag{4.10}$$

and the stress field is given by

$$\sigma_{xx} = \sigma_{yy}, \qquad \sigma_{zz}(z,t) = 0 \tag{4.11}$$

The following hypothetical functions for the temperature field and thermorheological properties using a Maxwell fluid model are assumed:

a) Temperature solution:

$$T(z,t) = 1.5 \cdot z \cdot t \qquad (^{\circ}C) \tag{4.12}$$

b) Temperature shift function:

$$X(T) = 1. + 20.0\ T \tag{4.13}$$

c) Relaxation moduli:

$$G_1 = 7.5757 \times 10^4 \, \mathrm{EXP}(-\xi / 0.44)$$
$$G_2 = 5 \times 10^5$$

(dyne/cm^2) (4.14)

with the equivalent creep compliance approximated by

$$J(\xi) = (1 + G_1/3G_2)/3G_1$$
$$= 4.622 \times 10^{-6} + 1.0 \times 10^5$$

(cm^2/dyne) (4.15)

d) Instantaneous elastic constants:

$$\nu_o = (3G_2 - 2G_1)/(6G_2 + 2G_1)\Big|_{\xi=0} = 0.4278$$

$$E_o = (9G_1G_2)/(3G_2 + G_1)\Big|_{\xi=0} = 2.1634 \times 10^5$$

(dyne/cm^2) (4.16)

and the coefficient of thermal expansion is

$$\alpha = 8 \times 10^{-5}$$

(1/°C) (4.17)

The analytical solution is expressed by the following form (cf. ref.[85]):

$$\sigma_{xx} = \frac{-\alpha E}{1-\nu} \, \mathrm{EXP}(-\beta \xi / \tau) \int_o^t \mathrm{EXP}(-\beta / \tau) \frac{\partial T}{\partial t'} dt' \quad (4.18)$$

where

$$\beta = \frac{1+\nu}{3(1-\nu)}$$

and τ_o denotes the initial relaxation time at $T = T_o$. Substitution of the above assumed data (4.12 - 4.17) into eqn.(4.18) yields the explicit form of

$$\sigma_{xx} = -45.37\ Z\ EXP(-1.89(t + 15.\ Z\ t^2)) \cdot \int_o^t EXP(1.89(t' + 15.\ Z\ t'^2))\ dt' \qquad (4.19)$$

The integral of eqn.(4.19) is numerically evaluated by the Romberg's extrapolation method and a small amount of numerical error may be introduced in computing analytical values.

Since the temperature function is selected to be symmetric with respect to the z axis, only half of the slab thickness is modeled by using 16 plane strain finite elements having 34 nodal points as shown in Figure 15. Comparisons between the non-dimensionalized axial stress from the presented FEM formulation and analytical solutions for different elapsed times are shown in Figure 16. The FEM results with $\theta = 1.0$ and $\tau = 0.1$ show good agreement with the analytical results, and the maximum error (4.5%) occurs near the free surface at $t \approx 0.175$, where the maximum compressive stresses are obtained. With increasing time, stress relaxation becomes evident and a uniform low stress value is obtained. Figure 17 shows the stresses at $z/a = 0.0125$, near the middle plane, and the maximum error (4.3%) is noted at the maximum stress when $t \approx 1.0$.

It is also noteworthy that the stresses in the higher temperature region (linearly increasing toward the free surface) relax faster than in the low temperature region (near the middle plane).

The FEM solutions up to t = 2.0 require a solution time of 7.4 seconds and the time increment ranges the initial increment 0.01 to 0.215 with increasing time.

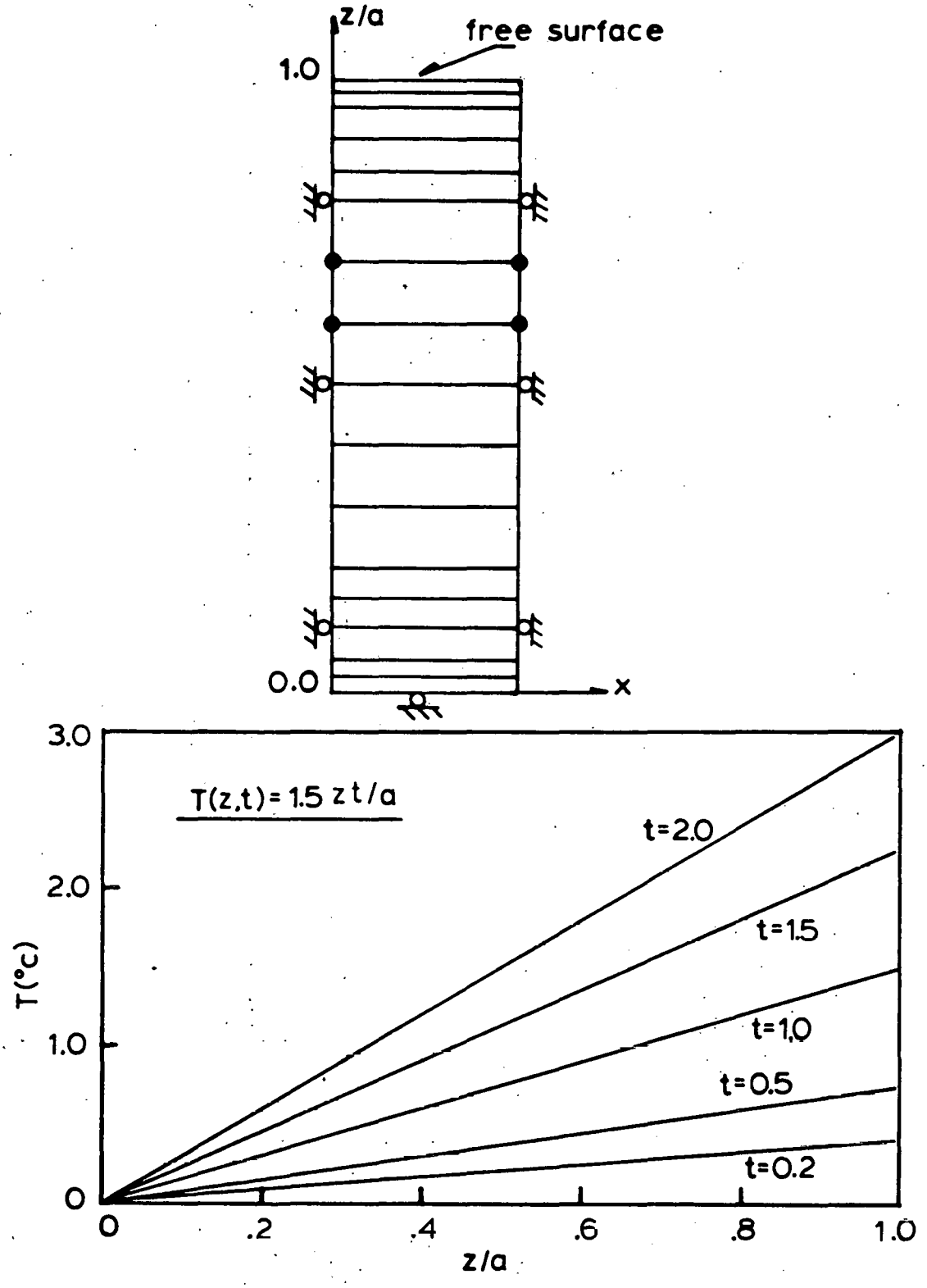

Figure 15: Plane Strain FEM Model and Prescribed Temperature Solutions for A Slab Problem

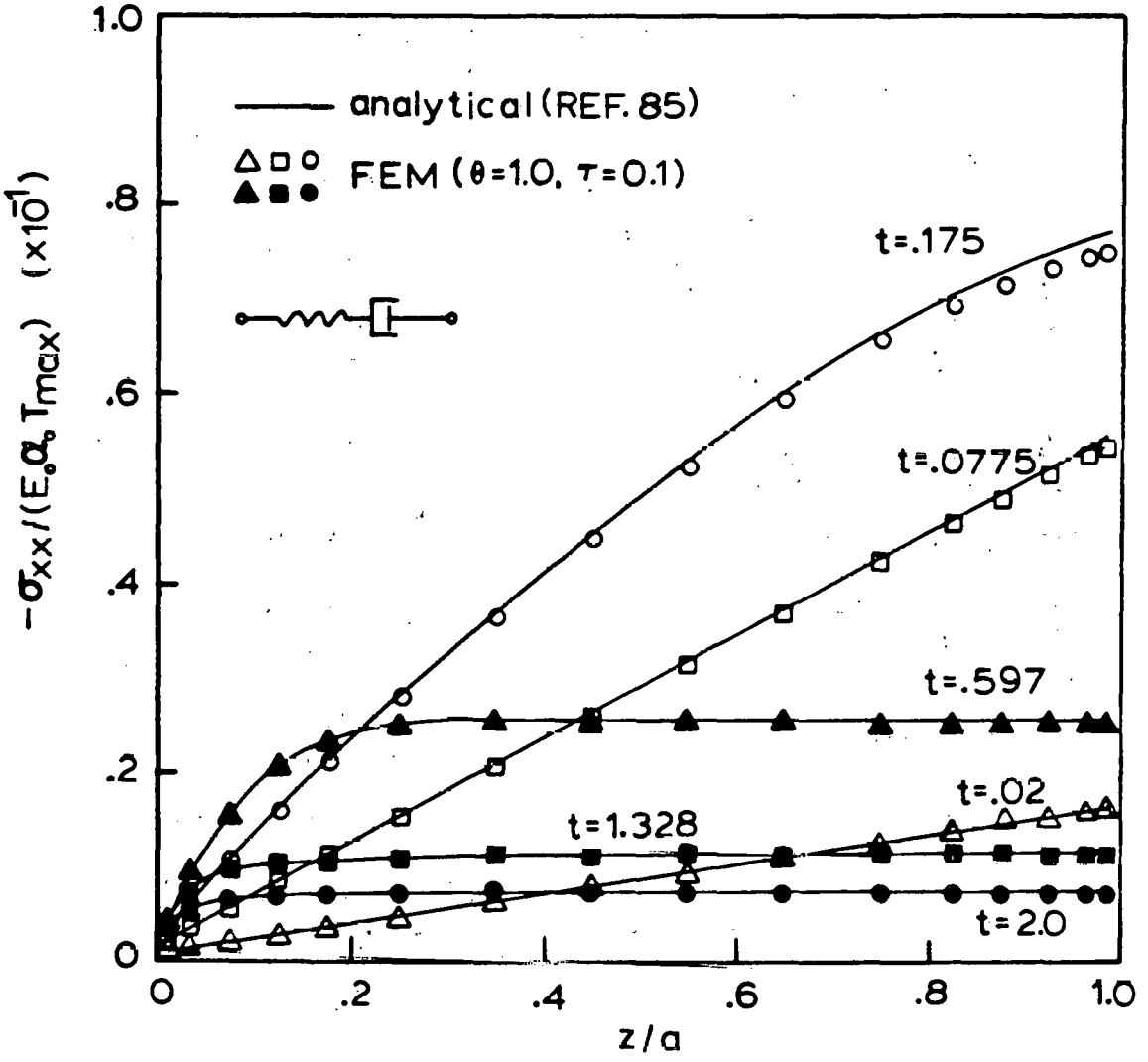

* T_{max}: temperature at t = 2.0 and z/a = 1.0

Figure 16: Axial Stress Comparisons using FEM and Analytical Solutions

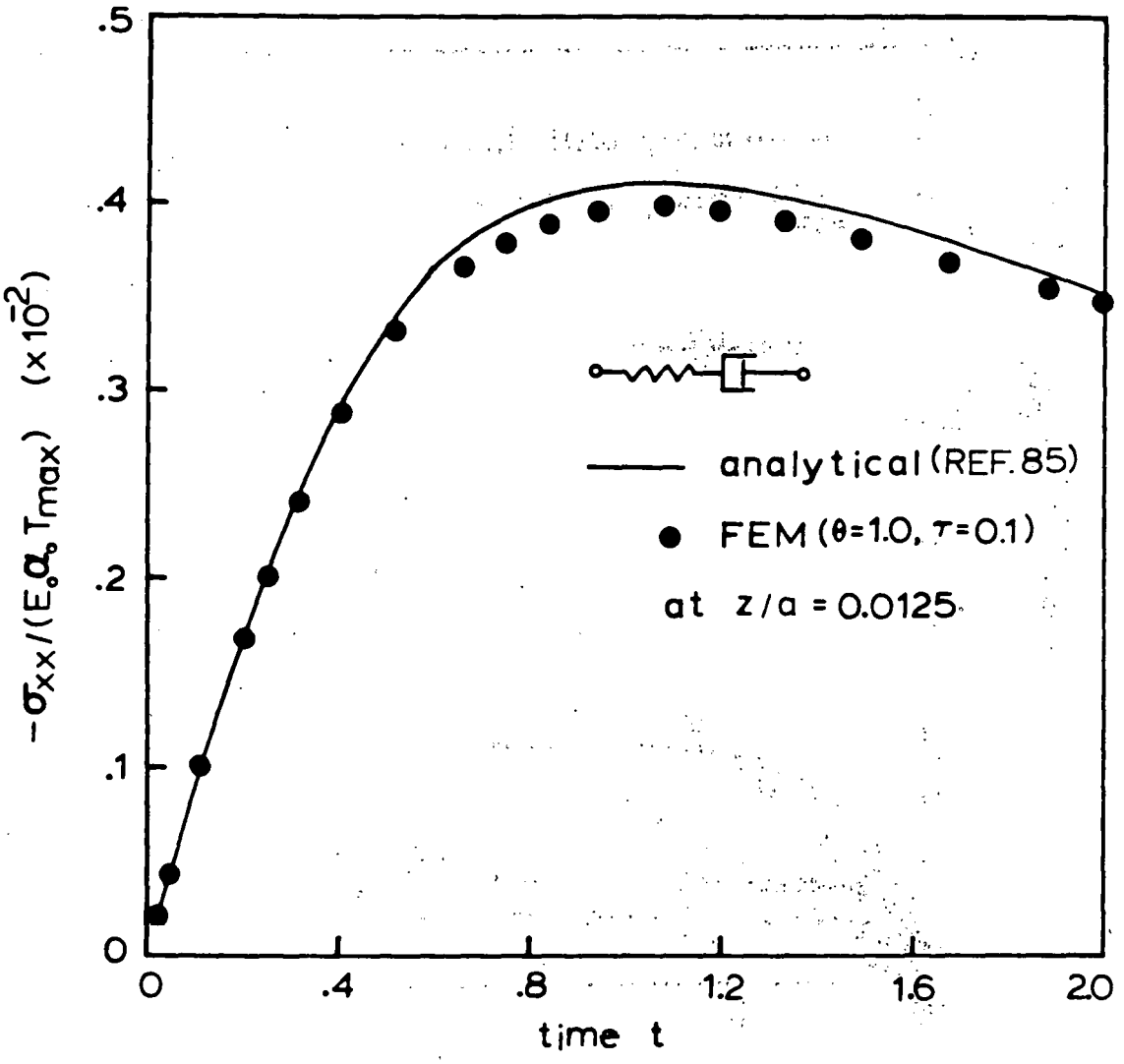

* T_{max}: temperature at t = 2.0 and z/a = 1.0

Figure 17: Comparisons of Axial Stress at z/a = 0.0125

4.2 THERMAL RESPONSES

In the absence of the thermo-mechanical coupling effects, the thermal responses are separated from the mechanical responses. Here, FEM models for the convective-diffusion equation and the transient heat conduction equation are demonstrated. The upwinding scheme presented in Section 3.1 is compared with other numerical schemes for the convective-diffusion model. Results from the two-point recurrence scheme for the transient heat conduction equation is compared with analytical solutions.

4.2.1 CONVECTIVE-DIFFUSION MODEL

To assess the effectiveness of the upwinding scheme described in Section 2.2, a series of numerical results obtained by Hughes and Brooks [56,57] are compared. In each scheme, the finite element descretization procedure is identical except for the treatments of the convective terms. The convective-diffusion equation in consideration is represented by

$$\nabla^2 T - 1\times10^6 \left(\cos\gamma T_{,x} + \sin\gamma T_{,y}\right) = 0 \tag{4.20}$$

where γ is the flow direction measured in the counter-clockwise direction. The boundary conditions and FEM model are shown in Figure 18.

Numerical comparisons are made between the following solutions; i) the standard Galerkin method (G), ii) the quadrature upwind scheme (QU), iii) the streamline upwind (SU1,SU2), iv) the upwind scheme proposed by Heinrich (HU) and v) the exact solution (E). Details of the quadrature

and streamline upwinding schemes are found in Hughes et al [20,56,57]. Denoting each solution by its abbreviation, the different convective skews are shown in Figure 19. It is evident that the solutions G and SU1 suffer from the most serious oscillations while the solution QU experiences significant cross-wind diffusion thereby degrading the solution accuracy. It is also evident that the above schemes suffer more oscillations and cross-wind diffusion in x or y dominant convection than the case of equally distributed convection ($\gamma = 45^{\circ}$). Meanwhile, the solutions SU2 and HU possess the same amount of cross-wind diffusion. However, SU2 tends to show slight oscillations in the vicinity of the region subjected to the steep variation of temperature. For the HU scheme, the results are far better than others in that HU maintains the most consistent accuracy for the different convection angles. The pertubation of upwind parameters, $\bar{\alpha}_i$ and $\bar{\beta}_i$ in HU, does not significantly affect the solutions although the full upwinding scheme has a tendency to cause more cross-wind diffusion than the half upwinding procedure.

It is recommended that the upwind scheme proposed by Heinrich et al [47,48] (HU) be used when a significant amount of convection must be considered in the energy equation, which arises from the flow of hot fluid through a channel. Modeling of moving boundary (with a constant velocity) would be another important case in which the convection term must be considered [21].

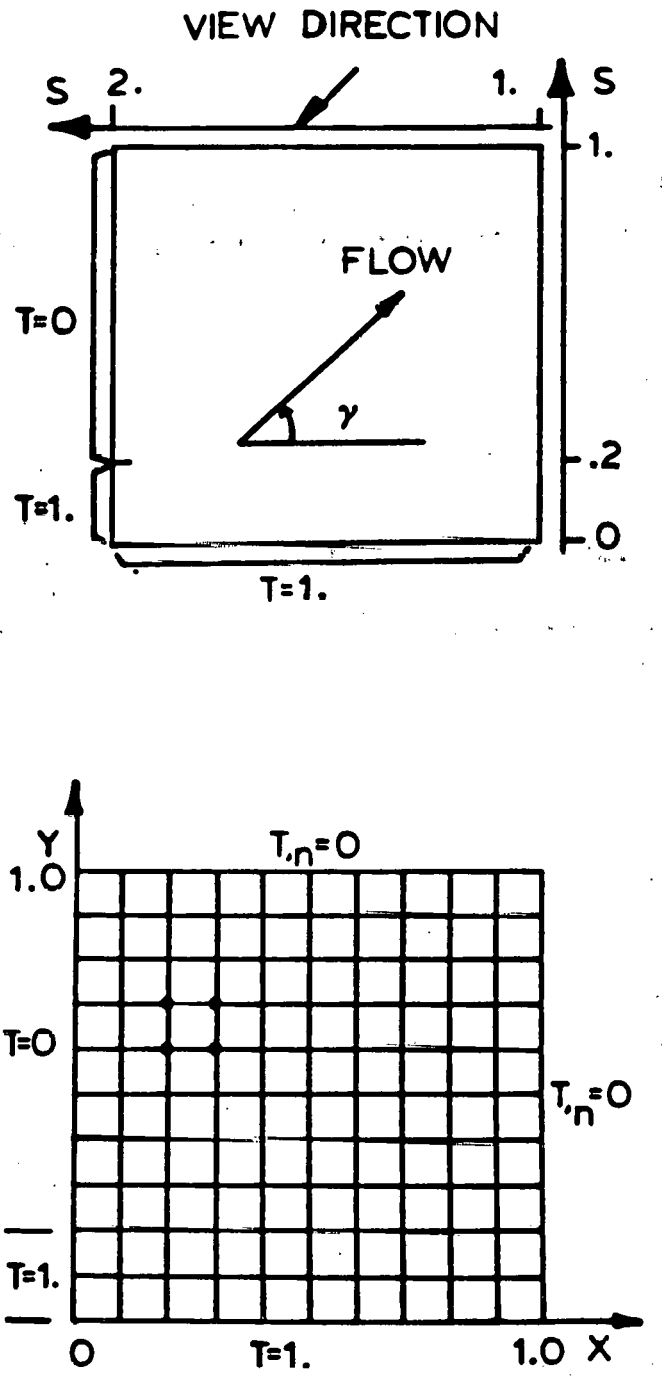

Figure 18: Boundary Conditions and FEM Model for Convective-Diffusion Test Problem

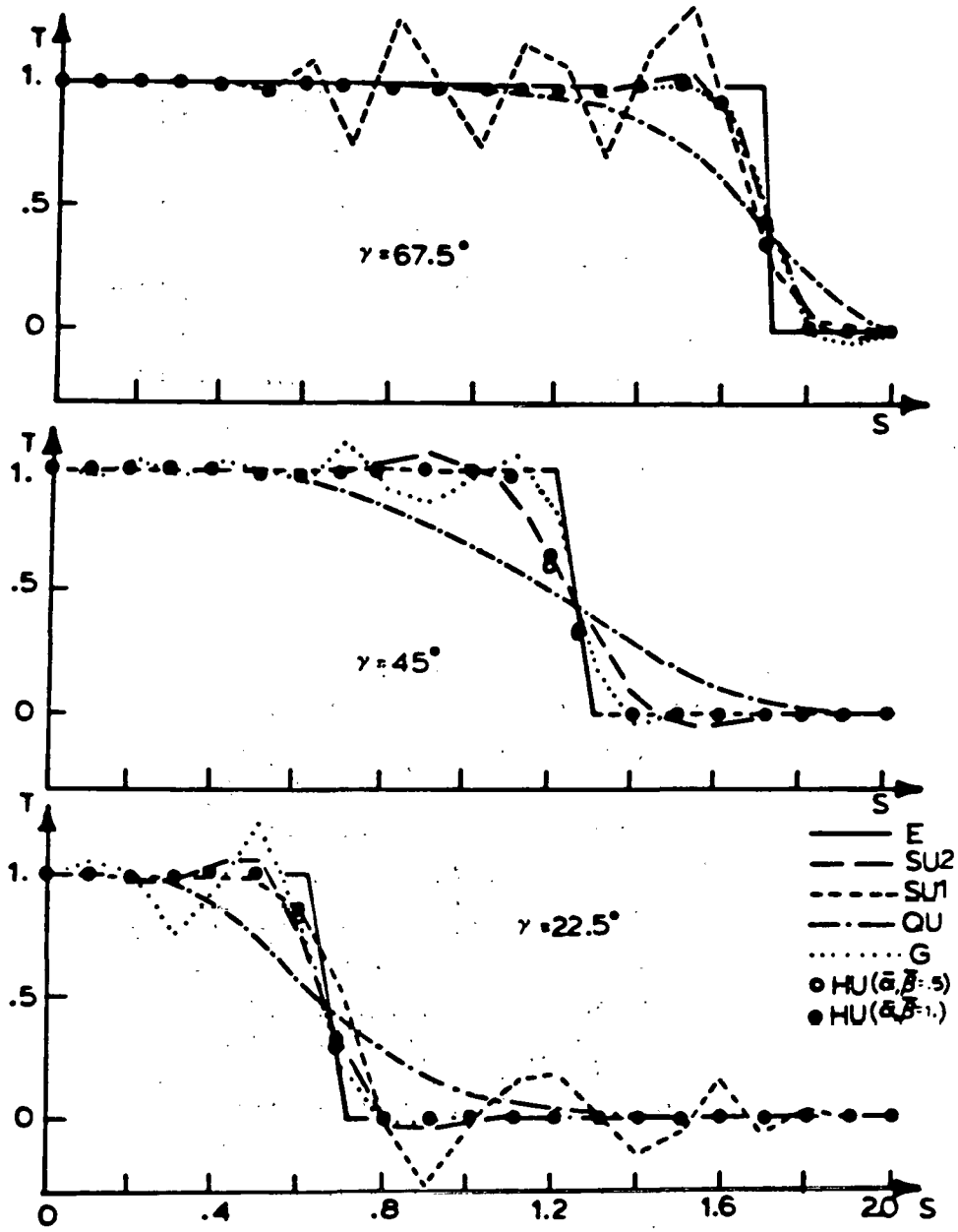

Figure 19: Temperature Profiles along S axis for Convective-Diffusion Test Model

4.2.2 TRANSIENT HEAT CONDUCTION MODEL

The infinitely long circular cylinder subjected to prescribed temperature boundary conditions is considered. The two-point recurrence scheme with the implicit algorithm, described in Chapter III, is employed. The presented FEM solutions are compared with the analytical series solutions [21].

FEM models are shown in Figure 20 wherein the boundary temperature is suddenly raised from zero to a constant temperature $\bar{T}_0 = 1.0$ and is thereafter maintained. The FEM model is generated under the planar and the axisymmetric cases so that the solutions are checked in both cases. A quarter of the circular domain is used by applying the zero temperature gradient conditions on the symmetric boundaries for the planar case. The material constants are normalized to yield

$$\bar{\nabla}^2 \bar{T} = \frac{\partial \bar{T}}{\partial \bar{t}} \tag{4.21}$$

The constant time step size 0.0025 according to eqn.(3.15) is used for both $\bar{\theta} = 0.5$ and 1.0. Figure 21 shows a good agreement between the FEM and analytical solutions. It is observed that the time step size selected from eqn.(3.15) yields stable and accurate results so that the temperature dependent properties can be favorably incorporated.

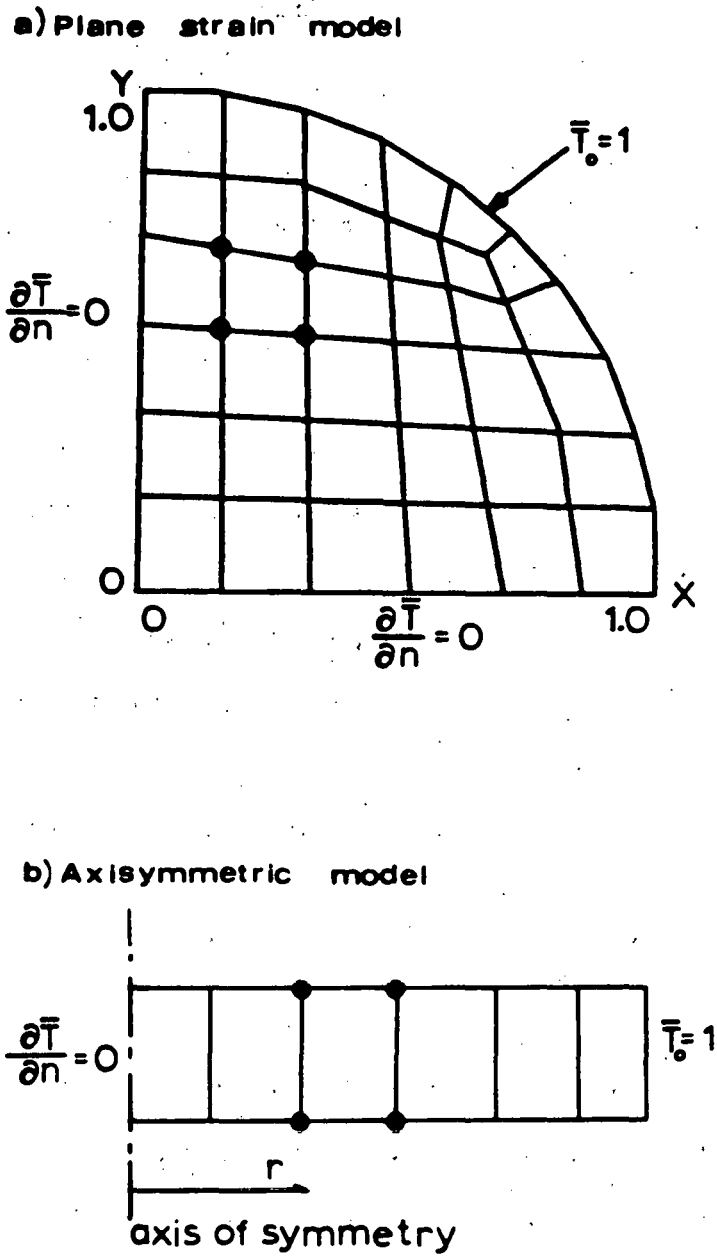

Figure 20: FEM Models for Transient Heat Conduction Test Problem

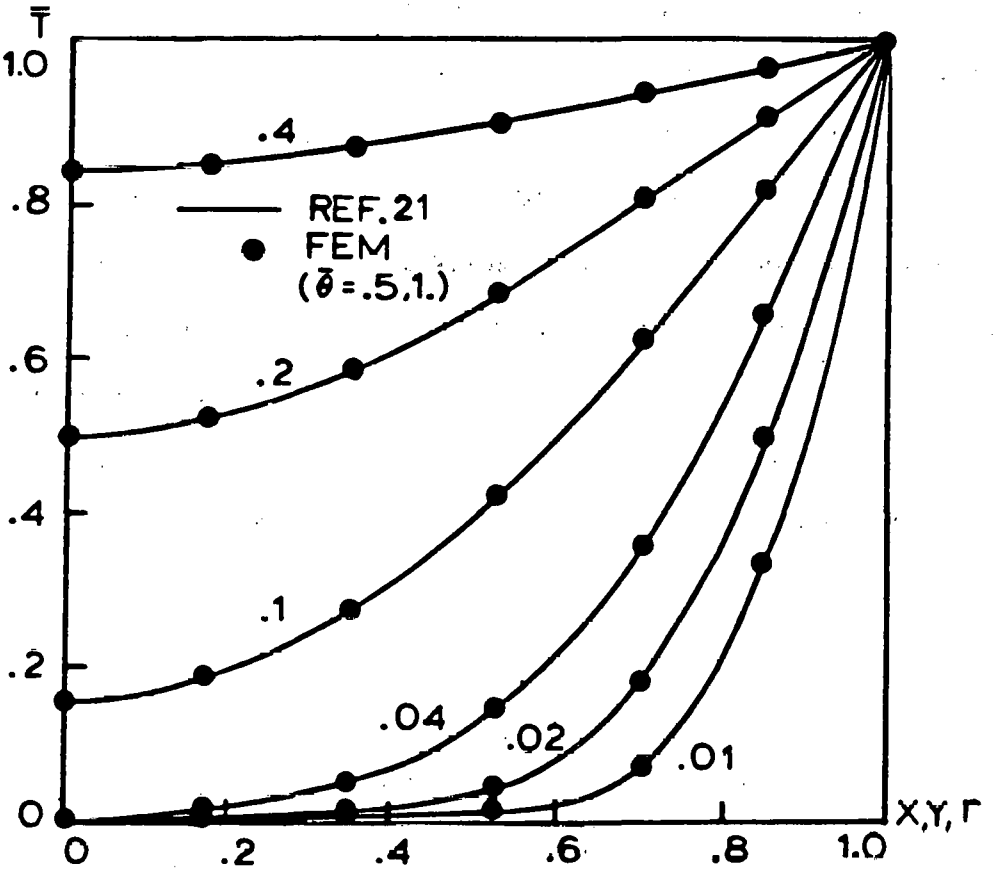

Note: Temperature solutions for the plane strain and axisymmetric cases coincide

Figure 21: Transient Temperature Profiles of FEM and Analytical Solutions

4.3 THERMOELASTIC FRACTURE RESPONSES

Solutions associated with the FEM models for the thermoelastic line crack problems described in Appendix A are demonstrated. The steady-state temperature, displacement and stress fields in a homogeneous, isotropic, elastic medium with a line crack are obtained. The temperature distribution in the body with the quasi-static uncoupled thermoelastic assumption, is determined independently. The selected material properties of rock for the fracture analysis are assumed to be independent of temperature and are listed in Table 2. The FEM results are compared with the analytical solutions [73,123,127] in terms of the stress intensity factors for mode I and mode II cases. The stress intensity factors obtained by two- and three-point Gaussian quadrature rule are also compared.

Properties	Symbol	Unit	
Thermal Conductivity	k	W/m °C	2.244
Coeff. of Linear Thermal Expansion	α	10^{-6}/ °C	2.5
Elastic Modulus	E	10^{4}MPa	1.378
Poisson's Ratio	ν		0.12

Table 2

Material Properties for Thermoelastic Line Crack Test Model

4.3.1 MODE I CASE

The prescribed constant temperature on the upper and the lower crack surface are assumed to be T_o and zero at infinity i.e.

$$T(x,y) = T_o \qquad \text{for} \qquad y = 0,\ |x| < a$$

$$\frac{\partial T}{\partial y} = 0 \qquad \text{for} \qquad y = 0,\ |x| > a$$

$$T(x,y) = 0 \qquad \text{at} \qquad \text{infinity} \tag{4.22}$$

The FEM model is shown in Figure 22 by taking a quarter of the entire domain due to the symmetry. The chosen domain size is 20 times the crack length. The degenerate singular elements are used around the crack tip and the eight-noded isoparametric elements are employed for the rest of the domain. The normalized temperature and the maximum principal stress distributions are shown in Figure 23.a and 23.b, respectively. The stress intensity factor K_I is non-dimensionalized to yield

$$\bar{K}_I = K_I/(\alpha G T_o \sqrt{\pi a}) \tag{4.23}$$

and $\bar{K}_I$ obtained by the two-point (2x2) and three-point (3x3) quadrature rule are 1.2987 and 1.3067, respectively and are within 2.5% error when compared to the analytical value of 1.273 (cf. eqn.(A.9)). It is observed that effects of the number of integration points on the singular elements are insignificant for both temperature and stress fields although the $\bar{K}_I$ value obtained from the two-point rule is slightly more accurate than the one from three-point rule.

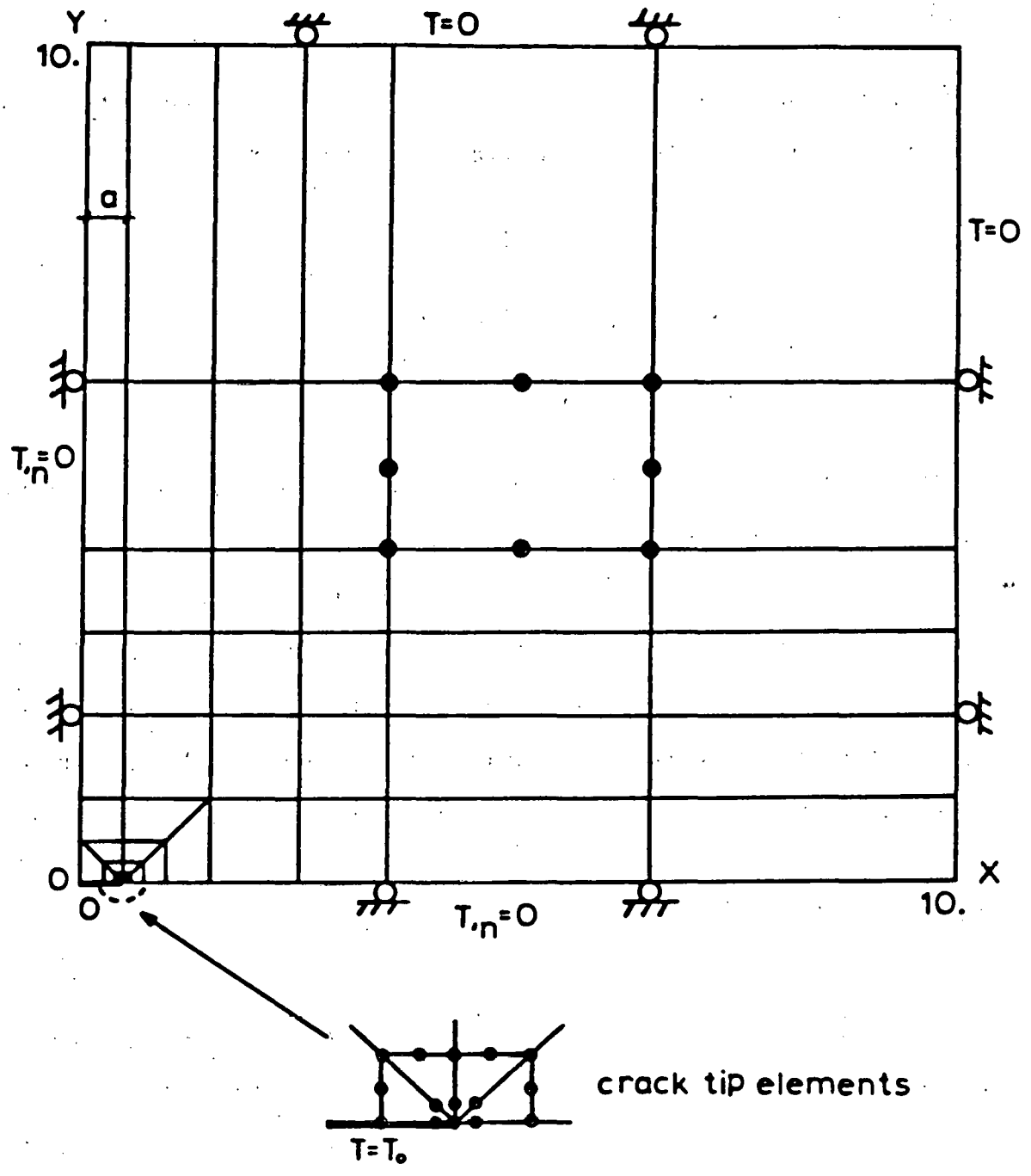

Figure 22: FEM Model for Mode I Case in Thermoelastic Line Crack Test Problem

a) Temperature distribution

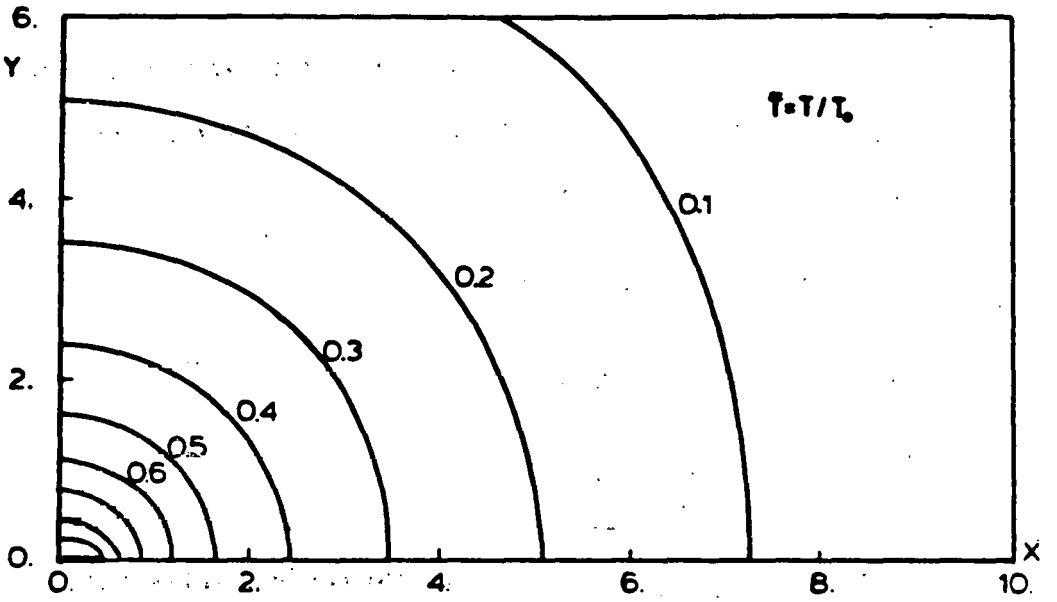

b) Maximum principal stresses

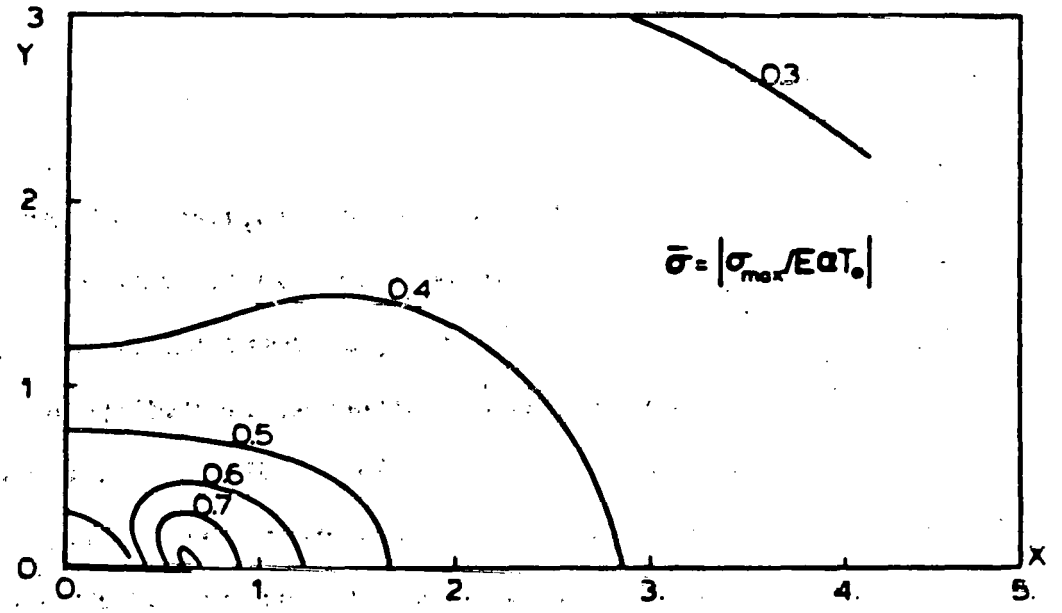

Figure 23: Temperature and Maximum Principal Stress Contours for Mode I Case

4.3.2 MODE II CASE

A line crack of length 2a is situated in an infinite plane subjected to a constant temperature gradient at the surface of the crack. The boundary conditions at y = 0 are

$$\frac{\partial T}{\partial y} = C = \text{constant} \quad \text{for } |x| < a$$

$$T(x,y) = 0 \quad \text{for } |x| > a$$

$$T(x,y) = 0 \quad \text{at infinity} \tag{4.24}$$

The domain size of FEM model is approximately 15 times the crack length as shown in Figure 24. The non-dimensionalized stress intensity factor $\bar{K}_{II}$ is expressed by

$$\bar{K}_{II} = K_{II}/(\alpha GC \sqrt{\pi}\, a^{3/2}) \tag{4.25}$$

FEM results of the stress intensity factor $\bar{K}_{II}$ are 0.643 for the two-point rule and 0.669 for the three-point rule while the analytical value is 0.636 (cf. eqn.(A.10)). It is again noted that the singular effects near the crack tip is slightly better represented by the two-point rule for both temperature and stress fields. Since the thermal and mechanical responses are symmetric with respect to x and y axes, the normalized temperature and stress distributions for a quadrant are shown in Figure 25.a and 25.b, respectively.

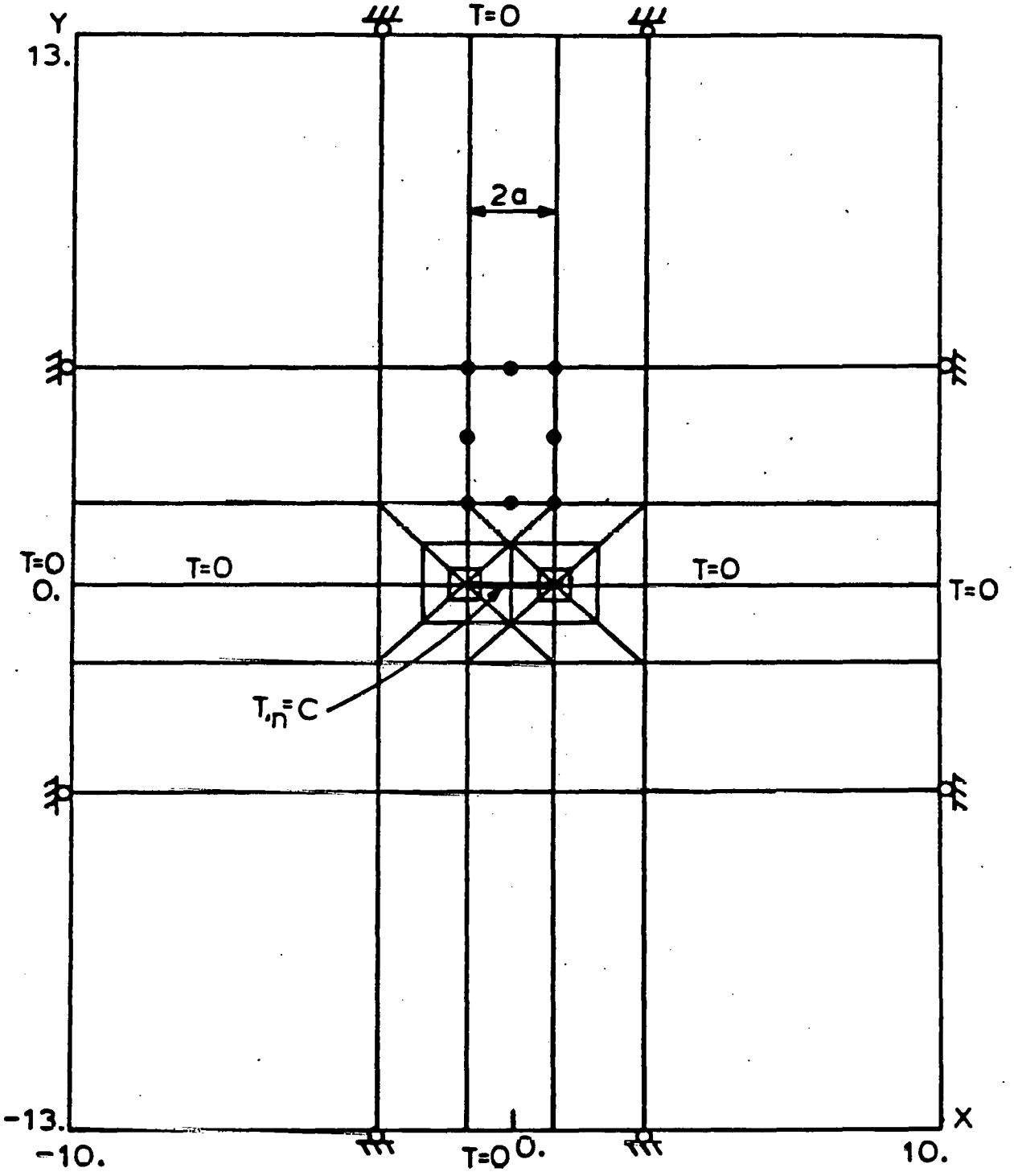

Figure 24: FEM Model for Mode II Case in Thermoelastic Line Crack Test Problem

a) Temperature distribution

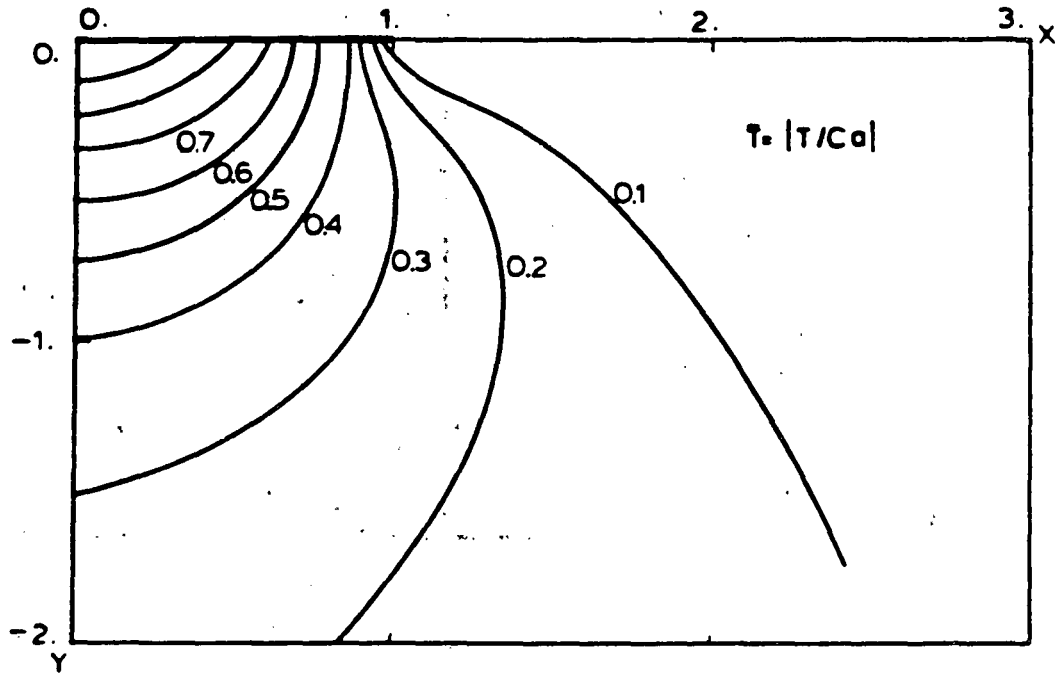

b) Maximum principal stresses

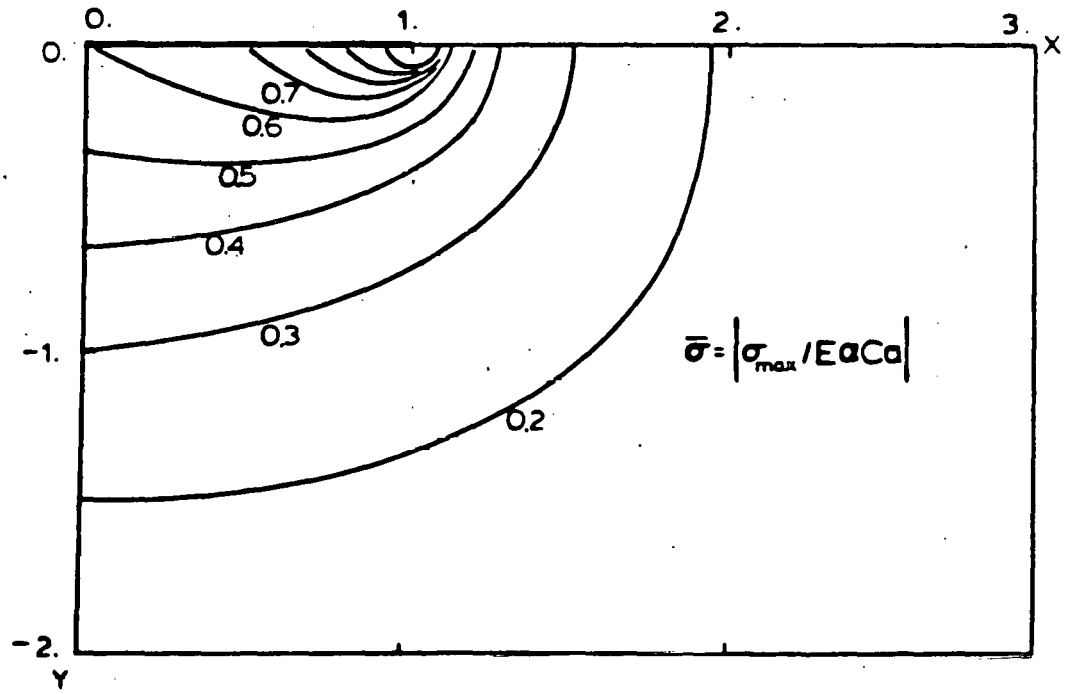

Figure 25: Temperature and Maximum Principal Stress Contours for Mode II Case

Chapter V

FIELD APPLICATIONS

In the formulation of design criteria for rock mechanics problems, the effects of time and temperature can be of considerable concern. In particular, problems involving elevated temperature such as underground coal conversion (UCC) process and nuclear waste disposal, the strong time and temperature dependence of geological materials may pose a potential hazard to process mechanisms and the host environment. In this chapter, the UCC post-burn response is simulated by using the preceding thermoviscoelastic and thermoelastic FEM model formulations with emphasis on the key variables involving temperature, stress, failure zones, and surface subsidence. A similar approach is also applied to possible nuclear waste disposal model in a low permeability salt medium.

5.1 UCC POST-BURN MODEL

Underground coal conversion has gained attention as a vital source of alternate energy in the U.S.A. since the early 70's energy crisis. As an innovative and efficient extraction technique, in-situ gasification of coal reserves has appeared to be a viable avenue for retrieving combustible gases from the carbon content of burning coal. The development of underground coal gasification (UCG) and basic principles are reviewed by Gregg and Olness [42] and Skafa [102]. Descriptions of various approaches and their mathematical modeling, laboratory and field results

have been presented mainly at the Annual Symposia on Underground Coal Conversion [117,118,119,120,121,122].

The typical UCC process is characterized in three main stages; namely, pre-burn, active-burn, and post-burn stages. The pre-burn stage includes drilling, fracturing and linking processes to enhance the permeability between wells. When the required permeability is established, gasification of coal is conducted by supplying gaseous oxidizing agents to the prepared coal seam. During the active-burn stage, the gasification chamber is expanded through the coal seam while the combustible gases are retrieved at the surface. In the post-burn stage, the supply of the oxidizing agents is stopped and the hot cavity gradually cools with time and has a potential for subsequent roof collapse and subsidence. For the sustained reliability of the UCC process, major structural concerns are placed on the control of in-situ gasification process mainly in the aspect of fracture mechanics, heat transfer and thermo-mechanical responses. In addition, the ground movement, especially the surface subsidence and the growth of gasification chamber in active and post-burn stages are the major problem areas associated with UCC (Figure 26). Structural finite element model investigations of various UCC cavity configurations have been conducted by Advani et al [1] and Thompson et al [112]. Closed form solutions for thermally stressed ellipsoidal cavities have been obtained by Advani et al [2]. Jegbefume and Thompson [62] have conducted a study on roof collapse and subsidence treating only the overburden rock as a linear viscoelastic material. Advani et al [3] have recently introduced FEM models which can be directly applicable to UCC field simmulations for active and post-burn stages. This includes

the moving boundary problem for the active-burn stage and the thermoviscoelastic modeling for the post-burn stage to predict the surface subsidence and the gasification chamber configuration. Other relevant research includes studies by Langland and Trent [71], Sutherland et al [107] and Turner et al [116].

In this section, the post-burn stage of Hoe Creek II site is simulated by use of the thermoviscoelastic FEM model presented in this study with temperature-dependent material properties. Thermorheological representations of coal and rock and detailed modeling procedures are presented in the appropriate sections.

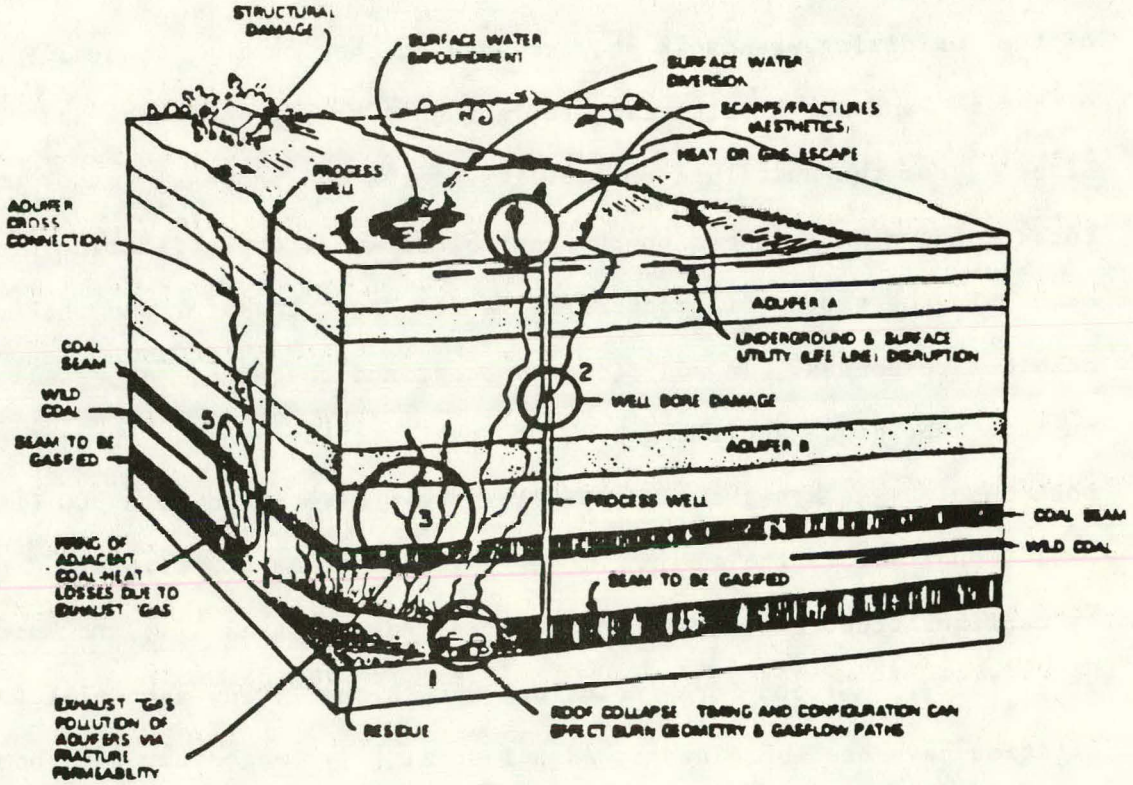

Figure 26: Typical UCC Site and Potential Environmental Impacts

5.1.1 THERMO-MECHANICAL AND RHEOLOGICAL BEHAVIOR OF COAL

Major laboratory tests for eastern bituminous coal at elevated temperatures have been conducted by Singer and Tye [101] and Shoemaker [99]. Based on the above references, Min [81] has presented a general thermal property trend for coal. This provides a basis for possible parametric studies and modifications of UCC models. Here, similar trends of the thermal and mechanical properties are adopted and associated nominal values are selected depending on a specific UCC site. Figure 27 illustrates normalized thermal trends for thermal conductivity, heat capacity, mass density, linear coefficient of thermal expansion, tensile strength, and compressive strength.

For the viscoelastic properties of coal, Fitzgerald [35] and Waters [124] have examined coals at the stage of carbonization and thermal softening. Compressive creep tests in the temperature range between 200°C and 370°C have been conducted by Sanada and Honda [93] revealing that creep of coal can be represented by a simple rheological model. Shoemaker [99] has presented directional viscoelastic properties of the Pittsburgh coal at elevated temperatures ranging from 24°C to 343°C. It is reported that the Pittsburgh coal can be treated as a thermorheologically simple material [99]. Lin [75] has adopted Shoemaker's data for the Pittsburgh coal and presented analytical creep functions using a four parameter fluid model(Burger's model). Due to insufficient creep data at elevated temperatures for field experimetal sites, the creep data for the four parameter fluid model of the Pittsburgh coal is adopted in the present UCC simulation. The selected trends of the uniaxial

creep compliance and the temperature shift function are shown in Figure 28. The creep compliance of Pittsburgh coal is calibrated according to available experimental data for Hoe creek II site [62,80] and the same temperature shift function is used. The appropriate numerical expressions are

$$J(\xi) = 1.1727\times10^{-6} + 7.1699\times10^{-26}\xi - 1.1621\times10^{-6}\ EXP(-2.\times10^{-19}\xi) \qquad (1/Pa) \tag{5.1}$$

and

$$\chi(T) = 1/a_T = \{180.6\ EXP(-2.2089 - 1.24\times10^{-1}T - 1.9661\times10^{-5}T^2)\}^{-1} \tag{5.2}$$

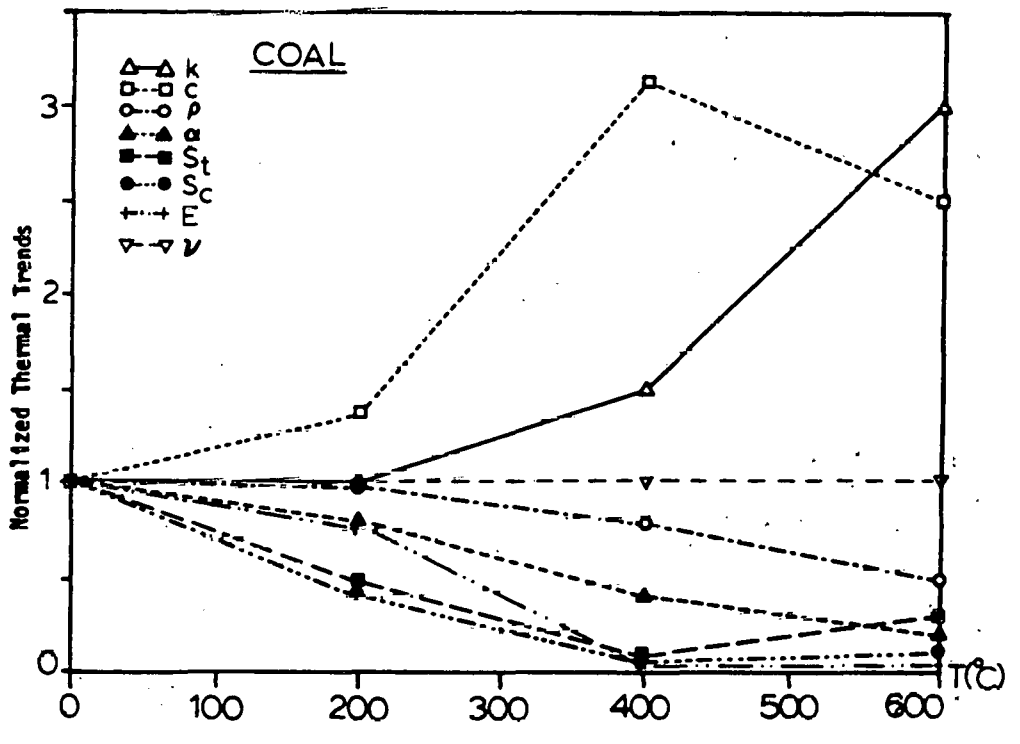

Figure 27: Normalized Thermal Trends for Coal Properties

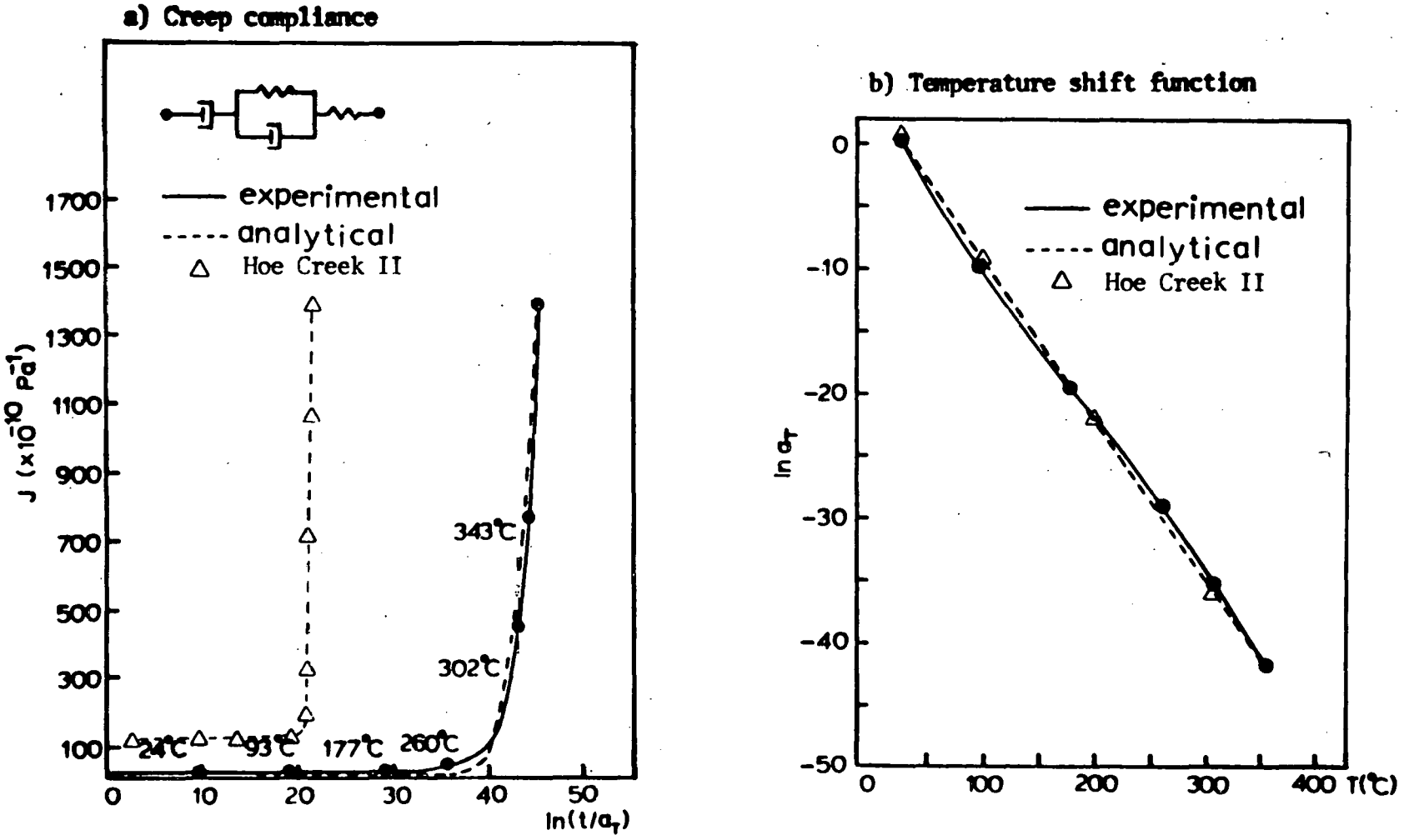

Figure 28: Thermal Trends of Creep Compliance and Temperature Shift Function of Coal (ref. 75)

5.1.2 THERMO-MECHANICAL AND RHEOLOGICAL BEHAVIOR OF ROCK

Extensive references on thermal and mechanical properties of different rock types can be found in Lama and Vutukuri [69]. The thermal trends for most of rock materials are known to be similar [81]. Here, based on the laboratory tests for oil shale [31], sandstone and limestone [17], and granite rocks [50], the selected general trends for thermal and mechanical properties are presented in Figure 29. The normalized thermal trends of rock materials are again calibrated by choosing proper nominal values for a specific UCC experimental site.

For the thermorheological properties of rock, Misra and Murrel [82] has conducted creep tests for a number of different rocks(dolomite, sandstone, marble) up to 750 °C under the uniaxial loading. It is reported that the creep strain is proportional to the logarithm of the time, stress and temperature at the low temperature range but increases exponentially as temperature increases. The analytical model for the rheological behavior of the dark gray shale associated with the UCC process has been proposed by Lin [75] using the creep data conducted by Gmeindl [40]. Figure 30 shows the creep compliance of the four parameter fluid model and the temperature shift function for the dark gray shale. These thermorheological properties are again adopted and scaled for the associated rock materials(siltstones) for the Hoe Creek II site. The selected thermorheological properties are

$$J(\xi) = 5.6394\times10^{-8} + 3.2603\times10^{-21}\xi - 4.6042\times10^{-8}\,EXP(-1\times10^{-9}\xi) \quad (1/Pa) \qquad (5.3)$$

and

$$x(T) = 1/a_T = \{4.795\ EXP(-2.297 + 0.118T - 5.919x10^{-4}T^2)\}^{-1} \qquad (5.4)$$

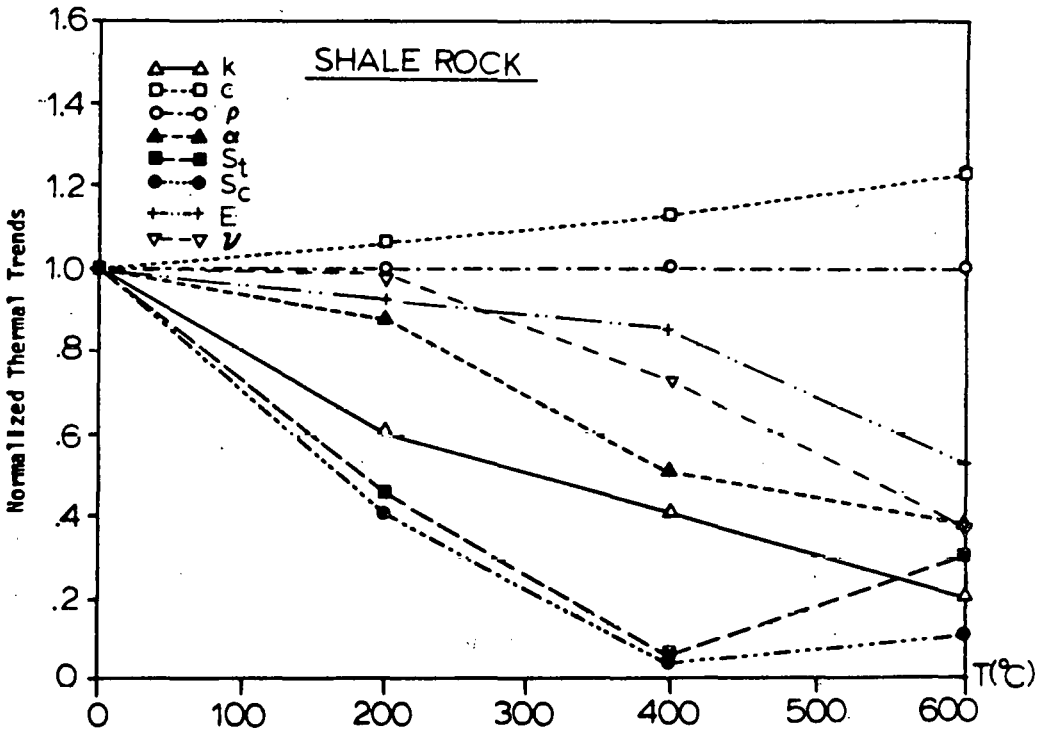

Figure 29: Normalized Thermal Trends for Rock Properties

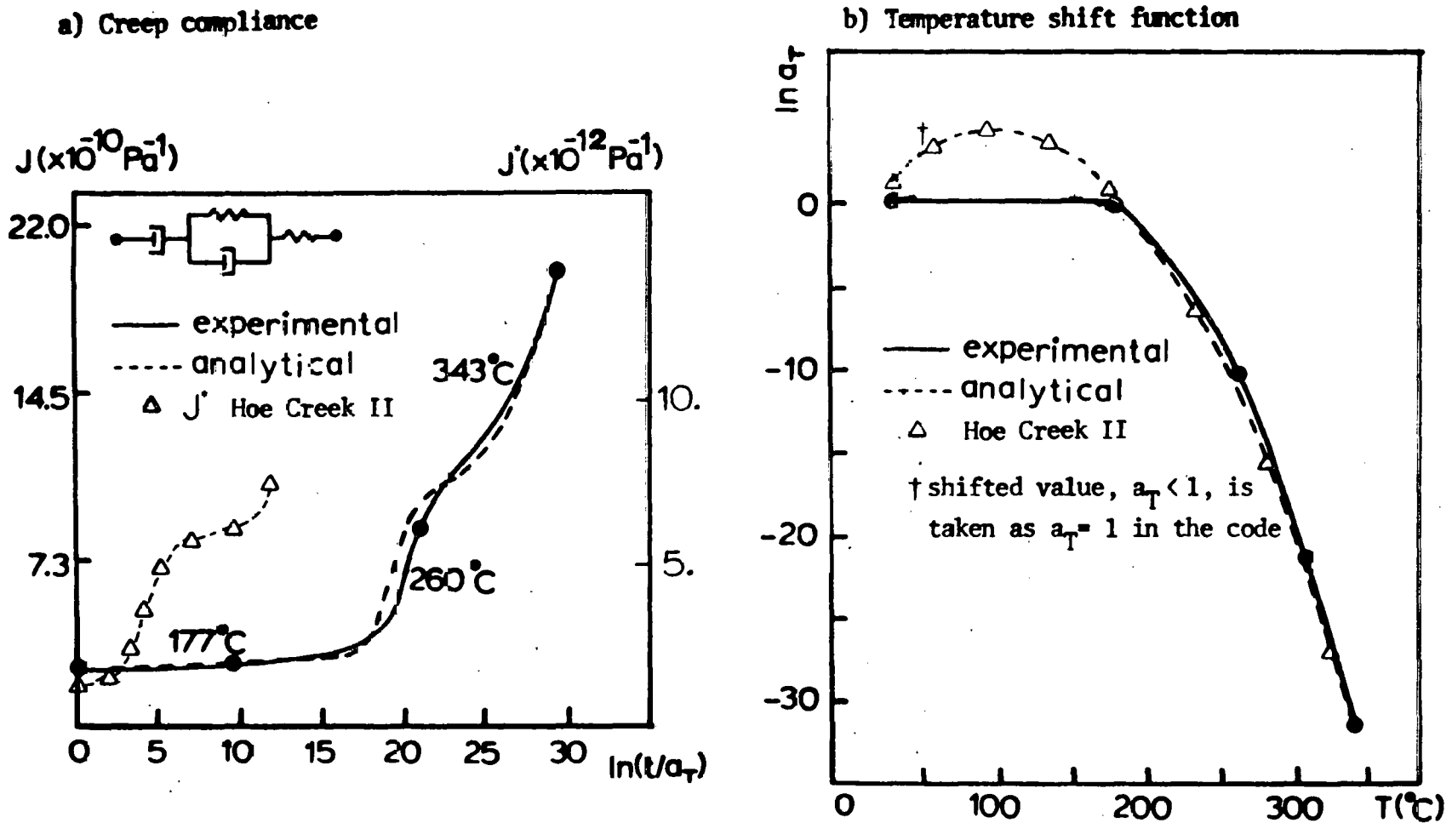

Figure 30: Thermal Trends of Creep Compliance and Temperature Shift Function of Shale (ref. 75)

5.1.3 POST-BURN MODELING PROCEDURE

Two issues are of primary concern in the simulation of the UCC post-burn process; namely the heating and cooling of the gasification chamber and the structural response of the chamber configuration. To simulate the heating and cooling effects, a time-dependent temperature condition on the chamber boundary is used for the thermal responses. Since the thermally-active zone is reported to be confined in the vicinity of the chamber boundary and it is preceded by failures during the active-burn stage [81], the thermal responses in the post-burn process are independently simulated. The assumed time-dependent chamber temerature is as follows;

a) The chamber temperature increases linearly from the ambient temperature(20°C) to the combustion temperature(600°C) within a short time interval at the early stage.

b) The chamber temperature remains constant at the combustion temperature for a certain time interval and starts to decrease slowly toward the ambient temperature. This simulates the natural cooling effect on the gasification chamber due to heat loss and water influx.

The choice of the temperature boundary condition is based on observations of the UCC experimental results. It also avoids numerical oscillations caused by abrupt changes in the boundary temperature at the beginning stage.

For the chamber configuration shown in Figure 31, the two-dimensional failure theories presented in Appendix A are incorporated in the model

to define the failed zones. Although the transient chamber configurations fall in the category of moving boundary value problems, a crude, yet economical, finite element model can be obtained by assuming that the failed elements are still attatched to the adjacent elements but do not show any structural strength. This assumption allows us to use the same mesh configuration during the entire solution procedure and simply discard the load increment for the failed elements at each solution step. During the entire simulation, the temperature-dependent thermal and mechanical properties are also incorporated.

5.1.4 FEM MODEL AND RESULTS FOR HOE CREEK II SITE

The selected plane strain FEM model for the Hoe Creek II site is simulated for 10 years post-burn. The prescribed chamber temperature and boundary conditions along with the idealized stratigraphy are shown in Figure 31. The selected chamber configuration is based on the field experiment conducted by LLNL [4]. Due to the symmetry of the initial chamber shape and the geological structure, the FEM model dimensions are selected to be 60m horizontal by 70m vertical. The 4-node quadrilateral isoparametric element is used throughout. The mesh discretization shown in Figure 31 has 267 elements and 309 nodal points. The geological materials at Hoe Creek II site have been reported to be very weak and the nominal values for thermal and mechanical properties listed in Table 3 are selected from sample data [80]. The rock materials at the top and bottom(seam 1,6) are treated as elastic materials while Felix 1 and 2(seam 3,5) and siltstones(seam 2,4) are represented by the thermorheological model for coal and rock respectively as described in Section 5.1.2 and 5.1.3.

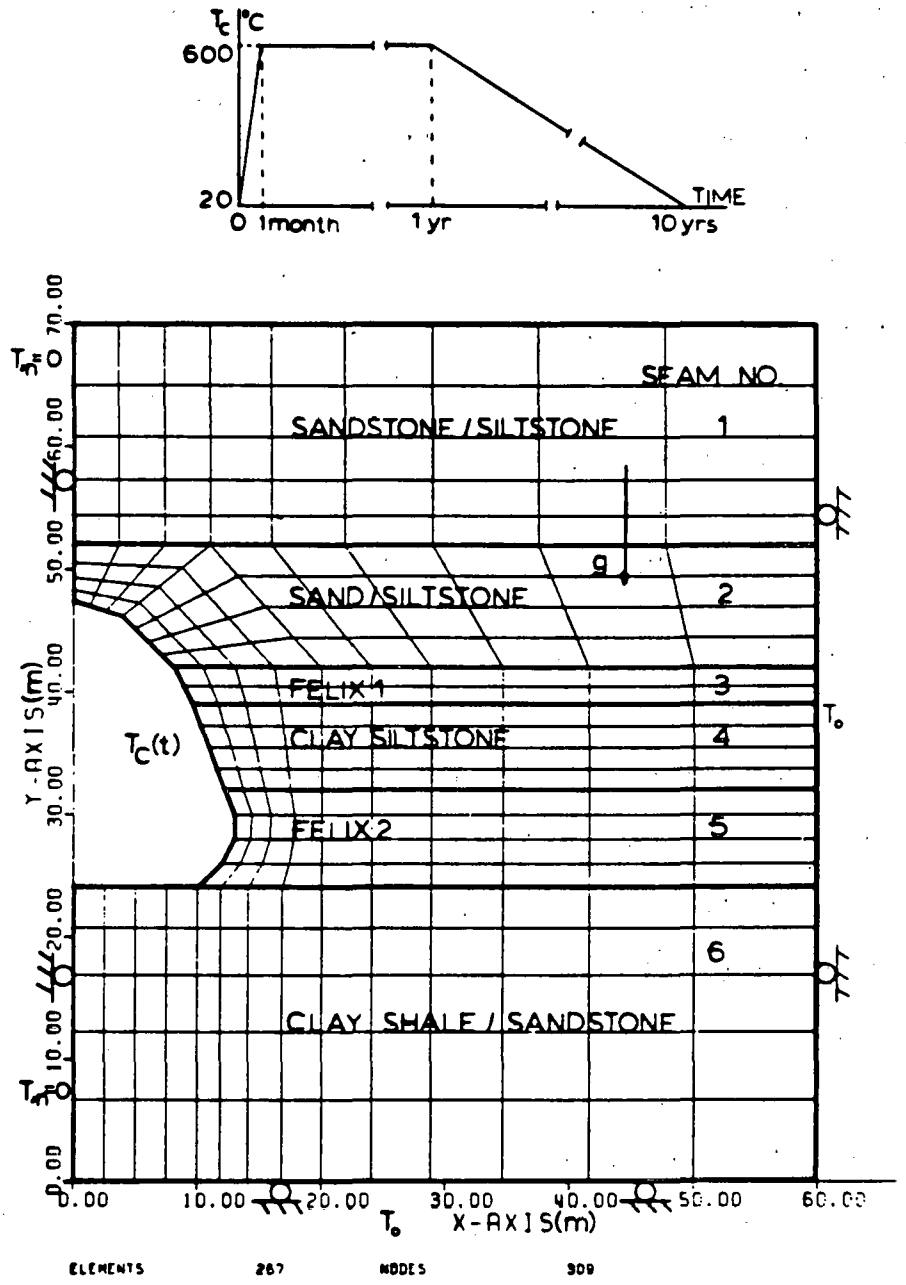

Figure 31: Two-Diemsional FEM Model, Stratigraphy, and Boundary Conditions for Hoe Creek II Post-Burn Simulation

Properties	Symbol	Unit	Seam No.					
			1	2*	3*	4*	5*	6
Mass Density	ρ	kg/m^3	2374.0	2259.0	1300.0	2259.0	1300.0	2323.0
Thermal Conductivity	k	W/m°C	2.0	2.0	.27	2.0	.27	2.0
Heat Capacity	C	J/kg°C	900.0	900.0	800.0	900.0	800.0	600.0
Coeff. of Linear Thermal Expansion	α	10^{-6}/°C	10.0	10.0	5.0	10.0	5.0	10.0
Tensile Strength	S_t	KPa	73.0	90.0	200.0	90.0	200.0	6000.0
Compressive Strength	S_c	MPa	-7.3	-6.5	-10.0	-6.5	-10.0	-30.0
Elastic Modulus	E	MPa	42.0	96.6*	94.*	96.6*	94.*	90.0
Poisson's Ratio	ν		.38	.37*	.32*	.37*	.32*	.37
Coeff. of Internal Friction	μ_f		1.0	1.0	1.0	1.0	1.0	1.0

* designates viscoelastic material and associated material properties are instantaneous values.

Table 3

Selected Nominal Values for Material Properties
at Hoe Creek II Site

The computed temperature profiles at different elapsed times are presented in Figure 32. A constant time step size, 0.04 year, resulting 250 transient steps for 10 years, is utilized with about 2 minutes 44 seconds of CPU time. A larger time step size can be used to reduce the number of time steps and the CPU time after the initial stage. However, the same time step size is used for the entire duration to provide a complete characterization of the viscoelastic responses. Slow thermal propagation, limited to the vicinity of the chamber boundary, is evident for the first 2 years. However, the solutions at 4.8 and 10 years show further temperature propagation and different characteristics in the thermal pattern as the chamber is cooled down to the ambient temperature. At 10 years elapsed time, the maximum temperature found to be approximately 115°C about 7m outside of the chamber boundary and steadly approaches the ambient temperature.

Figure 33 illustrates the thermo-mechanical responses characterized by the principal stress redistributions, uniform reference subsidence (S_o) due to the cavity, maximum differential surface subsidence ($\bar{S}^v_{max} = S^v_{max} - S_o$) and failed zones associated with the defined chamber configuration. Comparisons of the progressive failure zones and maximum surface subsidence, $\bar{S}^v_{max}$ and $\bar{S}^E_{max}$, for thermoviscoelastic and thermoelastic cases, respectively are also presented. For the thermoviscoelastic response evaluation, the instantaneous elastic responses are obtained from the gravitational loading which results in compressive stresses at the bottom of the base rock(seam 6). The steep increase in temperature at the earlier stages results in high stresses causing rapid element failures around the chamber boundary. With time, these high com-

pressive stresses are reduced for coal and siltstones while the elastic layer stresses(seam 1,6) are almost uniform. This behavior illustrates the effect of material softening due to the time-temperature dependence. Major shear failures occur in siltstones(seam 2,4) indicating potential roof collapse in the upper chamber region. The slow development of the failed zone between 5 and 10 years simulation time potentially indicates the final stablized chamber configuration. During the 10 year period, the computed subsidence increases an additional 40%, i.e. 0.1299m, compared to the instantaneous elastic responses of 0.0929m. The effects due to the gravitational loading, roof collapse and weak elastic materials near the surface may counteract the effect due to the thermal expansion which generally causes upheaval in various boundary value problems. The presented analysis with the implicit time stepping scheme ($\theta = 1.$) permits rather large time step size with 65 transient steps and utilizes approximately 3 minutes of CPU time for the entire solution. The selected time control parameter is $\tau = 0.2$ and time steps vary from 1 day to 2.3 years permitting larger steps toward the later stages of solution.

For the thermoelastic simulation, the normalized thermal trends (Figures 27 and 28) based on the nominal values (Table 3) for the elastic constants for coal and rock are used. At early stage, the thermoelastic and thermoviscoelastic cases reveal approximately similar responses for the surface subsidence and failed zones (Figures 33.b and 33.c). With ellapsed time, it becomes evident that the thermoelastic responses, in the absence of time dependence, are mainly affected by the thermal expansion resulting in structural upheavals. It is also noted that with progressive cooling, the thermoelastic surface subsidence increases

faster than the corresponding thermoviscoelastic value. However, the surface subsidence obtained by thermoviscoelastic model is much larger than by thermoelastic model in general due to the creeping of materials. At a simulated time of 10 years, the computed maximum subsidence for the thermoelastic case is 0.0319m, i.e. approximately 25% of the thermoviscoelastic value (0.1299m). A slow chamber growth rate is noted for the thermoelastic case. The thermoviscoelastic case, on the other hand, reveals further chamber growth especially in Felix 1 and siltstone layers (seam 3,4). It is apparent that both time and temperature dependence of coal and overburden should be considered to assess the effect of material softening for the long term structural response evaluation.

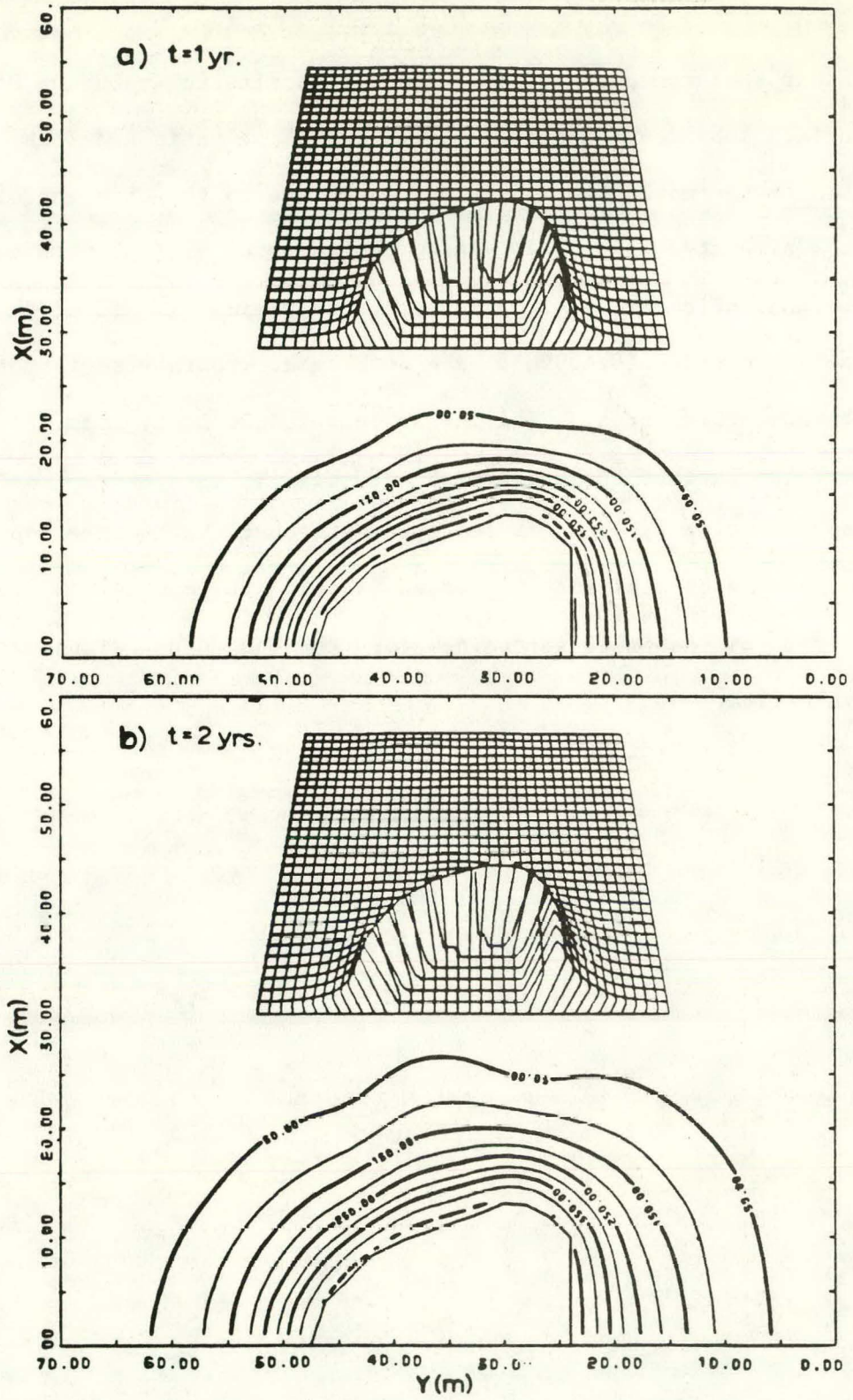

Figure 32: Temperature Profiles for Hoe Creek II Post-Burn Model

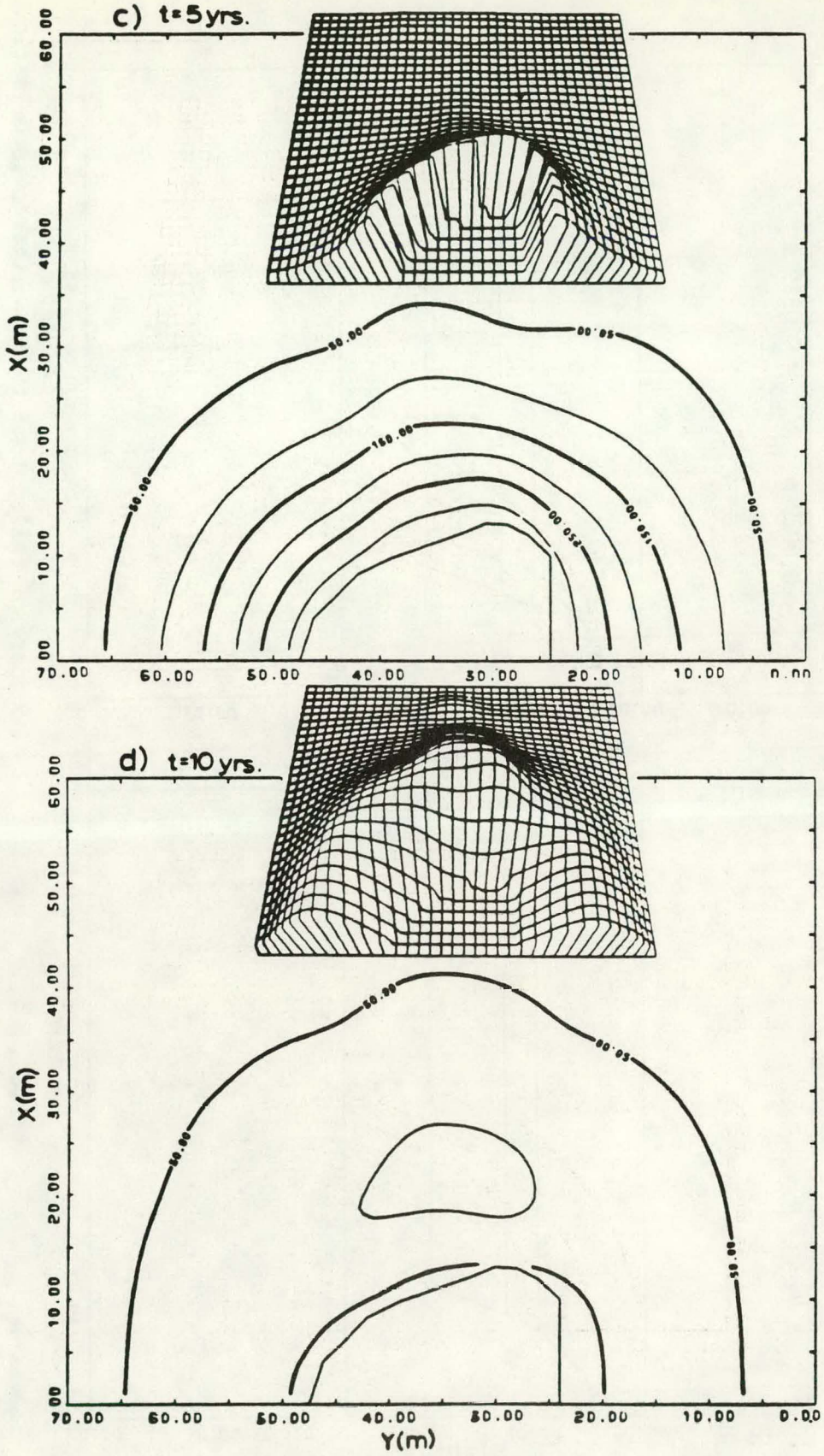

Figure 32: (continued)

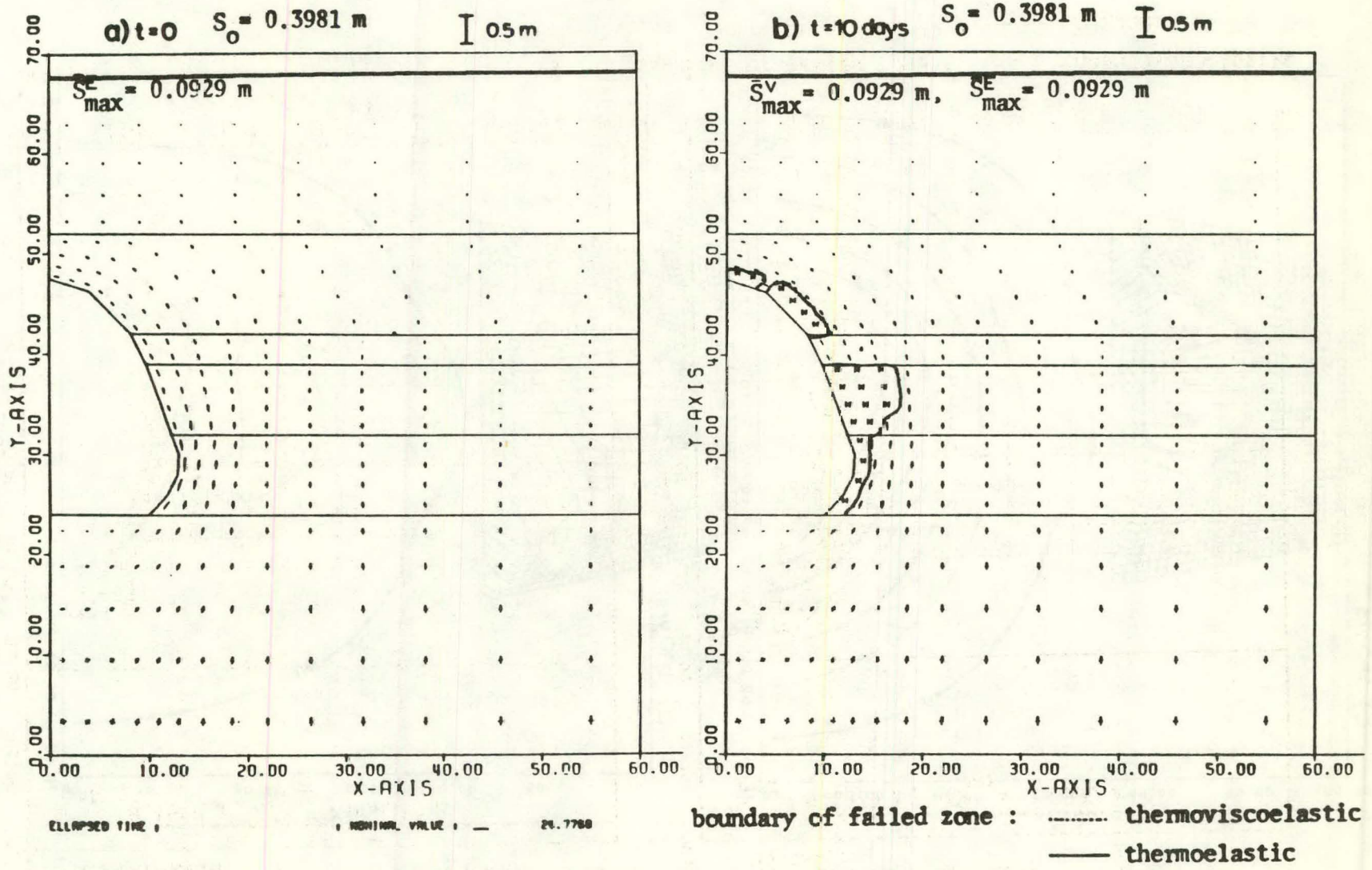

Figure 33: Computed Results for Hoe Creek II Post-Burn Simulation: Surface subsidence, principal stresses($\times 10^5$ Pa and bold line for tension), and failed element designated by * (thermoviscoelastic)

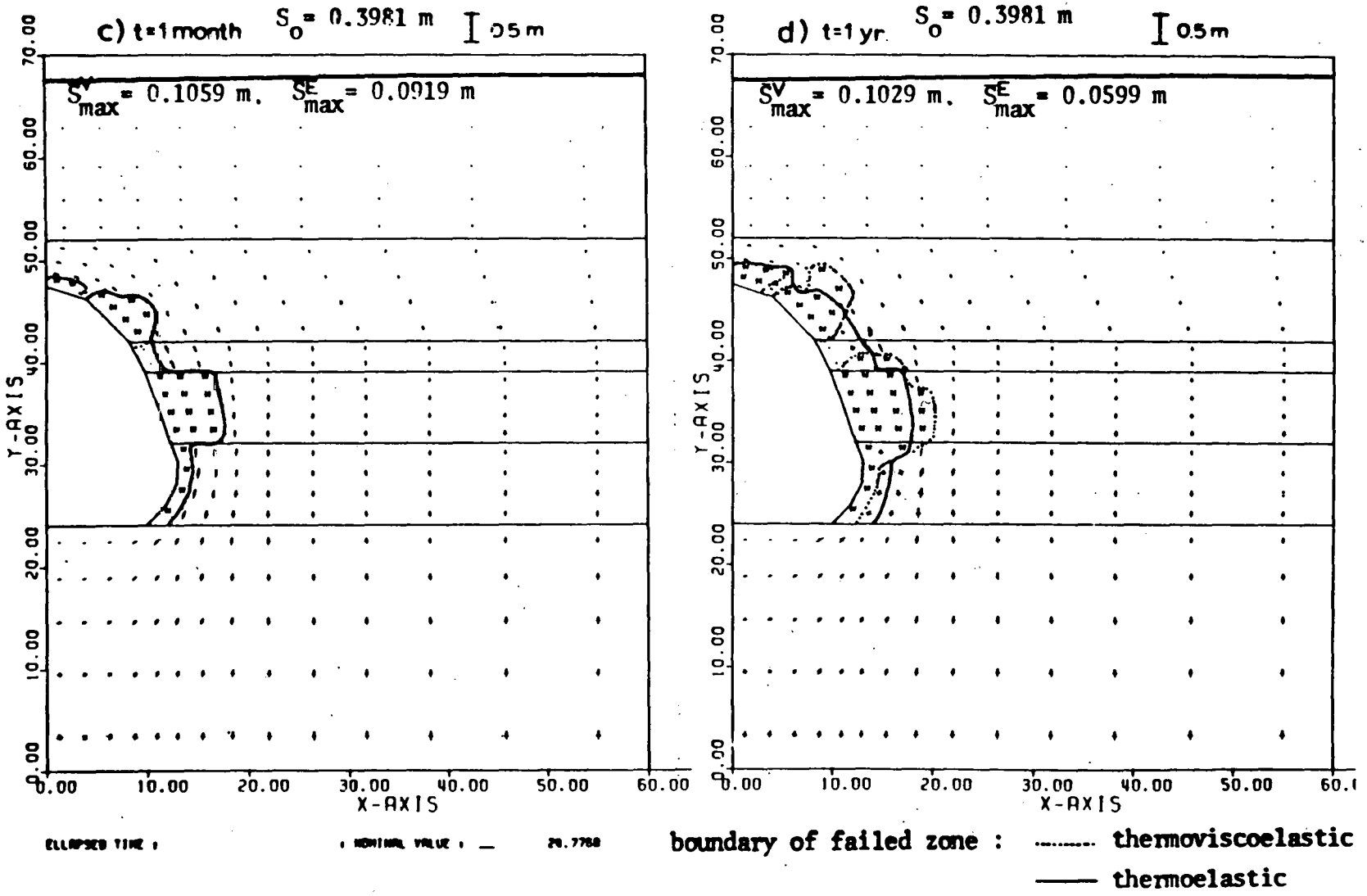

Figure 33: (continued)

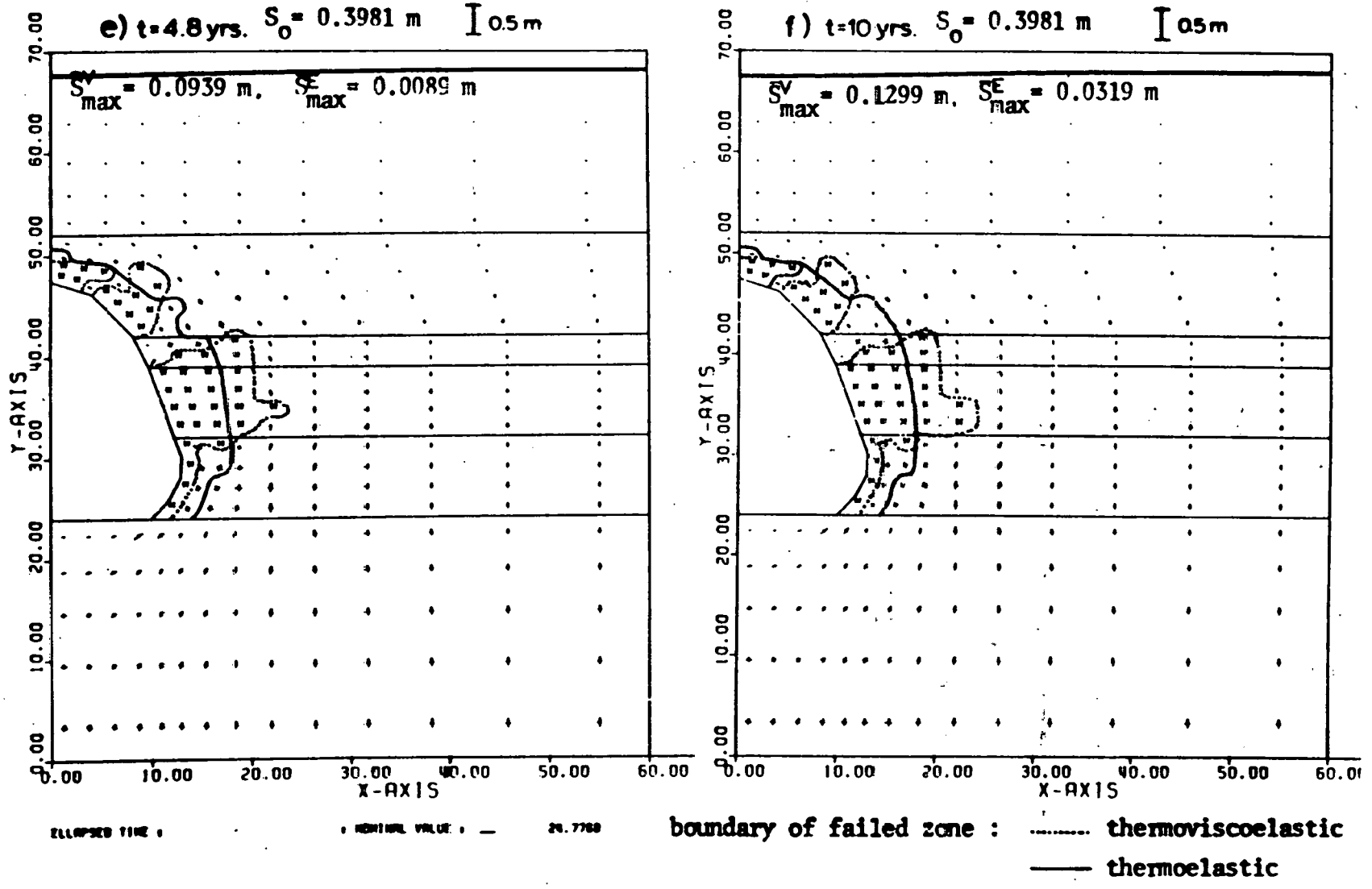

Figure 33: (continued)

5.2 UCC ELLIPTIC CAVITY MODEL WITH A LINKING CHANNEL

A successful UCC operation requires the coal to have sufficient permeability for allowing the oxidizing gas to flow through the coal seam. Various permeability enhancement methods have been employed with varying degrees of success, namely, reverse combustion method, electro-linking, pneumatic linking, and hydrofracturing. The choice of linking technique is critically dependent on the properties of the coal seam (cf. ref. [42,102]). A typical UCC cavity model with a linking channel is illustrated in Figure 34 along with potential thermo-mechanically-induced cracks and water influxis into the chamber. A common structural problem during the gasification process has linking channel closure or plugging. This closure or plugging phenomenon can occur due to the swelling characteristics of bituminous coals and the condensation of vaporized tars. Lee [73] and Wang [123] have analyzed the crack-closure response of the elastic porous-permeable media of coal under the thermo-mechanical loading conditions. The analytical expressions of the displacement and stress fields, obtained from the complex variable approach, are expressed in terms of the thermo-mechanical loading changes and stress intensity factors. It is shown that the fracture permeability is greatly influenced by factors such as thermal and/or pressure crack propagation and closure/plugging of cracks.

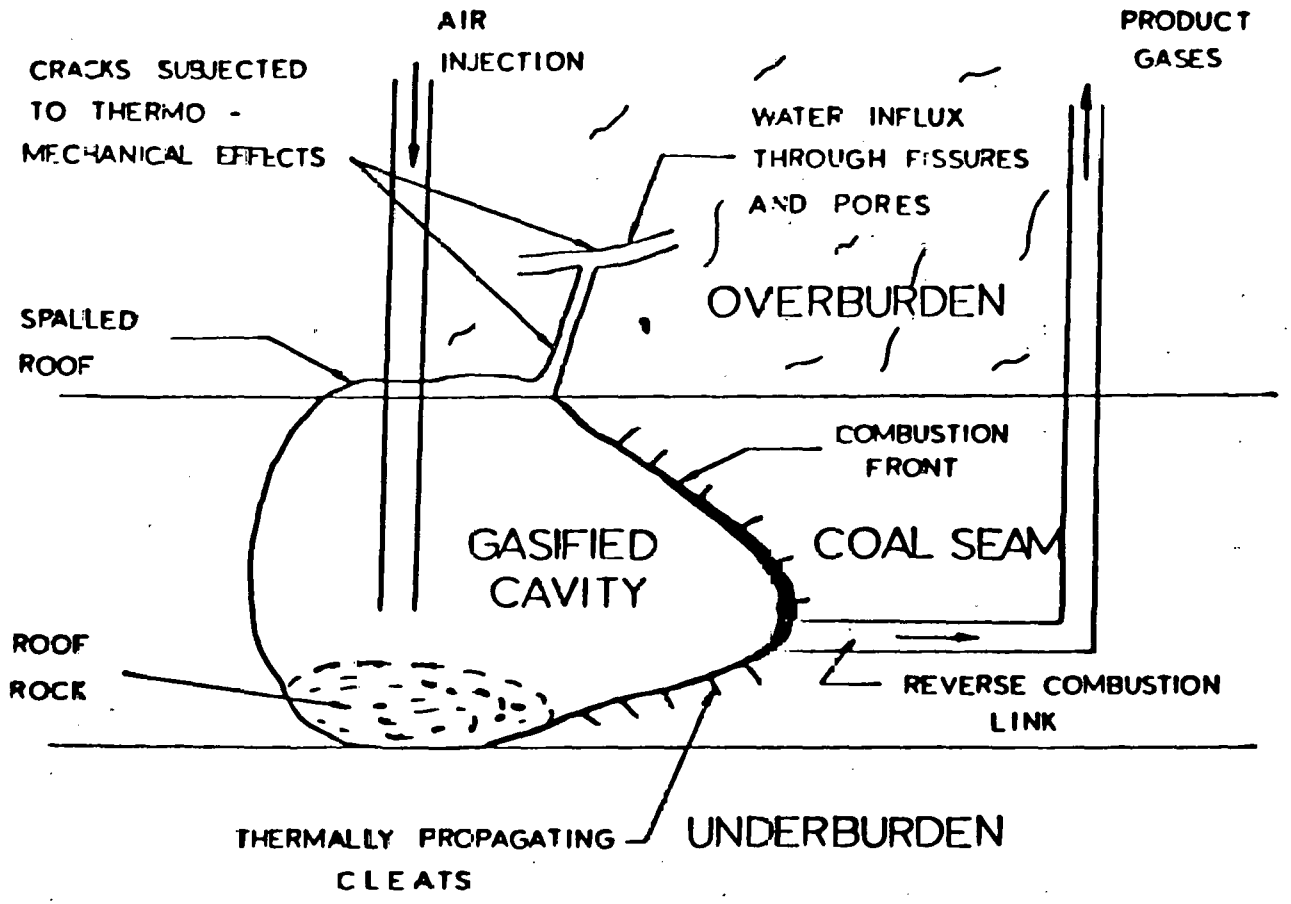

Figure 34: UCC Fracture Model with Linking Channel

Here, a preliminary FEM simulation of an elliptic cavity model with a horizontal linking channel is presented. Since the softened inelastic combustion front is known to be narrow and subjected to the immediate failure (cf. ref. [81,75]), a thermoelastic model with coal and sandstone layers is selected. Materials are assumed to be isotropic and homogeneous, and constant and temperature-dependent mechanical properties are used for sandstone and coal, respectively (Table 4). The steady-state thermal response is obtained with the prescribed temperature conditions for the cavity and linking channel. The plane strain FEM model shown in Figure 35 includes the overburden pressure, cavity pressure, and linking channel treated as a line crack. Quadratic quadlilateral isoparametric elements are used resulting 196 elements and 651 nodal points for the mesh, and at the end of the channel crack tip singular elements are included (cf. Figure 35).

Figure 36 shows the steady-state temperature contours with a prescribed temperature of 540°C for the cavity and channel and 7°C for the external boundary (i.e. ambient temperature). Based on the computed temperature profile, two cases of mechanical loading conditions are considered, i.e. i) overburden pressure of 3.45 MPa and ii) overburden pressure 3.45 MPa with an internal pressure 2.75 MPa on the cavity and linking channel. Figure 37 illustrates the deformed mesh for each case with a potential partial closure of the channel unless suffiicient internal pressure is applied. The maximum principal stresses along the minor and major axes are shown in Figure 38. It is noted that the material layering condition contributes significantly to the stress distribution along the vertical axis and the application of the internal

pressure of 2.75 MPa seems to relieve high stresses along the horizontal axis. Failure is observed at the two ends of the channel. The normalized stress intensity factors $\bar{K}_{I,II} = K_{I,II} / E_o \alpha_o T_c$ near the end of the linking channel are found to $\bar{K}_I = -2.017$, $\bar{K}_{II} = -0.109$ for the case with only overburden pressure, and $\bar{K}_I = -0.176$, $\bar{K}_{II} = 0.011$ for the case with both overburden and internal pressure. The computed stress intensity factors show that crack closing mode is dominant and the application of internal pressure will induce lower values of stress intensity factors.

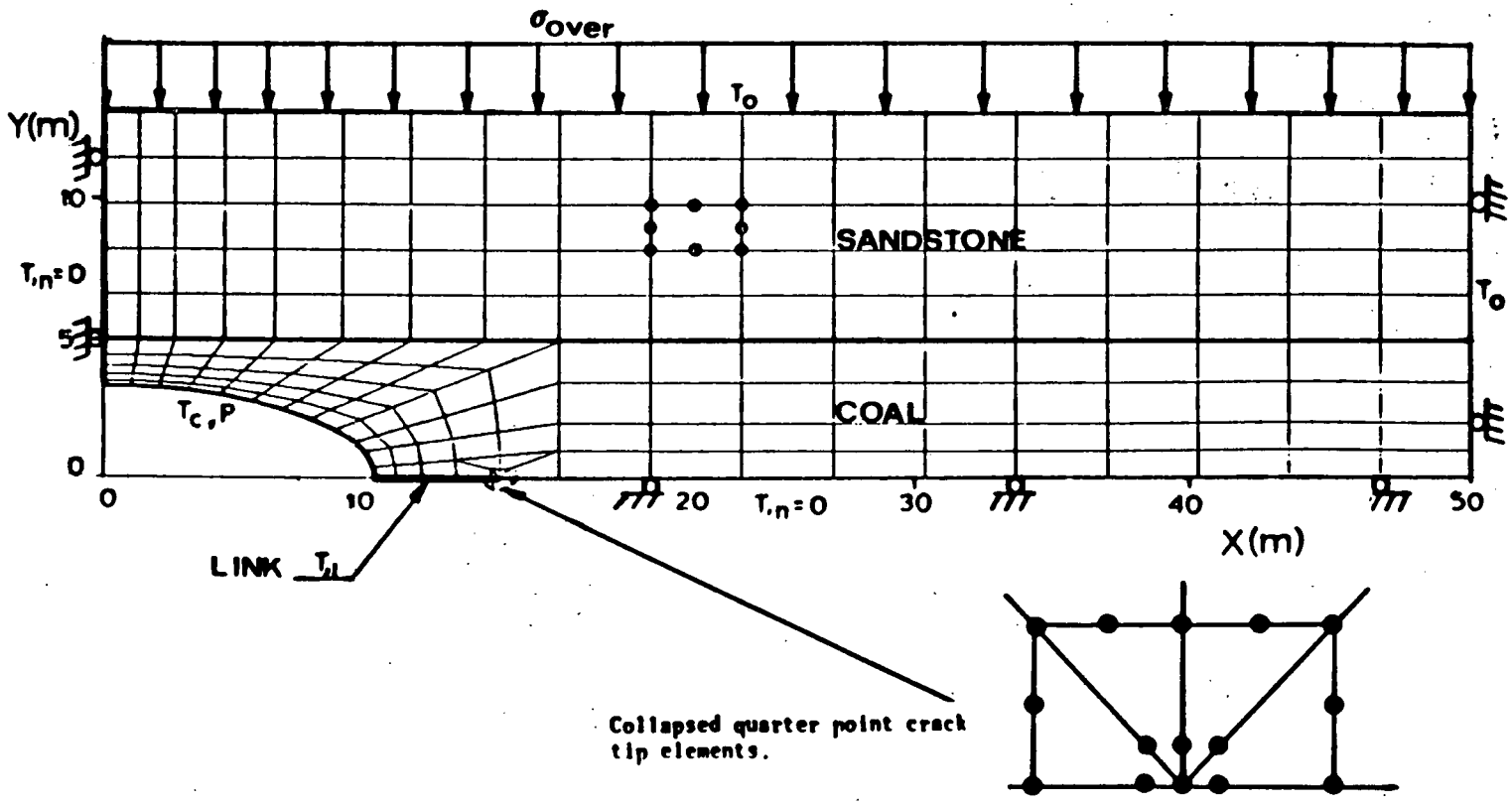

Figure 35: FEM Model for Elliptic Cavity Model with Linking Channel

COAL

Temperature(°C)	k(W/m°C)	E(MPa)	ν	α(X10^{-6}/°C)	S_c(MPa)	S_t(MPa)	μ_f
20	.208	1240.5	.44	2.6	-16.72	1.73	1.0
170	.208	1240.5	.44	2.6	-15.53	2.07	1.0
260	.208	592.7	.44	2.6	-10.86	1.12	1.0
282	.208	75.8	.44	2.6	-4.35	.45	1.0

SANDSTONE

	.187	13784.0	.12	2.5	-103.4	10.68	1.0

Table 4

Selected Material Properties for Elliptic Cavity Model

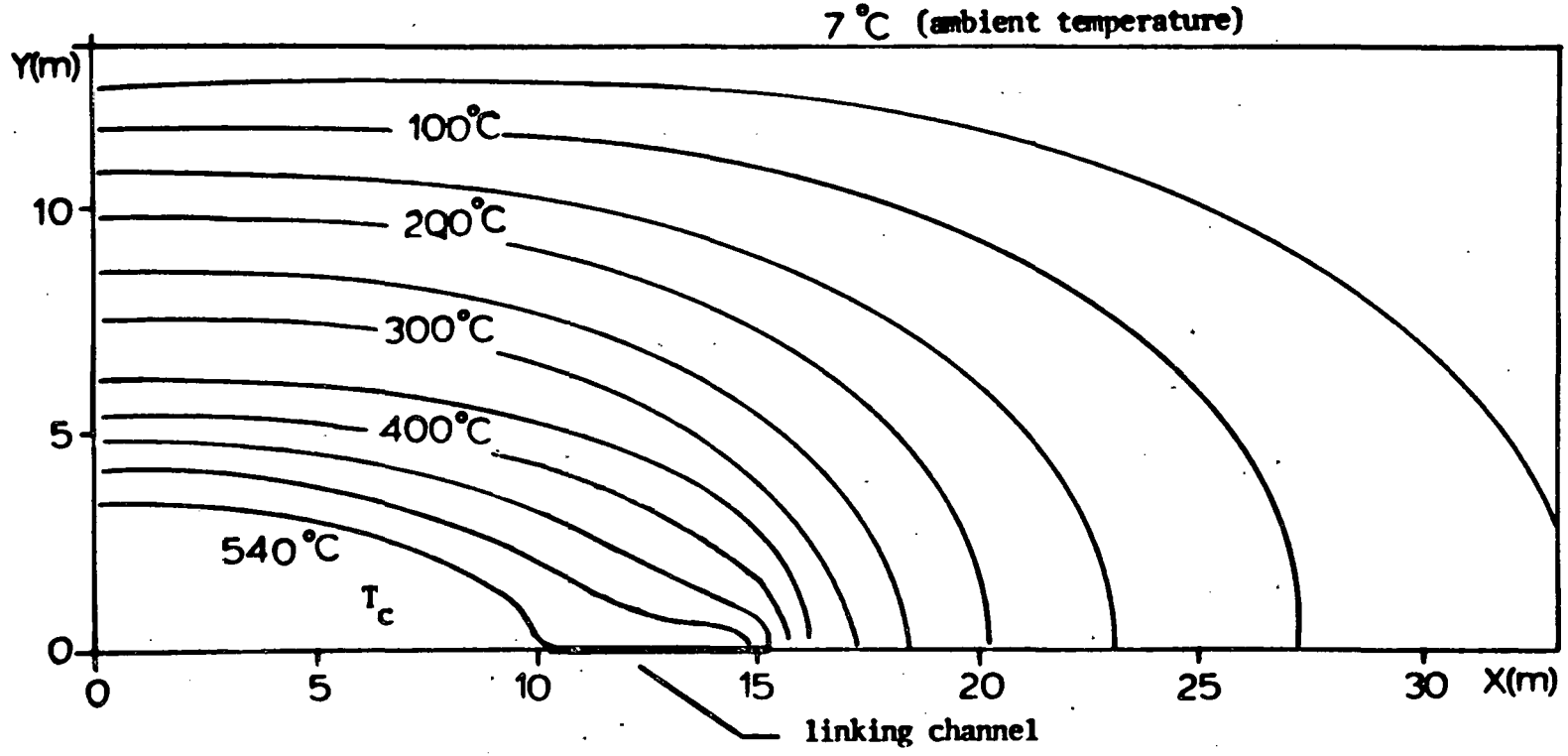

Figure 36: Steady-State Temperature Contours for Elliptic Cavity Model

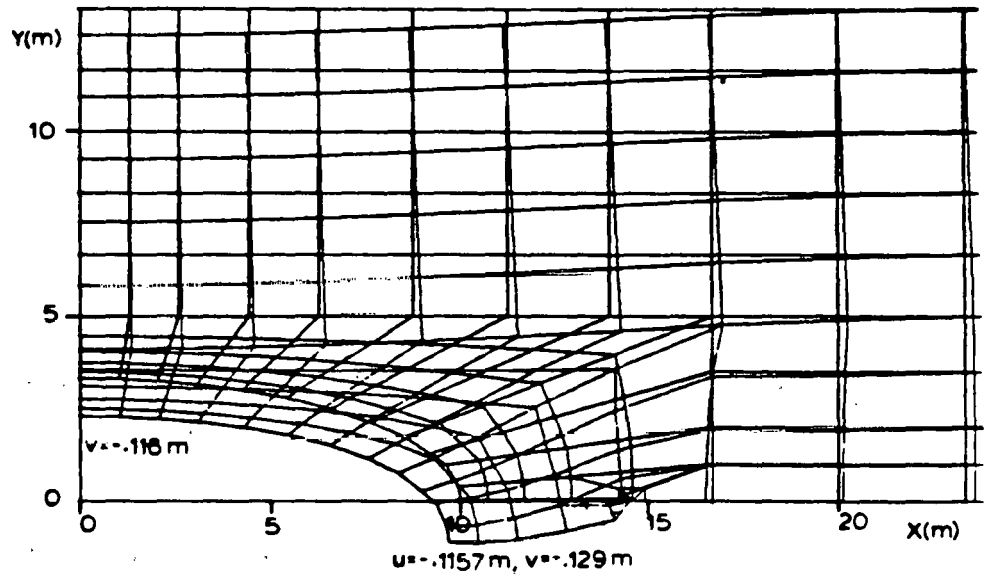

a) Overburden only

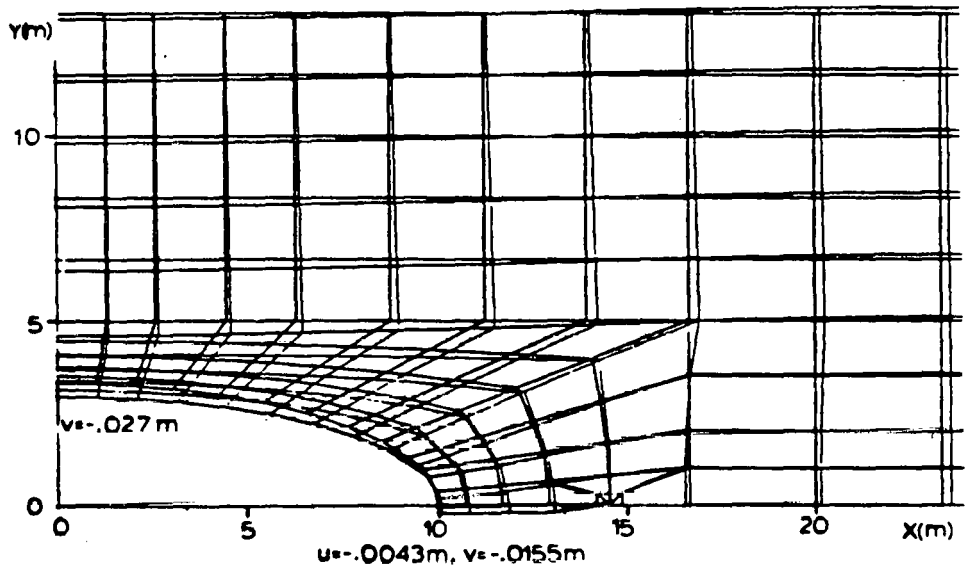

b) Overburden with internal pressure

Figure 37: Deformed Meshes of Elliptic Cavity Model: Magnification factors 8.4545 for case (a) and 16.126 for case (b)

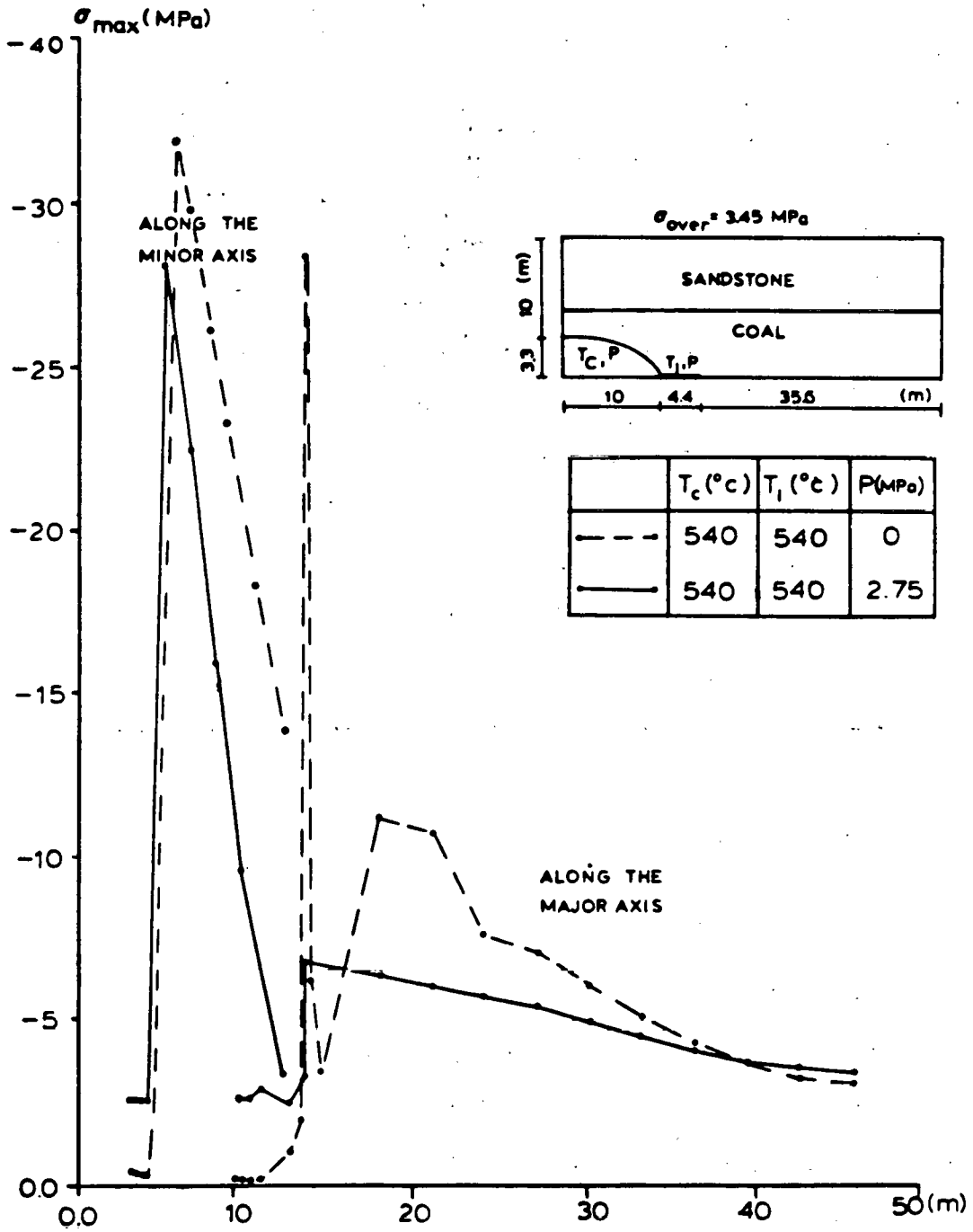

Figure 38: Maximum Principal Stresses along Minor and Major Axes

5.3 IN-SITU WASTE DISPOSAL MODEL

Although the developed FEM models have been primarily conducted for UCC field simulations, a possible application to the salt-dome mining problem can be considered in regard to in-situ nuclear waste management. Various options for radioactive waste disposal including extraterrestrial disposal, seabed disposal, ice-pack disposal, deep melt disposal, and others have been proposed. At present, deep, salt-dome disposal appears to be one of the most reliable techniques since the rock salt formation is stable and free of dissolution for hundreds of millions of years. The saltbed is fairly easy to mine and has very low permeability and water content. Although this behavior may be desirable in most instances, the long-term design criteria often require accurate prediction of the time dependent deformations under various combinations of stress and temperature.

Underground nuclear waste creates two types of disturbances to the rock mass: i) the disturbance resulting from the creation of the emplacement hole and ii) the disturbance resulting from the effects of temperature produced by the radioactive waste. The far-field effects of temperature include the upward motion of the overburden due to the thermal expansion of the rock mass. In particular, the large scale rock movements and their effect on the overall integrity of the geologic containment for the post-repose phase is of interest. Here, the FEM modeling for the post-repose phase is presented by using the preceding thermoviscoelastic formulation.

5.3.1 THERMO-MECHANICAL AND RHEOLOGICAL BEHAVIOR OF ROCK SALT

The thermal properties adopted here are based on the data used by Duddeck and Nipp [32]. Normalized thermal trends for the thermal conductivity, the heat capacity, and the coefficient of thermal expansion are shown in Figure 39.a. It is worth noting that the thermal trend associated with the coefficient of thermal expansion for rock salt is different from most of other rock materials as it remains almost constant for elevated temperatures. This may produce higher thermal expansion in rock salt when compared to other rock materials as temperature increases.

Creep data on rock salt associated with nuclear waste management problems has been recently presented by Langer et al [70], Nipp [88] and Pfeifle and Senseny [92]. A typical deformation-versus-time curve for rock salt s presented in Figure 39.b. The rate of deformation at ealier stages is high, but it decreases monotonically(transient creep) while the deformation continues at a constant rate(stationary creep). At elevated temeratures, the rate of deformation is further accelerated as temperature increases. The creep compliance test data shown in Figure 40 is fitted by a four parameter fluid model by applying the TSM postulate described in Chapter II. Coefficients of the creep compliance and the temperature shift function are obtained from a best-fit analytical curve for the experimentally available limited temperature range. The selected thermorheological properties are

$$J(\xi) = 0.1775\times10^{-2} + 0.18\times10^{-7}\xi - 0.1436\times10^{-2}\,EXP(-0.558\times10^{-2}\xi) \quad (1/MPa) \tag{5.5}$$

and

$$x(T) = 1/a_T = \mathrm{EXP}(53.58 - 0.252T + 0.241\times10^{-3}T^2) \qquad (5.6)$$

Figure 41 illustrates the temeperature shift fuction of rock salt for the temperature range 285°K to 375°K.

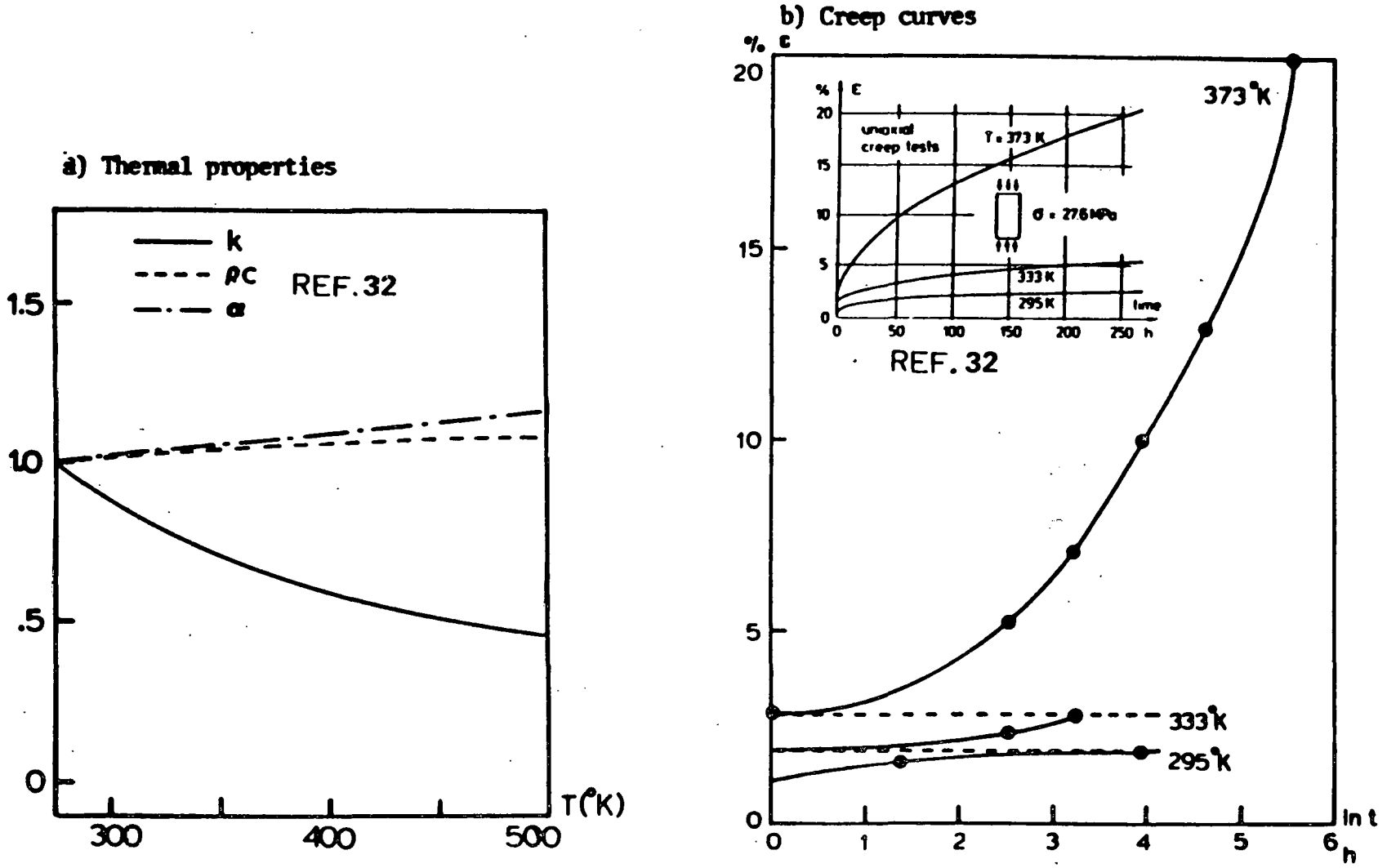

Figure 39: Normalized Thermal Trends and Creep Behavior of Rock Salt (ref. 32)

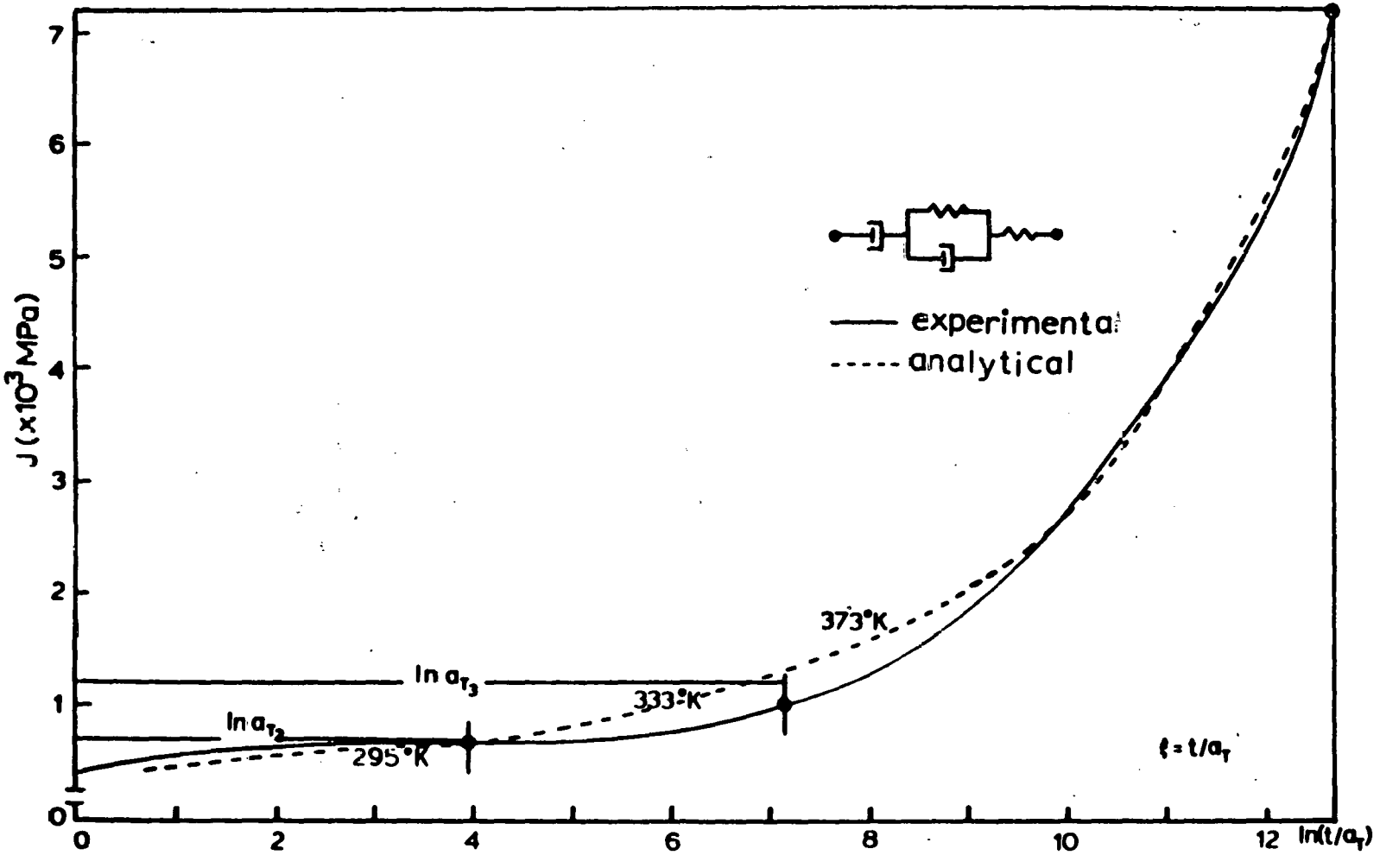

Figure 40: Creep Compliance of Rock Salt under TSM Postulate

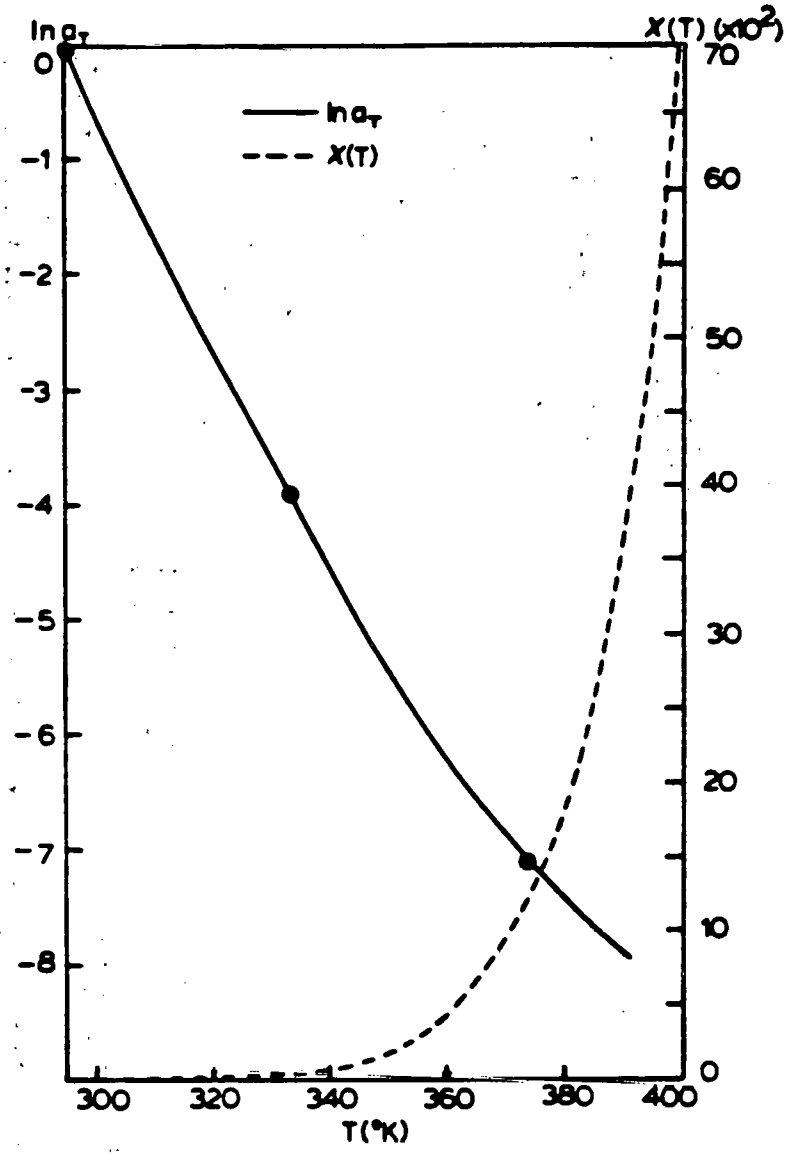

Figure 41: Temperature Shift Fuction of Rock Salt

5.3.2 FEM MODEL AND RESULTS FOR SALT-DOME MINING SITE

The presented axisymmetric FEM model parameters and the geological structure are selected from the study conducted by Nipp [88]. FEM model and boundary conditions shown in Figure 42 with 182 elements and 210 nodal points are used by adopting quadrilateral isoparametric element. Although an explicit expression of the heat source/sink function can be treated in the presented formulation, a simple time-dependent temperature is prescribed over the heat source due to the lack of proper representation of this term. The initial temperature varies linearly from 285°K at the surface to 315°K at the base (simulating the geothermal gradient of 0.035 °K/m). The selected nominal values for different rock materials are listed in Table 5 and only the properties of rock salt are assumed to be temperature-dependent. Temperature profiles up to 260 years simulation time are shown in Figure 43 and the constant time step size, 4 years, is used with 38 seconds solution CPU time. It is shown that the maximum temperature 445°K is reached 54 years later and further propagation of the thermal front continues while the temperature of the heat source slowly decreases. The results also indicate relatively narrow thermally-active zones around the heat source and slow thermal propagation during the entire simulation.

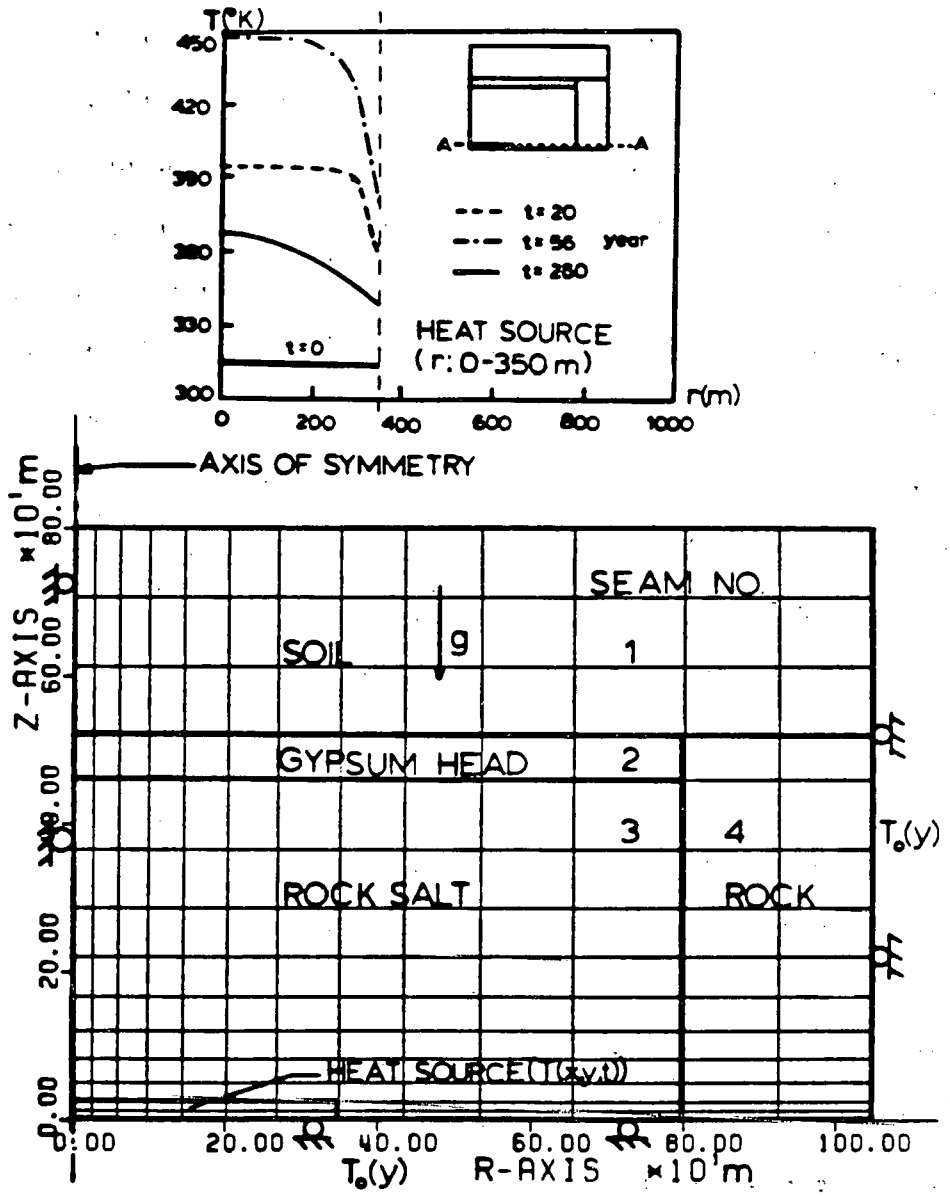

Figure 42: FEM Model, Stratigraphy, and Boundary Conditions for Salt-Dome Mining Site

Properties	Symbol	Unit	Seam No.			
			1	2	3*	4
Thermal Conductivity	k	W/m°K	1.6	1.5	6.06	1.6
Mass Density and Heat Capacity	ρC	$MJ/m^3°K$	2.13	1.5	21.8	1.52
Coeff. of Linear Thermal Expansion	α	$\bar{1}0^5/°K$	9.0	7.5	3.9	8.0
Elastic Modulus	E	10^2MPa	2.5	5.0	146.00*	50.0
Poisson's Ratio	ν		0.3	0.3	0.25*	0.3

* designates viscoelastic material and associated material properties are instantaneous values.

Table 5

Selected Nominal Values for Material Properties
in Salt-Dome Waste Disposal Model

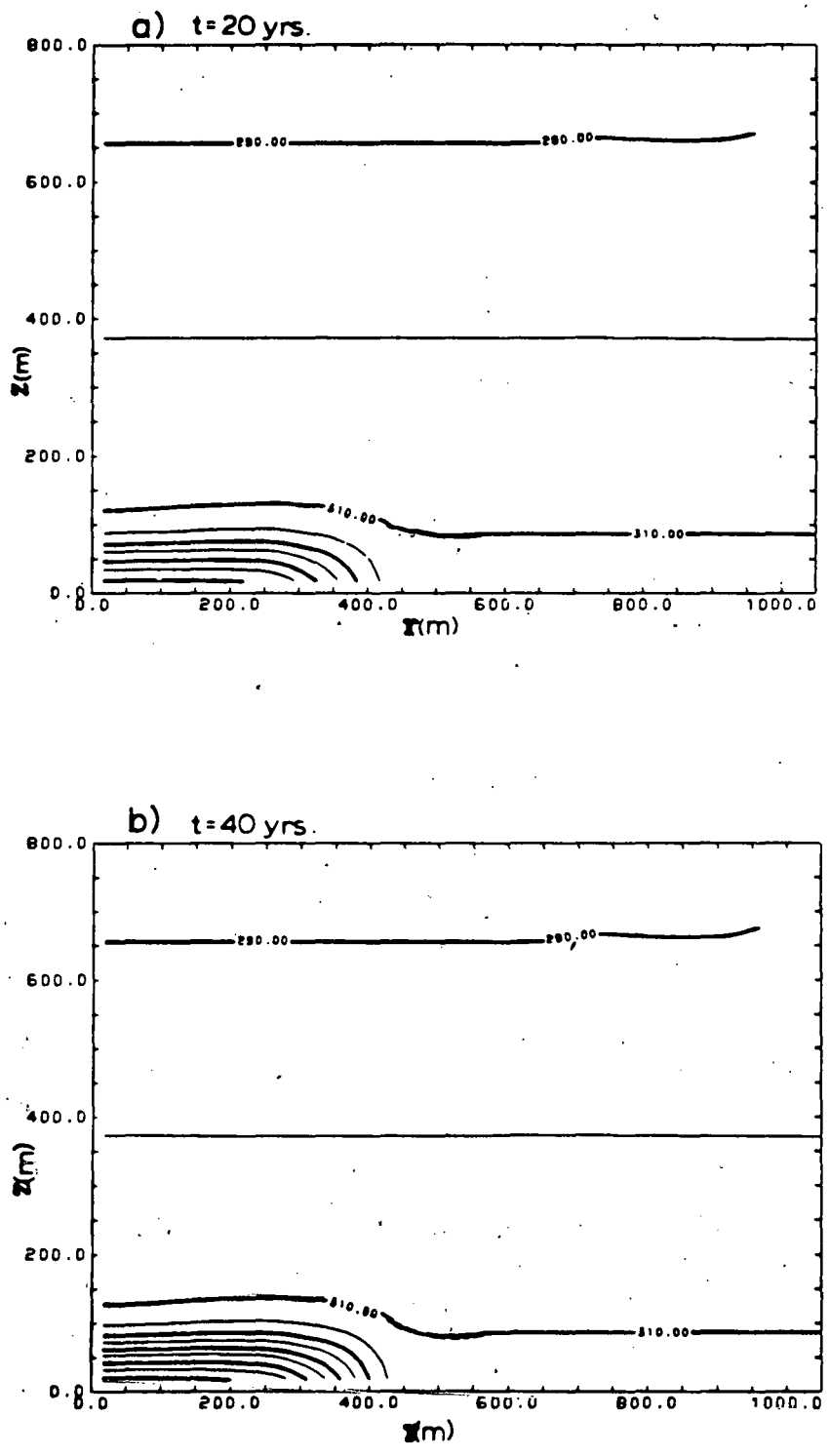

Figure 43: Computed Temperature Profiles for Salt-Dome Waste Disposal Model

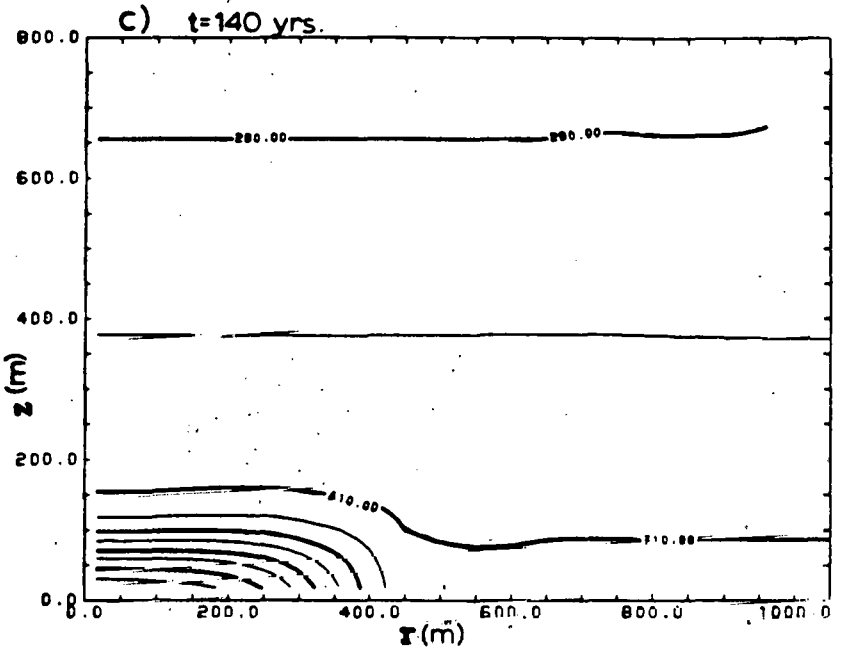

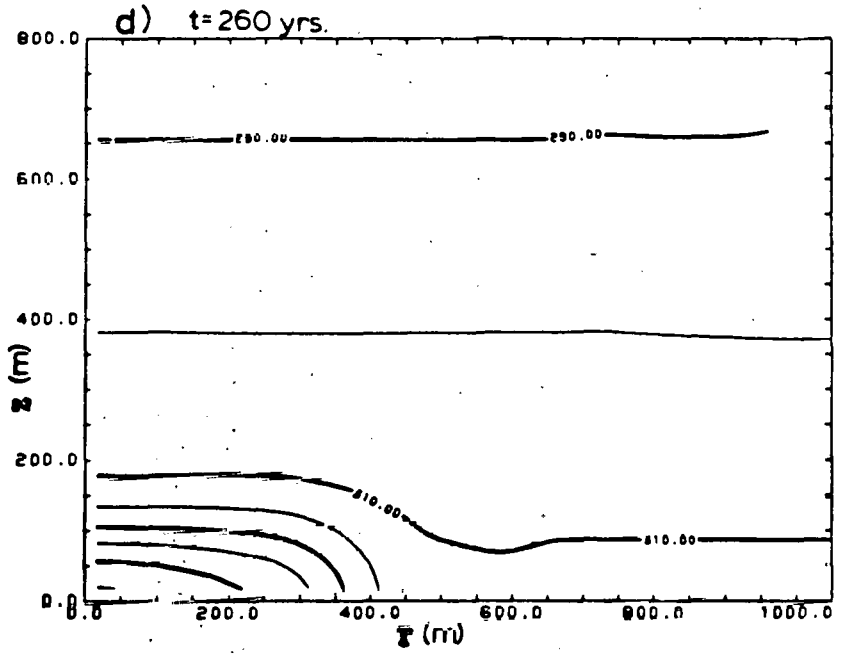

Figure 43: (continued)

e) Along r axis

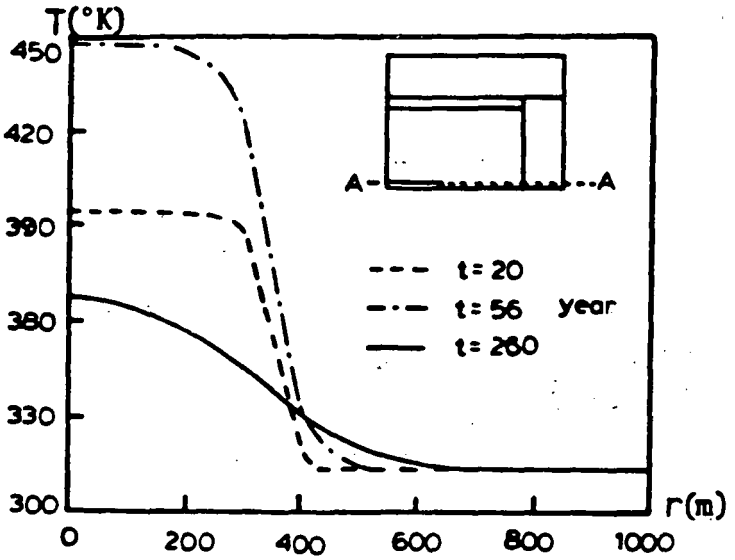

f) Along z axis

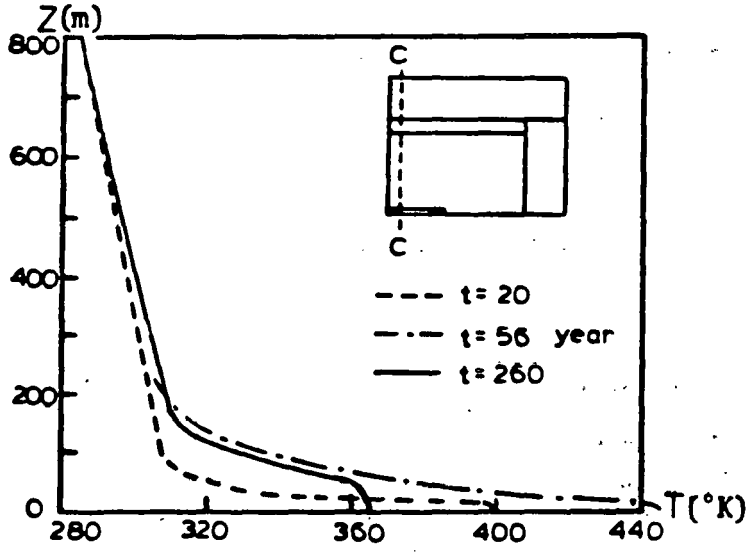

Figure 43: (continued)

Based upon the above temperature solutions, viscoelastic responses are obtained by adopting the thermorheological properties described in Section 5.3.1 for rock salt and constant elastic properties for the other layers. The hydrostatic stresses varying along the distance from the surface are assumed to represent instantaneous elastic stresses and simulate the gravitational loading with $\rho g = 0.024$ MN/m selected from Nipp [88]. Figure 44 illustrates the deformed mesh configurations at each of the selected transient steps. It reveals that the maximum upheaval is 0.992m (above the heat source) and deceases to 0.305m at the surface after 58.3 years of simulation time. This illustrates large deformations due to the thermorheological behavior of rock salt and the thermal expansion in the active thermal zone. The elastic material near the surface experiences less deformations. As the steady-state thermal trends at the lower temperature level are established, the deformation magnitudes are reduced leading to a stable structural configuration. Figure 45 shows typical stress redistributions along the major axes at 11.52, 58.3, 80.44 and 260 years elapsed time. Stress relaxtion with a relatively low stress build-up at earlier stages is noticed while a typical transition from high compressive stresses to low stresses is apparent in the region subjected to steep temperature variations. As the temperature front propagates (80.44 and 260 years), the stresses in the heat source region are relaxed and the high stress zone expands toward the outer region. The entire solution with 38 transient steps utilizes 1 minute 20 seconds solution CPU time and the maximum stress build-up reaches a value 5.7% higher than the instantaneous stress level. It is observed that the presented rheological model for rock salt does not

produce a significant stress build-up while the effects of thermal expansion mainly account for the structural upheaval.

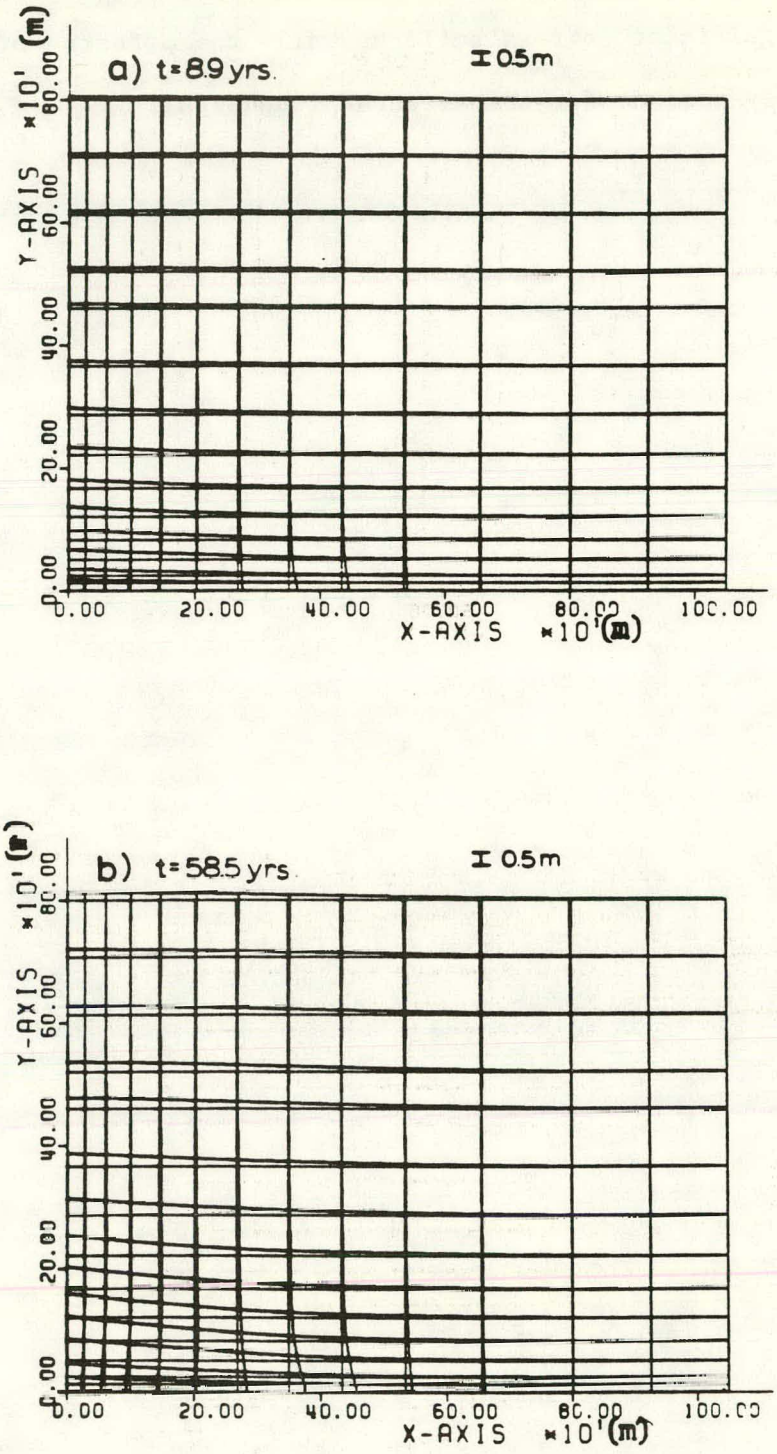

Figure 44: Deformed Mesh Configurations for Salt-Dome Waste Disposal Model: Bold line for deformed shape

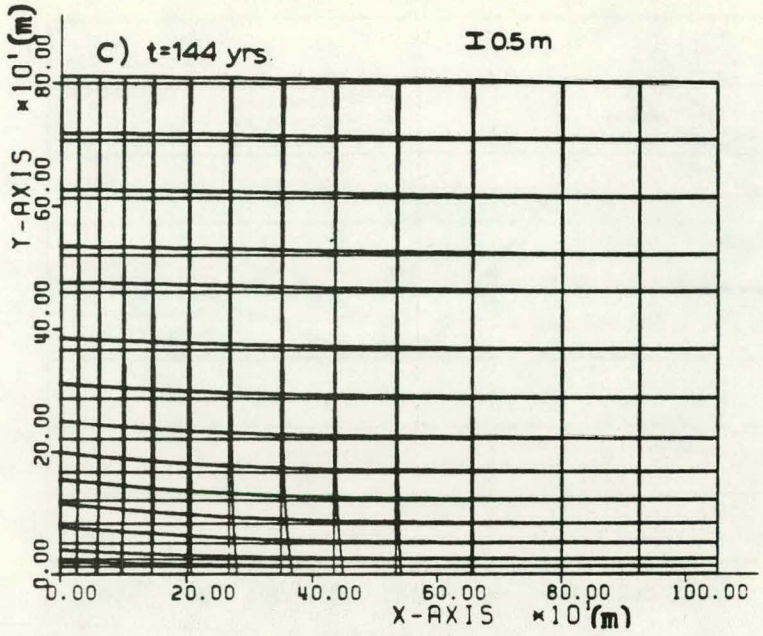

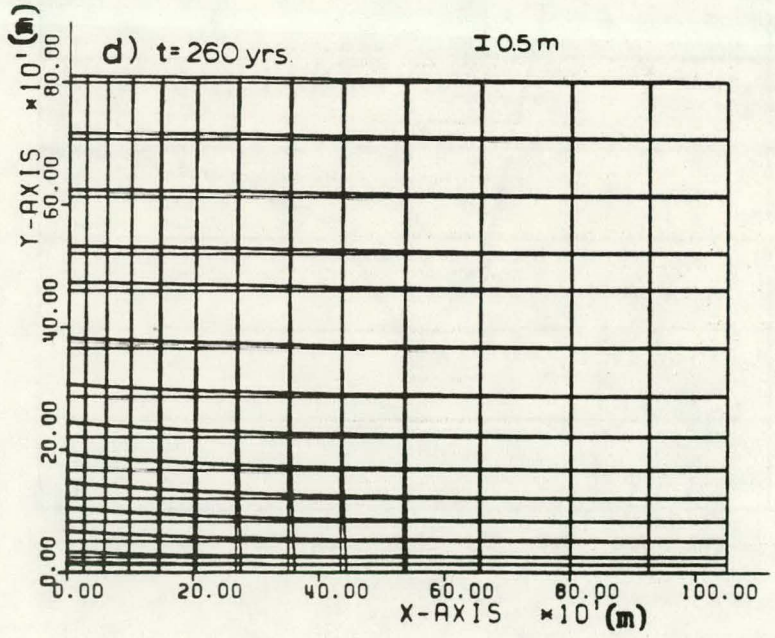

Figure 44: (continued)

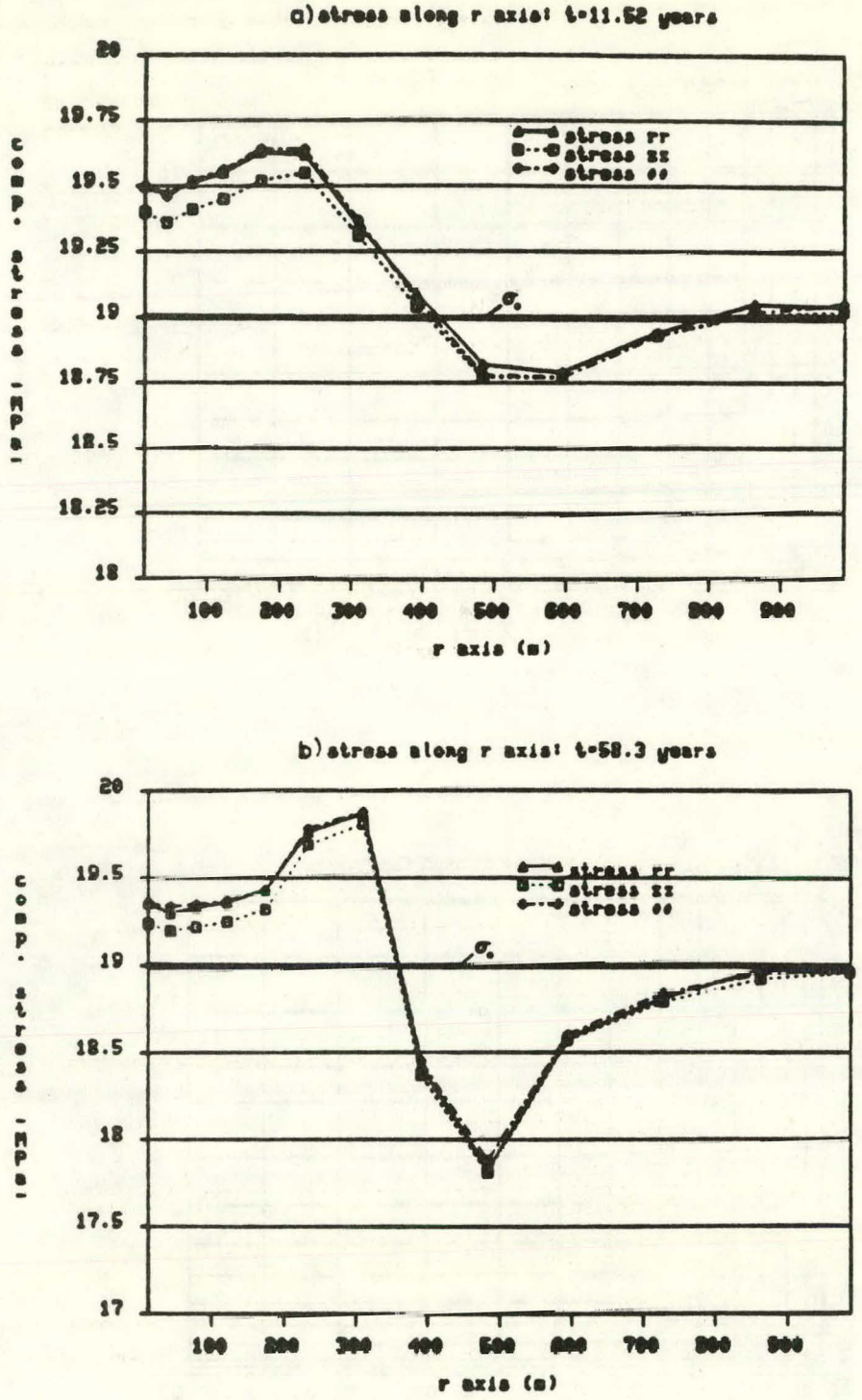

Figure 45: Normal Stress Redistributions along r and z Axes

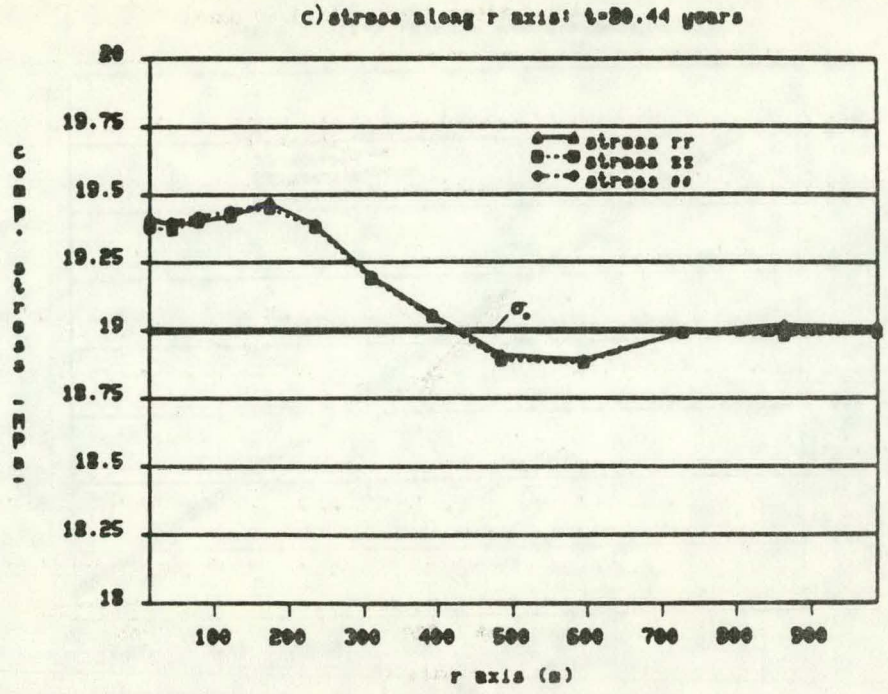

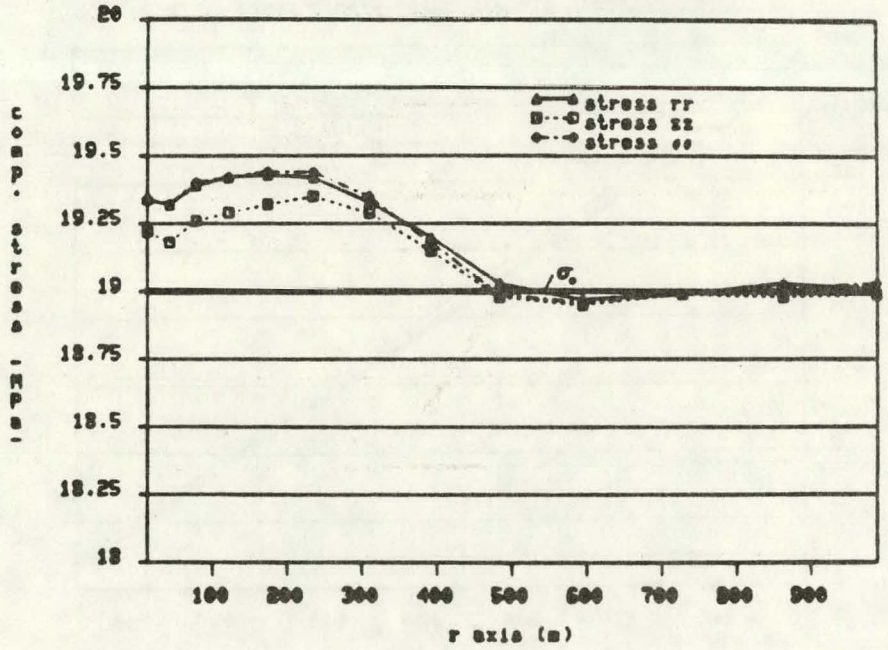

Figure 45: (continued)

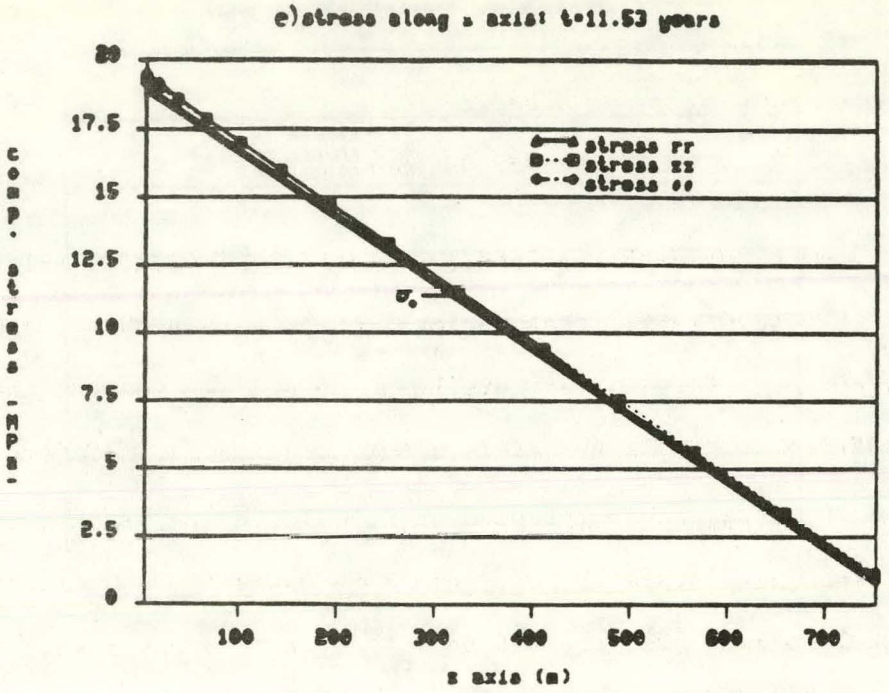

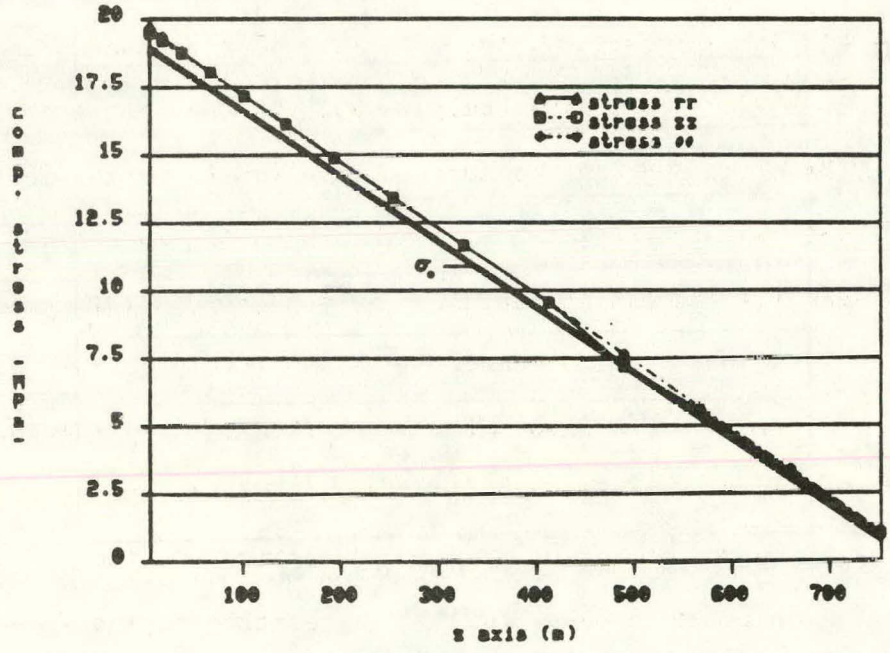

Figure 45: (continued)

Chapter VI

CONCLUSIONS AND RECOMMENDATIONS

Finite element formulations and associated solution algorithm for continua thermoviscoelastic response evaluation have been developed in this dissertation. Formulations are based on one way coupled theory in which the effects on the stress field is considered but not vice versa. The time and temperature correspondence concept is utilized along with the thermorheologically simple material (TSM) assumption. Although the presented applications are focussed on rock mechanics problems, various other applications such as thermal stress analyses in structural mechanics can be made.

Two types of energy equations, the transient heat conduction and convective-diffusion equations, are analyzed for the thermal response determination. The transient heat conduction equation is formulated by using the weighted residual approach with the two-point recurrence scheme in time. Linear time-dependent boundary temperature conditions are used for field applications. This condition simulates physical boundary temperature variations, and also minimizes numerical oscillations subjected to abrupt changes in the boundary temperature at the onset of the solution. Temperature-dependent thermal properties are incorporated in the transient analysis to account for the temperature-dependent material nonlinearity. This formulation provides a versatile application from the viewpoint that the temperature can be replaced by a relevant variable

such as pressure or moisture function or a combined temperature-moisture shift function can be utilized.

The upwinding scheme is used for the FEM formulation of the convective-diffusion equation. The temperature solutions from several upwinding schemes and conventional Galerkin formulation are compared with the exact solution for the quasi-static convection-dominant diffusion equation. Each upwinding scheme depends on the choice of weight functions and quadrature techniques. The weight functions proposed by Heinrich (HU) yields the best result while the other techniques, streamline upwind (SU1,SU2), quadrature upwind (QU), and Galerkin formulation (G), suffer from the cross-wind diffusion and numerical oscillations in varying degrees for several cases of different flow directions. The pertubation of the upwinding parameters in HU, half and full upwindings, shows insignificant effects on the solution accuracy. This transport equation has various applications in areas such as flow through porous-permeable media (advective-diffusion equation), thermodynamic line drive models, and viscous boundary layer problems depending on the coefficients associated with the convective/advective terms.

Based on the determined temperature responses, the time and temperature correspondence concept (TSM postulate) is adopted for the thermoviscoelastic responses. The uniaxial creep compliance with the reduced time scale and the temperature shift function represents the thermorheological behavior of viscoelastic media along with the temperature history. It is assumed that a large amount of creep occurs due to the deviatoric stress while the volumetric behavior is elastic. This assumption

permits the use of a constant Poisson's ratio for creep strains and provides an easy access to currently available creep data at elevated temperatures. The four parameter fluid model (Burger's model) is selected and the creep compliance is expressed as a function of the reduced time. The creep strain rate expression is obtained by approximating the integral expression in summations and the recurrence relationship for the creep strain rate is expressed in terms of the creep strain rate at the previous time step. Use of the implicit time stepping scheme in the creep strain increment leads to a new matrix for the material constants composed of instantaneous elastic constants, reduced time increment, scheme control parameter, and rheological model constants. This matrix, incorporated in the incremental expression of equilibrium equations, is evaluated at each time step unless the scheme control parameter is selected to be zero. In order to reduce computing time, a variable time interval scheme is presented with the time step size selected by limiting the effective creep strain increment as a fraction of the total effective strain. Two cases representing a thermoviscoelastic thin-walled tube, with internal pressure or temperature effects, and a slab of infinite extent are studied in detail to validate the formulation and to assess the effectiveness of the proposed solution algorithm. The results obtained by the presented FEM formulation are compared with other available numerical and analytical results. The presented FEM results compare well in each case and show better time discretization requiring 27 time cycles compared to 100 and 40 time cycles for the finite difference method [77] and Taylor's FEM formulation [111], respectively. Comparisons with the analytical solution for a slab problem show maximum

error of 4.5% based on the hypothetical temperature and thermorheological functions.

The thermally-induced line crack problems are formulated by introducing a degenerate quadratic isoparametric element (cf. Appendix B). The element shape functions incorporating the quarter point mid-side nodes are further modified to maintain the correct strain singularity. The modified shape functions vary quadratically in both ξ and η directions even for pertubation of the mid-side nodes across the the collapsed node. The expression for the stress intensity factor is obtained by equating the coefficient of the $r^{-1/2}$ term in the analytical and numerical expressions of displacements near the crack tip. This expression is generalized for mode I and II plane strain or stress problems. Mode I and II cases for the thermoelastic line crack problems are examined and the results for the FEM formulation stress intensity factors show less than 3% error for both cases when compared with the analytical values. It is also noted that the singular effects near the crack tip are slightly better represented for the two-point (2x2) Gaussian integration rule than the three-point (3x3) rule.

Two field problems associated with the underground coal conversion (UCC) process have been illustrated by using the presented thermoviscoelastic and thermoelastic fracture formulations. The physical and mechanical properties of geological materials show large quantitative variations with temperature. It is almost impossible to have a comprehensive set of material data required for a detailed UCC simulation. A set of normalized thermal trends for coal and rock mass have been qualitatively

estimated so that one set of nominal values can be chosen for a specific UCC site. The experimental data for the thermorheological properties of geological materials appear to be limited and are only available in terms of the creep compliance for the eastern bituminous coal and shale. These materials are found to approximate the thermorheologically simple material behavior. The rheological behavior of coal and rock are assumed to have the same thermal trends for bituminous coal and overburden shale and are calibrated for a specific UCC site based on the available experimental data.

A UCC post-burn simulation for Hoe Creek II site has been presented with emphasis on the gasification chamber configuration and surface subsidence. Two-dimensional failure criteria described in Appendix A are incorporated to define the failed zones. The time-dependent boundary temperature condition simulates the heating and cooling effects on the gasification chamber boundary. During 10 years simulation time, major shear failures occur in the upper chamber region indicating potential roof collapse, and stress relaxations are also noticed in the viscoelastic layers as the thermal front propagates. A modest increase in the surface subsidence is obtained for the Hoe Creek experiment with gravitational loading, roof collapse, and weak elastic materials at the surface. The thermoelastic simulation with temperature dependent elastic constants reveals less surface subsidence and slow chamber growth rate than the thermoviscoelastic case. It is clearly noted that the time dependence of coal and overburden must be included to assess the effect of material softening for the long term simulation of UCC experiment.

To demonstrate a UCC fracture model simulation, an elliptic cavity model with a horizontal linking channel is selected. Temperature-dependent elastic material constants are used on the basis of the computed steady-state temperature solution. The prescribed overburden pressure is applied on the top surface to simulate the gravitational effect. The linking channel treated as a line crack is incorporated with degenerate quadratic singular elements at the end of the linking channel. Comparisons between two cases, i.e. with and without the internal pressure on the cavity and link channel, indicates that an optimum internal pressure should be provided to have a stable burn front configuration controlling the roof collapse and the closure of the linking channel.

As a secondary application of the presented thermoviscoelastic FEM formulation, the post-repose phase of the nuclear waste management in a salt-dome mining site is selected. The thermal trends for the physical and mechanical properties for rock salt appear to be different from the ones selected for the UCC simulation models. In particular, the coefficient of thermal expansion remains almost constant for the temperature range 280°K to 500°K. The thermorheological behavior based on uniaxial creep data is represented by a four parameter fluid model with the TSM postulate. The temperature of the heat source (treated as boundary temperature) is prescribed as a function of time and space. The transient temperature solutions reveals relatively narrow thermally-active zones around the heat source and slow thermal propagation during 260 years of simulation. The thermally-active zone around the heat source experiences large deformations as the temperature increases. The computed stress results show a low stress build-up at ealier stages and a typical stress

relaxation in the region subjected to steep temperature variations. It is clearly noted that the presented thermorheological model for rock salt produces insignificant stress redistributions while the effect of the thermal expansion contributes significantly to the structural upheaval.

Considering the effectiveness of the presented thermoviscoelastic FEM solution algorithm, the variable time interval scheme can allow a fairly large time step size with stable solutions requiring a reasonable amount of computing time for the UCC and in-situ waste disposal model simultions studied here. The presented approximation of the strain rate expression is general and can be used for different mechanical models by establishing recurrence relationships with appropriate creep functions. In particular, the incremental procedure with the implicit time stepping scheme is effectively adopted for the field appications minimizing computational efforts and computing time.

In order to improve the numerical simulations for the UCC process and in-situ nuclear waste disposal, the following recommendations are suggested for furture research:

a) Development of a thermovisco-elsto-plastic model with large deformation.
b) Coupling of in-situ fluid flow and the chemical/radioactive reaction kinetics for the thermally-active zone by heat source/sink terms.
c) Consideration of viscoelastic crack propagation with convective creep flow for the fracture model.
d) Effects of anisotropy/heterogenity of geological materials.

e) Development of formulation for predicting hygrothermal responses, i.e. formulation of the moisture shift function by analogy of the time and temperature shift.

f) Use of the moving boundary FEM formulation for defining the progressive chamber configuration.

g) Establishment of site specific and accurate data for the thermophysical and thermo-mechanical properties for in-situ model simulations.

BIBLIOGRAPHY

1. Advani, S.H., Lin, Y.T., Gmeindl, F.D. and Powell, W.R., "Coupled Roof Fracture Responses and Surface Subsidence Elevations Related to Underground Coal Gasification", Proc. 4th Annual UCC Symp., pp. 507-514, 1978.

2. Advani, S.H., Lee, J.K. and Min, O.K., "Formulations, Simulations and Evaluations Associated with Thermomechanical Models for Underground Coal Gasifications", In Situ, Vol.7(2), pp.121-142, 1983.

3. Advani, S.H., Lee, J.K., Min, O.K. and Lee, S C.," Status of Technology Associated with Cavity and Subsidence Responses Prediction Associated with Underground Coal Conversion", Proc. 8th Annual UCC Symp., pp.271-286, Aug.,1982.

4. Aiman, W.R., Ganow, H.C. and Thorsness, C.B., "Hoe Ceek II Revisited: Boundaries of the Gasification Zone", UCRL-83498, Oct., 1979.

5. Akay, H.U. and Gurdogan, O., "An Investigation of Degenerate Isoparametric Finite Element of Stress Intensity Computation", 5th Int. Conf. on Structural Mech. in Reactor Technology, Part M, Berlin, W.Germany, 1979.

6. Alfrey, T., "Mechanical Behavior of High Polymers", Interscience, N.Y., 1948.

7. Anderson, C.A. and Bridwell, R.J., "A Finite Element Method for Studying the Transient Nonlinear Thermal Creep of Geological Structures", Int. J. Num. Analy. Mtd. in Geomechanics, Vol.4, pp.255-276, 1980.

8. Anderson, C.A., "An Investigation of the Steady Creep of Spherical Cavity in a Half Space", J. Appl. Mech., pp.254-258, June, 1976.

9. Argyris, J.H., Vaz, L.E. and Willam, K.J., "Inelastic Finite-Element Analysis of Coupled Thermovisco-plastic Problems", J. Thermal Stresses, Vol.4, pp.121-153, 1981.

10. Argyris, J.H. and Scharpf, D.W., "Finite Element in Time and Space", Nucl. Engng. Design, Vol.10, pp.456-469, 1969.

11. Barrett, K.E. and Demunshi, G., "Finite Element Solutions of Convective-Diffusion Problems", Int. J. Num. Mtd. Engng., Vol.14, pp.1511-1524, 1979.

12. Barsoum, R.S., "On Use of Isoparametric Finite Elements in Linear Fracture Mechanics", Int. J. Num. Mtd. Engng., Vol.10, pp.25-37, 1976.

13. Bathe, K.J. and Wilson E.I., "Numerical Methods in Finite Element Analysis", Prentice-Hall, Inc., N.J., 1976.

14. Batra R.C., Levinson, M. and Betz, E., "Rubber Covered Rolls- The Thermoviscoelastic Problems. A Finite Element Solution", Int. J. Num. Mtd. Engng., Vol.10, pp.267-285, 1976.

15. Batra, R.C., "Cold Sheet Rolling, The Thermoviscoelastic Problem, A Numerical Solution", Int. J. Num. Mtd. Engng., Vol.11, pp.671-682 1977.

16. Biot, M.A., "Linear Thermodynamic and Mechanics of Solids", Proc. 3rd U.S. Nat. Congr. Appl. Mech., 1958.

17. Birch, F. and Clark, H., "The Thermal Conductivity of Rocks and its Dependence upon Temperature and Composition", American J. Sci., Vol.238, pp.529-558, 1940.

18. Bloom, J.M., "An Evaluation of a New Crack Tip Element, The Distorted 8-node Isoparametric Elements", Int. J. Frac. Mech., Vol.11, pp.705-707, 1975.

19. Bonacina, C., Comini, G. Fasano, A., and Prinicerio, M., "Numerical Solution of Phase-Change Problems", Int. J. Heat Mass Transfer, Vol. 16, pp.1825-1832, 1973.

20. Brooks, A. and Hughes, T.J.R., "Streamline-Upwind/Petrov-Galerkin Methods for Advection Dominant Flows", 3rd Int. Conf. on Finite Element Methods in Fluid Flow, 1980.

21. Carslaw, H.C. and Jaeger, J.C., "Conduction of Heat in Solids", pp.200, Oxford Press, 2nd Ed., 1959.

22. Christensen, R.M. and Naghdi, P.M., "Linear Non-Isothermal Viscoelastic Solids", Acta Mechanica 3, 1967.

23. Christensen, R.M., "Theory of Viscoelasticity", Academic Press, pp.79-109, 1971.

24. Christie, I. Griffiths, D.F., Michell, A.R. and Zienkiewicz, O.C., "Finite Element Methods for Second Order Differential Equations with Significant First Derivative", Int. J. Num. Mtd. Engng., Vol.10, pp.1389-1396, 1976.

25. Comini, G. Del Guidice, S., Lewis, R.W. and Zienkiewicz, O.C., "Finite Element Solution of Nonlinear Heat Conduction Problems with Special Reference to Phase Change", Int. J. Num. Mtd. Engng., Vol.8, pp.613-624, 1974.

26. Cormeau, I., "Numerical Stability in Quasi-Static Elasto/Visco-Plasticity Int. J. Num. Mtd. Engng., Vol.9, pp.109-127, 1975.

27. Cost, T.L., "A Free Energy Functional for Thermorheologically Simple Material", Acta Mechanica, Vol.17, pp.153-167, 1973.

28. Crochet, M.J. and Naghdi P.M., "A Class of Simple Solids with Fading Memory", Int. J. Engng. Sci. 7, pp.1173, 1969.

29. Cyr, N.A. and Teter, R.D., "Finite Element Elastic-Plastic-Creep Analysis of Two-Dimensional Continuum with Temperature-Dependent Material Properties", Computers & Structures, Vol.3, pp.849-863, 1973.

30. Dong, R.G., Pister, K.S. and Dunham, R.S., "Mechanical Characterization of Nonlinear Viscoelastic Solids for Iterative Solution of Boundary Value Problems", Report No. 68-11, Structural Engineering Laboratory, Univ. of California, Berkeley, Ca., 1968.

31. Dubow J. and Rajaw, K., "Thermophysical Properties of Oil Shale", DOE-EF-77-5-03-1584, Colorado State University, 1980.

32. Duddeck, H.W. and Nipp, H.S., "Time and Temperature Dependent Stress and Displacement Field in Salt Domes", Proc. 23rd Symp. on Rock Mechanics, Berkeley, Ca., pp.596-603, Aug., 1982.

33. Ferry, J.D., "Mechanical Properties of Substances of High Molecular Weight: VI. Dispersion in Concentrated Polymer Solutions and Its Dependence on Temperature and Concentration", J. Amer. Chem. Soc. 72, pp.3746, 1950.

34. Ferry, J.D., "Viscoelastic Properties of Polymers", John Wiley & Sons, Inc., 2nd Ed., 1970.

35. Fitzgerald, D., "Viscoelastic Properties of Coal During Carbonization", Fuel, Vol.36, pp.389, 1957.

36. France, P.W., Parkesh, C.J., Peters, J.C. and Taylor, C.J., "Numerical Analysis of Linear Free Surface Seepage Problems", Proc., ASCE, Vol.97, pp.165-179, 1971.

37. Freudenthal, A.M., "On Inelstic Thermal Stresses in Flight Structures", J. Aero. Sci., Vol.21, pp.772, 1954.

38. Fried, I., "Finite Element Analysis of Time Dependent Phenomena", J. AIAA., Vol.7, pp.1170-1173, 1969.

39. Gallagher, R.H., Zienkiewicz, O.C., Oden, J.T., Morandi, C.M. and Taylor, C. "Finite Element in Fluids", Vol.3, John Wiley & Sons, Inc. 1978.

40. Gmeindl, F.D., "Mechanical Properties of Pennsylvania Shale at Elevated Temperature", MSME Thesis, West Virginia University, Morgantown, W.Va., 1977.

41. Greenbaum, G.A. and Rubinstein, M.F., "Creep Analysis of Axisymmetric Bodies Using Finite Elements", Nucl. Engngn. Design, Vol.7, pp.379-397, 1968.

42. Gregg, D.W. and Olness, D.U., "Basic Principles of Underground Coal Gasification", UCRL-52107, Lawrence Livermore Laboratory, 1976.

43. Griffith, A.A., Phil. Trans. Roy. Soc. London, Series A221, pp.163-198, 1921.

44. Griffith, A.A., "Theory of Rupture", Proc. 1st Int. Congress for Applied Mechanics, pp.53-63, 1924.

45. Haisler, W.E. and Sanders, D.R., "Elastic-Plastic-Creep-Large Strain Analysis at Elevated Temperature by the Finite Element Method", Computers & Structures, Vol.10, pp.375-381, 1979.

46. Heinrich, J.C., Huyakorn, P.S., Zienkiewicz, O.C. and Mitchell, A.R., "An Upwind Finite Element Scheme for Two-Dimensional Convective-Transport Equations", Int. J. Num. Mtd. Engng., Vol.11, pp.131-143, 1977.

47. Heinrich, J.C. and Zienkiewicz, O.C., "Quadratic Finite Element Scheme for Two-Dimensional Transport Problems", Int. J. Num. Mtd. Engng., Vol.11, pp.1831-1844, 1977.

48. Heinrich, J.C., "On Quadratic Element in Finite Element Solution of Steady-state Convection-Diffusion Equation", Int. J. Num. Mtd. Engng., Vol.5, pp.1041-1052, 1980.

49. Henshell, R.D. and Shaw, K.D., "Crack Tip Finite Elements Are Unnecessary", Int. J. Num. Mtd. Engng., Vol.9, 1975.

50. Heuze, F.E., "High-Temperature Mechanical, Physical, and Thermal Properties of Granite Rocks", UCRL-86967, Lawrence Livermore Laboratory, Nov., 1981.

51. Hibbit, H.D., "Some Properties of Singular Isoparametric Elements", Int. J. Num. Mtd. Engng., Vol.11, pp.180-184, 1977.

52. Hibbit, H.D. and Marcal, P.V., "Numerical Thermo-Mechanical Model for the Welding and Subsequent Loading of a Fabricated Structure", Computers & Structures Vol.3, pp.1145-1174, 1973.

53. Hilton, H.H., "Thermal Stress in Thick-Walled Cylinders Exihibiting Temperature-Dependent Viscoelstic Properties of the Kelvin Type", Proc. 2nd U.S. Nat. Cong. Appl. Mech., ASME, pp.547, New York, N.Y., 1954.

54. Hughes, T.J.R., "Unconditionally Stable Algorithms for Nonlinear Heat Conduction", Comp. Mtd. Appl. Mech. Engng., Vol.10, pp.135-139, 1977.

55. Hughes, T.J.R. and Taylor, R.L., "Unconditionally Stable Algorithms for Quasi-Static Elasto/Viscoplastic Finite Element Analysis", Computers & Structures, Vol.8, pp.169-173, 1978.

56. Hughes, T.J.R. and Brooks, A., "A Multi-Dimensional Upwinding Scheme with No Crosswind Diffusion", 3rd Int. Conf. on Finite Element Methods in Fluid Flow, 1980.

57. Hughes, T.J.R., "A simple Scheme for Developing Upwind Finite Elements", Int. J. Num. Mtd. Engng., Vol.12, pp.1359-1365, 1978.

58. Inglis, C.E., Trans. Roy. Inst. Naval Architects, Vol.60, pp.219-230, 1913.

59. Irons, B.M., "Application of a Theorem on Igenvalues to Finite Element Problems", CR/132/70, Univ. of Wales, Dept. of Civil Engng., Swansea, 1970.

60. Irwin, G.R., "Analysis of Stresses and Strains near the End of a Crack Transversing a Plate", I. Appl. Mech., 24, Vol.79, pp.361-364, 1957.

61. Irwin, G.R., "Fracture Mechanics", Structural Mechanics, Pegamon Press, N.Y., pp.361-364, 1957.

62. Jegbefume, E.U. and Thompson, T.W., "The Influence of Temperature and Nonelastic Behavior on Roof Collapse and Subsidence Resulting from Underground Coal Gasification", In Situ, Vol.7(2), pp.143-174, 1983.

63. Kanchi, M.B., Zienkiewicz, O.C. and Owen, D.R.J., "The Visco-Plastic Approach to Problems of Elasticity and Creep Involving Geometric Nonlinear Effects", Int. J. Num. Mtd. Engng., Vol.12, pp.169-181, 1978.

64. King, I.P., "Finite Element Analysis of Two-Dimensional, Time-Dependent Stress Problem , Report No. 65-1, University of California, Berkely, 1965.

65. Knott, K.N., "Fundamentals of Fracture Mechanics", Butterworths, London. 1973.

66. Koteras, J.R., "A Hybrid Finite Element for Determination of Stress Intensity Factors at a Crack Tip", Timco Report 73-2, The university of Texas at Austin, 1973.

67. Kotowski, M.D. and Gunn, R.D., "Theoretical Aspects of Reverse Combustion in the Underground Gasification of Coal", Laramie Energy Center, Laramie, Wyoming, March, 1976.

68. Kumar, V., Morjaria, M. and Mukherjee, S., "Numerical Integration of Some Stiff Constitutive Models of Inelastic Deformation", J. Engng. Mat. Tech. Vol.102, pp.92-96, 1980.

69. Lama, R.D. and Vutukuri, V.S., "Handbook on Mechanical Properties of Rock", Series on Rock and Soil Mechanics, Vol.II, 1978.

70. Langer, M. et al, "Das Verformungs und Bruchverhalten von Steinsalz", Bundesanstalt fur Geowissenschaften und Rohstoffe, Hannover, 1980.

71. Langland, R.T. and Trent, B.C., "Computer Models to Support Investigations of Surface Subsidence and Associated Ground Motion Induced by Underground Coal Gasification", Proc. 7th Annual UCC Symp., pp.303-314, Sept., 1981.

72. Leaderman, H., "Elastic and Creep Properties of Filamentous Materials and Other High Polymers", Textile Foundation, pp.175, 1943.

73. Lee, K.Y., "Thermo-Mechanical Responses for Porous Permeable Media with Applications to Underground Coal Gasification", METC/CR-78/17, Morgantown, W.Va., 1978.

74. Lees, M., "A Linear Three Level Difference Scheme for Quasilinear Parabolic Equations", Math. Comp., Vol.20, pp.516-622, 1966.

75. Lin, Y.T., "Structural Mechanics Simulations Associated with Underground Coal Gasification", MERC/E(40-1) 5088, Morgantown, W.Va. 1978.

76. Liu, Y.T. and Hsu, T.R., "On the Multidimensional Creep Deformation of Ice by Finite Element Analysis", J. Energy Resource Tech., Vol.104, pp.193-198, 1982.

77. Lockett, F.J. and Morland, L.W., "Thermal Stresses in A Viscoelastic Thin-Walled Tube with Temperature Dependent Properties", Int. J. Engng. Sci., Vol.5, pp.879-898, 1967.

78. Lubliner, J. and Sackman, J.L., "On Uniqueness in General Linear Viscoelasticity", Quart. Appl. Mech., Vol.25, pp.129-138, 1967.

79. McClintock, F.A. and Walsh, J.B., "Friction on Griffith Cracks in Rock under Pressure", 4th U.S. National Congress for Applied Mechanics, Berkeley, Ca., pp.1015-1021, 1962.

80. Mead, S.W., Campbell, J.H., Ganow H.C., Langland, R.T., Greenlaw, F.T., Wong, F.T. and Homsy, R.V., "LLL Environmental Studies of In-Situ Coal Gasification", UCRL-50032, Lawrence Livermore Laboratory, Aug., 1978.

81. Min, O.K., "Finite Element Modeling of Thermo-Mechanical Responses Associated with Underground Coal Conversion", DOE/1c/10335-t1, Feb., 1983.

82. Misura, A.K. and Murrel, S.A.F., "An Experimental Study of the Effect of Temperature and Stress on the Creep of Rocks", Geophys. J., Vol.9, pp.509-539, 1965.

83. Morjaria M. and Mukherjee S. "Finite Element Analysis of Time-Dependent Inelastic Deformation in The Presence of Transient Thermal Stresses", Int. J. Num. Mtd. Engng., Vol.17, pp.909-921, 1981.

84. Morland, L.W. and Lee, E.H., "Stress Analysis for Linear Viscoelastic Materials with Temperature Variations", Transactions, Society of Rheology, Vol.4, 1960.

85. Muki, R. and Sternberg, E., "On Transient Thermal Stresses in Viscoelastic Materials with Temperature-Dependent Properties", J. Appl. Mech., Vol.28, pp.193-207, June, 1961.

86. Muskhelishvili, N.I., "Some Basic Problems in the Theory of Elasticity", Noordhoff, Gronigen, Netherlands, 1953.

87. Nayak, G.C. and Zienkiewicz, O.C., "Elasto-Plastic Stress Analysis, A Generalization for Various Constitutive Relations Including Strain Softening", Int. J. Num. Mtd. Engng., Vol.5, pp.113-135, 1972.

88. Nipp, H.K., "Temperatureinflusse auf Rheologische Spannungzustande im Salzgebirge", Bericht Nr. 82-36, Institut fur Statik, Techmische Universitat Braunschwg, 1982.

89. Oden, J.T., "Finite Elements of Nonlinear Continua", McGraw-Hill Co., 1972.

90. Owen, D.R.J. and Hinton, E., "Finite Element in Plasticity", Pineridge Press, 1980.

91. Penny, R.K. and Mariott, D.L., "Design for Creep", McGraw-Hill, London, 1971.

92. Pfeifle, T.W. and Senseny, P.E., "Steady-state Creep of Rock Salt in Geoengineering", Proc. 23rd Symp. on Rock Mechanics, Berkeley, Ca., pp.307-314, 1982.

93. Sanada, Y. and Honda, H., "Creep in Coal over the Temperature Range 200°C to 370°C", Fuel, Vol.42, pp.479-486, 1963.

94. Sandhu, R.S., Wilson, E.L. and Raphael, J.M., "Two-Dimensional Stress Analysis with Incremental Construction and Creep", Report No. 67-34, University of California, Berkely, Ca., 1967.

95. Schapery, R.A., "Application of Thermodynamics to Thermomechanical Fracture and Birefringent Phenomena in Viscoelastic Media", J. Appl. Phys., 35, pp.1451-1465, 1964.

96. Schwarzl, F. and Staverman, A.J., "Time-Temperature Dependence of Linear Viscoelastic Behavior", J. Appl. Phys., Vol.23, pp.838, 1952.

97. Segerlind, L.J., "Applied Finite Element Analysis", John Wiley & Sons, Inc., 1976.

98. Sharma, M.G. "Seminar on Mechanics of Polymers", The Penn. State University, University Park, Pa., June, 1967.

99. Shoemaker, H.D., Shuck, L.Z., Haynes, R.R. and Advani, S.H., "Directional Viscoelastic Properties of the Pittsburg Coal at Elevated Temperature in Compression and Shear", MERC/RI-76/5, 1976.

100. Sih, G.C., "On the Singular Character of Thermal Stresses near a Crack Tip", J. Appl. Mech., Vol.29, pp.587-589, 1962.

101. Singer, J.M. and Tye, R P., "Thermal, Mechanical, and Physical Properties of Selected Bituminous Coals and Cokes", RI-8364, U.S. Bureau of Mines, 1979.

102. Skafa, P.V., "Underground Gasification of Coal", UCRL-TRANS-10880, English Translation(1975) from Russian(1960).

103. Smith, J.M. and Van Ness, H.C., "Introduction to Chemical Engineering Thermodynamics", McGraw-Hill Co., 3rd Ed., 1975.

104. Srinatha, H.R. and Lewis, R.W., "A Finite Method for Thermoviscoelastic Analysis of Plane Problems", Comp. Mtd. Appl. Mech. Engng., Vol.25, pp.21-23, 1981.

105. Sternberg, E. and Gurtin, M.E., "Uniqueness in the Theory of Thermo-Rheologically Simple Ablating Viscoelastic Solids", Prog. Appl. Mech., The Prager Aniversary Volume, The Macmillan Company, pp.373-384, 1963.

106. Stricklin, J.A , Haisler, W. and Reisemann, W., "Evaluation of Solution Procedure of Material and/or Geometrically Nonlinear Structural Analysis", AIAA, Vol.11, pp.292-299, 1973.

107. Sutherland, H.J., Schuler, K.W. and Benzley, S.E., "Observation and Analytic Calculations of Strata Movement above Idealized Mine Structure", Proc. 7th Annual UCC Symp., pp.290-302, Sept., 1981.

108. Sutherland, W.H., "AXICRP-Finite Element Computer Code for Creep Analysis of Plane Stress, Plane Strain and Axisymmetric Bodies", Nucl. Engng. Design, Vol.11, pp.769-785, 1970.

109 Tada, H., "The Stress Analysis of Cracks. Handbook", Del Research Corp., Lellertown, Pa., 1973.

110. Taylor, R.L. and Chang, T.Y., "An Approximate Method for Thermoviscoelastic Stress Analysis", Nucl. Engng. Design, Vol.4, pp.21-28, 1966.

111. Taylor, R.L., Pister, K.S. and Goudreau, G.L. "Thermomechanical Analysis of Viscoelastic Solids", Int. J. Num. Mtd. Engng., Vol.2, pp.45-59, 1970.

112. Thompson, T.W., Menezes, J.J. and Gray, K.E., "Roof Stabilities and Subsidence on In-Situ Gasification of Coal", Proc. 18th U.S. Symp. on Rock Mechanics, pp.2b1-1 to 2b1-5, 1977.

113. Thorsness, C.B., Rozsa, R.B. and Wong, R., "Two-Dimensional Modeling of In-Situ Coal Gasification", Lawrence Livermore Laboratory UCRL-79528, June, 1977.

114. Thresher, R.W. and Smith, F.W., "Stress Intensity Factors for a Surface Crack in a Finite Solid", J. Appl. Mech., Vol.39, 1972.

115. Tong, P., Pian, T.H. and Larry S.J., "A Hybrid Finite Element Approach to Crack Problems in Plane Elasticity", Int. J. Num. Mtd. Engng., Vol.7, pp.297-308, 1973.

116. Turner, S.M., Stephenson, D.E. and Shaw, D.E., "The Thermal Effects on Subsidence Induced by UCG Process", Proc. 7th Annual UCC Symp., pp.738-757, Sept., 1981.

117. "Proceedings of the 2nd Annual Underground Coal Gasification Symposium", MERC/SP-7613, Morgantown, W.Va., Aug., 1976.

118. "Proceedings of the 3rd Annual Underground Coal Conversion Symposium", CONF-770652, Fallen Leaf Lake, Ca., June, 1977.

119. "Proceedings of the 5th Annual Underground Coal Conversion Symposium", CONF-790630, Alexandria, Va. June, 1979.

120. "Proceedings of the 6th Annual Underground Coal Conversion Symposium", CONF-800716, Shangri-La, Ok, July, 1980.

121. "Proceedings of the 7th Annual Underground Coal Conversion Symposium , CONF-810923, Fallen Leaf Lake, Ca., Sept., 1981.

122. "Proceedings of the 8th Annual Underground Coal Conversion Symposium", Keystone, Colorado, Aug., 1982.

123. Wang, H.F., "Thermoelastic Solutions for In-Situ Gasification of Coal", Ph.D. Dissertation, Dept. of Mechanical Engineering and Mechanics, West Virginia University, Morgantown, W.Va., 1978.

124. Waters, P.L., "Rheological Properties of Coal during the Early Stage of Thermal Softening", Fuel, Vol.41, pp.3-14, 1962.

125. Willam, K.J., "Numerical Solution of Inelstic Rate Process", Computers & Structures, Vol.8, pp.511-531, 1978.

126. Wilson, E.L. and Nickell, R.E., "Application of Finite Element Method to Heat Conduction Analysis", Nucl. Engng. Design, Vol.4, pp.276-286, 1966.

127. Wit R.D. and Cooly W.E., "Mechanics of Brittle Fracture", pp.795-804, McGraw-Hill Co., 1979.

128. Wood, W.L. and Lewis, R.W., "A Comparison of Time Marching Schemes for the Transient Heat Conduction Equation", Int. J. Num. Mtd. Engng., Vol.9, pp.679-689, 1975.

129. Yamada, Y., "Constitutive Modeling of Inelastic Behavior and Numerical Solution of Nonlinear Problems by the Finite Element Method", Computers & Structures, Vol.8, pp.543-553, 1978.

130. Zienkiewicz, O.C., "The Finite Element Methods", McGraw-Hill Co., 3rd Ed., 1977.

131. Zienkiewicz, O.C., "A New Look at the Newmark, Houbolt, and Other Time Stepping Schemes, A Weighted Residual Approach", Int. J. Earthq. Engng. Struct. Dynamics, Vol.5, pp.413-418, 1977.

132. Zienkiewicz, O.C. and Cheung Y.K., "The Finite Element Method in Structural and Continuum Mechanics", McGraw-Hill, 1967.

133. Zienkiewicz, O.C. and Cormeau, I.C., "Viscoplasticity and Creep in Elastic Solids - A Unified Solution Procedure", Int. J. Num. Mtd. Engng., Vol.8, pp.821-845, 1974.

134. Zienkiewicz, O.C., Gallagher, R.H. and Hood, P., "Newtonian and Non-Newtonian Viscous Incompressible Flow. Temperature Induced Flow. Finite Element Solution", Int. Conf. Math. Finite Element Appl., Brunell Univ., 1975.

135. Zienkiewicz, O.C. and Parkesh, C.J., "Transient Field Problems - Two and Three Dimensional Analysis by Isoparametric Finite Elements", Int. J. Num. Mtd. Engng., Vol.2, pp.61-71, 1970.

136. Zienkiewicz, O.C., Watson, M. and King, I.P., "A Numerical Method of Viscoelastic Stress Analysis", Int. J. Mech. Sci., Vol.10, pp.807-827, 1968.

137. Zudans, Z., Reddi, M.M., Fishman, H.M., and Tsai, H.C., "Elastic-Plastic Creep Analysis of High Temperature Nuclear Reactor Components", Nucl. Engng. Design, Vol.28, pp.414-445, 1974.

Appendix A

FAILURE CRITERIA AND THERMOELASTIC LINE CRACK PROBLEMS

The significance of intense and localized concentration of stress along sharp notches was first emphasized by Inglis [58]. Further development of fracture mechanics theory were initiated by Griffith and Irwin [43,60,61] who found that the characteristics for initiation and propagation of brittle cracks could be expressed as a function of the stress, flaw size, geometry, etc. This also made it possible that the stress intensity factor, which represents the singularity of the stress field near the crack tip, can provide a useful index for investigations of the brittle fracture strength. Here, the failure criteria based on the principal stresses are presented along with a brief review of two-dimensional thermoelastic line crack problems and stress intensity factor expressions.

A.1 FAILURE CRITERIA

The following two-dimensional failure theories are adopted and incorporated within the framework of the thermomechanical response models:

a) The compressive failure criterion, defined by McClintock and Walsh [79], is

$$S_c(T) = \sigma_3 - \sigma_1 \frac{[(1 + \mu_f^2)^{1/2} + \mu_f]}{[(1 + \mu_f^2)^{1/2} - \mu_f]} \qquad (A.1)$$

where σ_1 is the major principal stress, σ_3 is the minor principal stress, $S_c(T)$ is the uniaxial compressive strength, and μ_f is the internal friction coefficient.

b) Following Griffith [43] with $3\sigma_1 + \sigma_3 > 0$, tensile failure occurs when

$$S_t(T) = \sigma_1 \tag{A.2}$$

and shear failure occure for $3\sigma_1 + \sigma_3 < 0$ when

$$8\, S_t(T) = -(\sigma_1 - \sigma_3)^2 / (\sigma_3 + \sigma_1) \tag{A.3}$$

where $S_t(T)$ is the uniaxial tensile strength and temperature-dependent strength of materials can be incorporated for thermomechanical analyses.

A.2 THERMOELASTIC LINE CRACK PROBLEMS

The first rational approach to linear elastic fracture mechanics(LEFM) was established by Griffith [43]. The basic concept is to evaluate the decrease of elastic energy associated with a specified crack length. Reasoning that this amount of energy must be equal to the energy required to form new crack surfaces at the point of fracture initiation, the critical stress for the crack length 2a is given by

$$\sigma_c = (2E\gamma / \pi a)^{1/2} \tag{A.4}$$

where E is the Young's modulus and γ is the specific surface energy of the material.

Introducing a material parameter K_c, the fracture toughness/the critical value of stress intensity factor,

$$K_c = \sigma_c(\pi a)^{1/2} \tag{A.5}$$

the magnitude of the stress field around the crack tip is measured by the stress intensity factors, $K_{I,II,III}$, when the load or crack size is kept below the point of unstable crack extension [43,65,109]. It is also noted that the singular effects and prediction of the stress field around the crack tip can deviate from the response of real materials, in that plastic deformations occur right at the crack tip and the crack tip stresses are finite instead of infinite. However, when the plastic zone is small compared to the crack length and uncracked dimensions, the stress intensity factors serve to characterize the crack tip stress field.

For thermoelastic crack problems, it is known that when a temperature field is disturbed by the presence of cracks or flaws, the resulting high elevation of thermal stresses can cause crack propagation. Sih [100] has shown that, for a steady-state temperature distribution, the crack tip stresses are identical to those for the isothermal problems involving mechanical responses. Lee [73] and Wang [123] have analyzed the line and elliptic crack problems with constant temperature and heat flux on the crack surface. These analyses are based upon the conformal

mapping method combined with the complex variable technique developed by Muskhelishvili [86] for steady-state thermoelasticity. The general procedure of the above analysis and the results of two specific problems are only presented here.

An infinite plate containing a single line crack of length 2a is considered a homogeneous, isotropic and elastic medium. The thermomechanical properties are assumed to be independent of temperature. With the complex variable formulation of temperature field, the analytical solution procedure is as follows;

a) The conformal mapping technique is applied to map the line crack into the unit circle using the mapping function

$$Z = W(\xi) = a(\xi + 1/\xi)/2 \tag{A.6}$$

where Z represents the real plane and ξ designates the mapped plane.

b) The thermal dislocation term due to the slit, which permits free deformation under the temperature distribution, is expressed by

$$U^* + iV^* = \bar{\alpha} \int_1^2 W(z)\, dz \tag{A.7}$$

where U^* and V^* are the x and y components of the relative displacement respectively, $\bar{\alpha}$ is the coefficient of thermal expansion and W(z) is the analytic function for the thermal dislocation.

c) The stress and displacement fields are expressed in terms of the Kolosov functions and the thermal dislocation terms are added to the displacement term for the isothermal case.

d) The coefficients of the Kolosov functions are determined by applying boundary conditions such as a stress-free crack surface and the conditions of the single-valuedness of displacement.

e) The stress field near the crack tip is evaluated in terms of the Kolosov functions and stress intensity factors are represented by the real and imaginary part of the complex quantity.

$$K_I + i\, K_{II} = 2\, \phi'(\xi)/\sqrt{a}\Big|_{\xi=1} \tag{A.8}$$

where $\phi'(\xi)$ is the derivative of the complex Kolosov function with respect to ξ .

The details of the above procedure can be found in Wang [123] and two specific problems for Mode I and II cases are given with the boundary conditions as shown in Figure A.1. Analytic expressions of stress intensity factors under the plane strain condition are expressed as follows;

Mode I:

$$K_I = -\sqrt{\pi}\,\frac{(1+\nu)}{(1-\nu)}\,\alpha\, G\, T_0\, a^{1/2} \tag{A.9}$$

Mode II:

$$K_{II} = \sqrt{\pi}\,\frac{(1+\nu)}{2(1-\nu)}\, a^{3/2}\, \alpha\, G\, C \tag{A.10}$$

and for the plane stress condition ν is replaced by $\nu/(1-\nu)$.

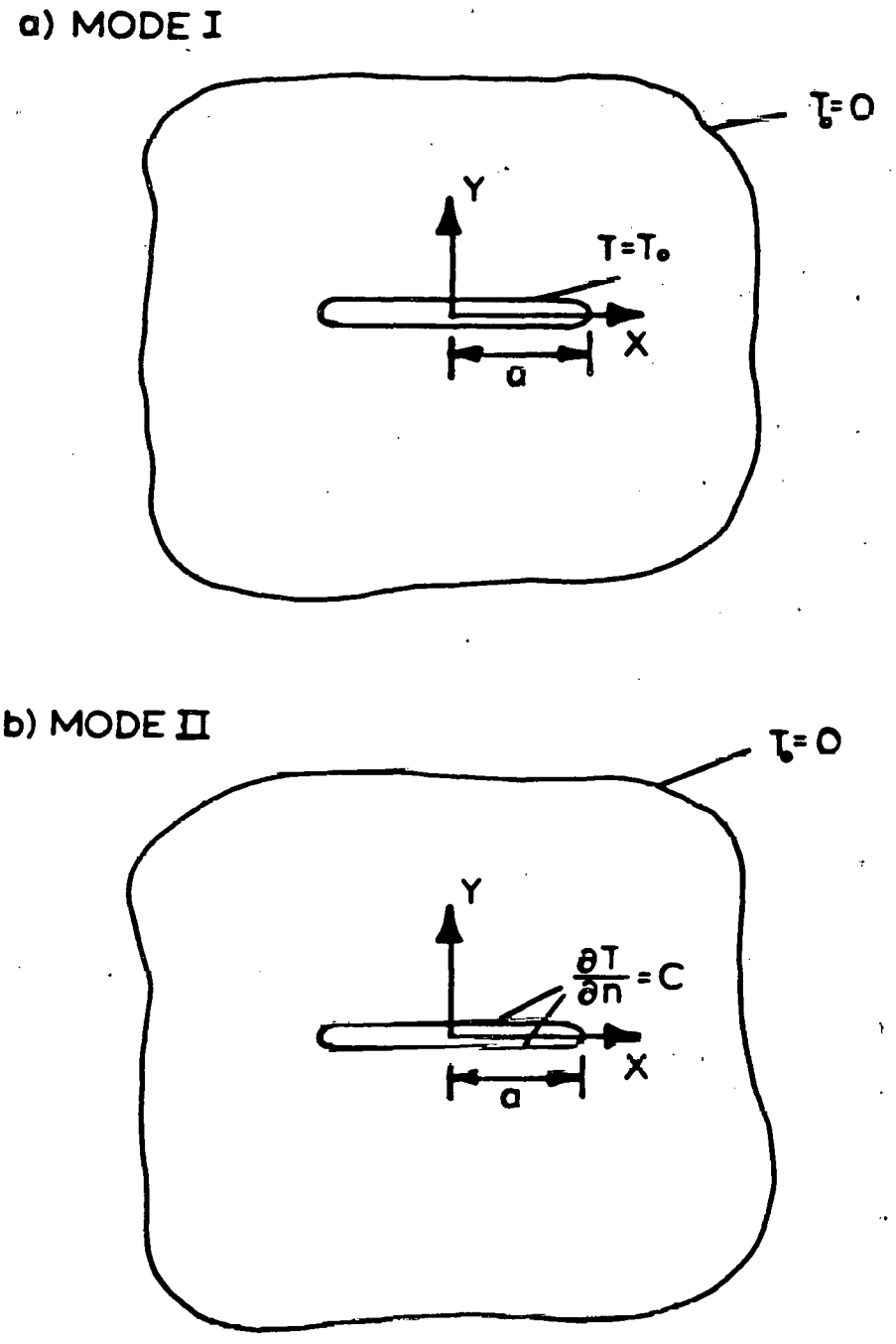

Figure A.1: Thermoelastic Line Crack Problems and Boundary Conditions

Appendix B

FORMULATION OF FRACTURE MECHANICS

It has been known that there exists a singularity in the stress field associated with the crack tip and that the strains and stresses along any radial line in the vicinity of crack are proportional to $r^{-1/2}$ for an isotropic medium. Thus, the convergence of the finite element solution is no longer ensured in the vicinity of crack tip due to this strain singularity. For the standard constant strain element, the convergence of the solution is no longer valid since by definition, the strain within each element is constant and as such can not adequately represent the true strain which approaches infinity near the tip. The treatment of the strain singularity in the finite element method entails use of special elements which embed the singularity for the crack tip region [66,115] or use of the conventional isoparametric element modified for the crack tip singularity [5,18,12,49].

Here, the singularity at the crack tip in a homogeneous, isotropic elastic medium is incorporated by suitably distorting the conventional isoparametric element. The displacement method is presented to compute the stress intensity factors in the LEFM problems associated with thermal loads.

B.1 ISOPARAMETRIC DEGENERATE SINGULAR ELEMENT

Hibbit [51], Barsoum [12] and Henshell and Shaw [49] have indicated that the standard quadratic isoparametric element can be used successfully by shifting the mid-side node to a quarter point toward the crack tip. It has been observed that these elements behave even better when one side of the quadratic quadrilaterals are collapsed to form degenerate triangles. However, the degenerate triangles often lead to unstable results if the mid-side node across the tip is not located precisely on a straight line, because an incorrect strain singularity is obtained due to pertubation of mid-side nodes. For this investigation, Akay [5] introduced the following modification on the shape functions to prevent the indeterminate slope situation at the collapsed corner.

A typical eight-noded isoparametric parent element is shown in Figure B 1.a for which the shape functions in curvilinear coordinates are given by [130]:

$$N_i = \frac{1}{4}(1 + \xi_0)(1 + \eta_0)(\xi_0 + \eta_0 - 1) \quad \text{for corner nodes}$$

$$N_i = \frac{1}{2}(1 + \xi^2)(1 + \eta_0) \quad \text{for } \xi_i = 0$$

$$N_i = \frac{1}{2}(1 - \eta^2)(1 + \xi_0) \quad \text{for } \eta_i = 0 \qquad \text{(B.1)}$$

where

$$\xi_0 = \xi\,\xi_i, \quad \eta_0 = \eta\,\eta_i \qquad \text{(B.2)}$$

A collapsed triangular element is obtained by superimposing the nodes 1, 4 and 8 of the parent square element as shown in Figure B.1.b. Since the shape function varies linearly for constant η and quadratically in the other direction, a nonpolynomial surface with indeterminate slopes is formed at the collapsed node as illustrated in Figure B.1.c.

For obtaining correct responses from the trianglar element, the above shape functions are modified so that they also vary quadratically in the ξ direction. This is accomplished by modifying N_6 to yield

$$N_6^* = N_6(1 + \xi)/2 = (1 - \eta^2)\ (1 + \xi)^2/4 \qquad \text{(B.3)}$$

with N_2 and N_3 are subsequently modified by replacing N_6 by N_6^* . Therefore, the quadratic isoparametric quadrilateral degenerates successfully into a quadratic triangular by assigning the same coordinate for the nodes at the collapsed corner and modifying the related mid-side node as suggested above.

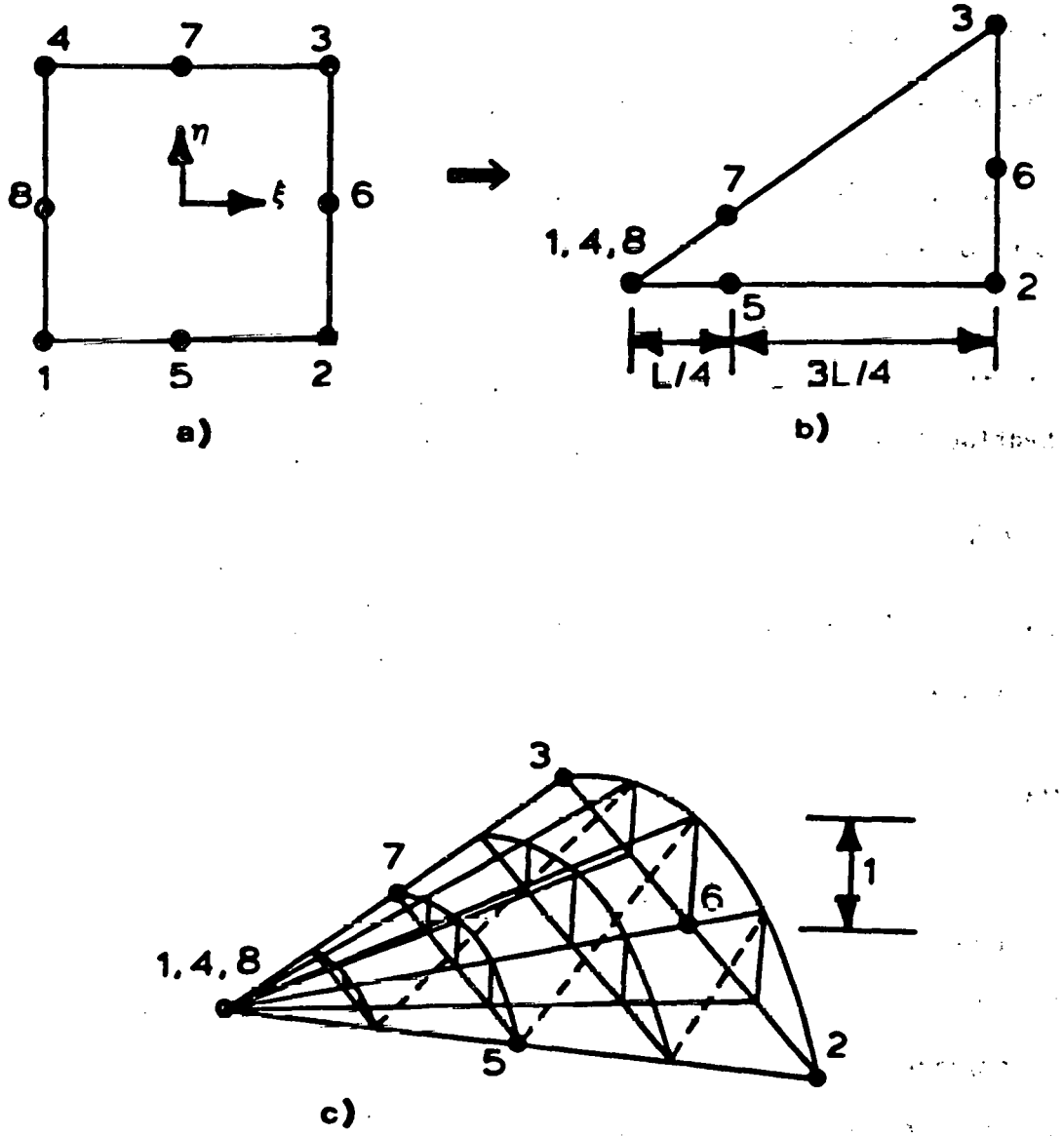

Figure B.1: Quadratic Isoparametric and Degenerate Singular Element

B.2 COMPUTATION OF STRESS INTENSITY FACTORS

The four most common techniques for obtaining stress intensity factor values are i) displcement method, ii) stress method, iii) energy release method, and iv) J integral method [65].

For the purpose of minimizing computational errors, the displacement method is widely adopted in finite element methods. When the mid-side nodes of the collapsed triangle are moved to the quarter point toward the collapsed node, the variation of the displacement in the radial direction is of the form [49]

$$U_i = A_i + B_i\, r^{1/2} + C_i\, r \tag{B.4}$$

where A_i, B_i and C_i are constants. Subsequently, the strain components vary as

$$\varepsilon_{ij} = a_{ij} + b_{ij}\, r^{-1/2} \tag{B.5}$$

Since it is precisely the $r^{1/2}$ term in eqn.(B.4) which contributes to the $r^{-1/2}$ strain singularity in eqn.(B.5), a consistent way of obtaining expressions for stress intensity factors in sufficiently small crack tip elements is to equate the coefficient of the $r^{1/2}$ term in the analytical and numerical displacement expression near the tip. The displcement variation along the crack surface of crack tip element takes the form

$$U = U_1 + (4U_2 - U_3 - 3U_1)\,(r/L)^{1/2} + (2U_3 + 2U_1 - 4U_2)\,(r/L) \tag{B.6}$$

where U_i are nodal displacements on the crack surface and L is the surface length of the crack element. For the crack opening mode, the coefficient of the $r^{1/2}$ term in the analytical expression is given by [114]

$$B_i = K_I (K^* + 1)/(G\sqrt{8\pi}) \tag{B.7}$$

where $K^* = (3 - \nu)/(1 + \nu)$ for the plane stress condition, $K^* = 3 - 4\nu$ for the plane strain condition and the shear modulus G is invariant.

Equating the coefficient in eqn.(B.6) to the corresponding value in eqn.(B.7), the expression for the stress intensity factors is [4]

$$K_{I,II} = [2G\sqrt{2\pi}/(K^* + 1)]\,[(4U_2 - U_3 - 3U_1)/\sqrt{L}] \tag{B.8}$$

where U_i are the nodal displacements on the crack surface with normal and horizontal displacements designated for the mode I and mode II cases, respectively. The finite element formulation described in Section 3.2 is adopted for the thermally-loaded crack problems. For problems subjected to the surface traction or the heat flux prescribed on the crack surface, the equivalent nodal forces for the crack tip element are computed from the surface integration. Table B.1 lists equivalent nodal forces for the quadratic isoparametric and crack tip singular elements.

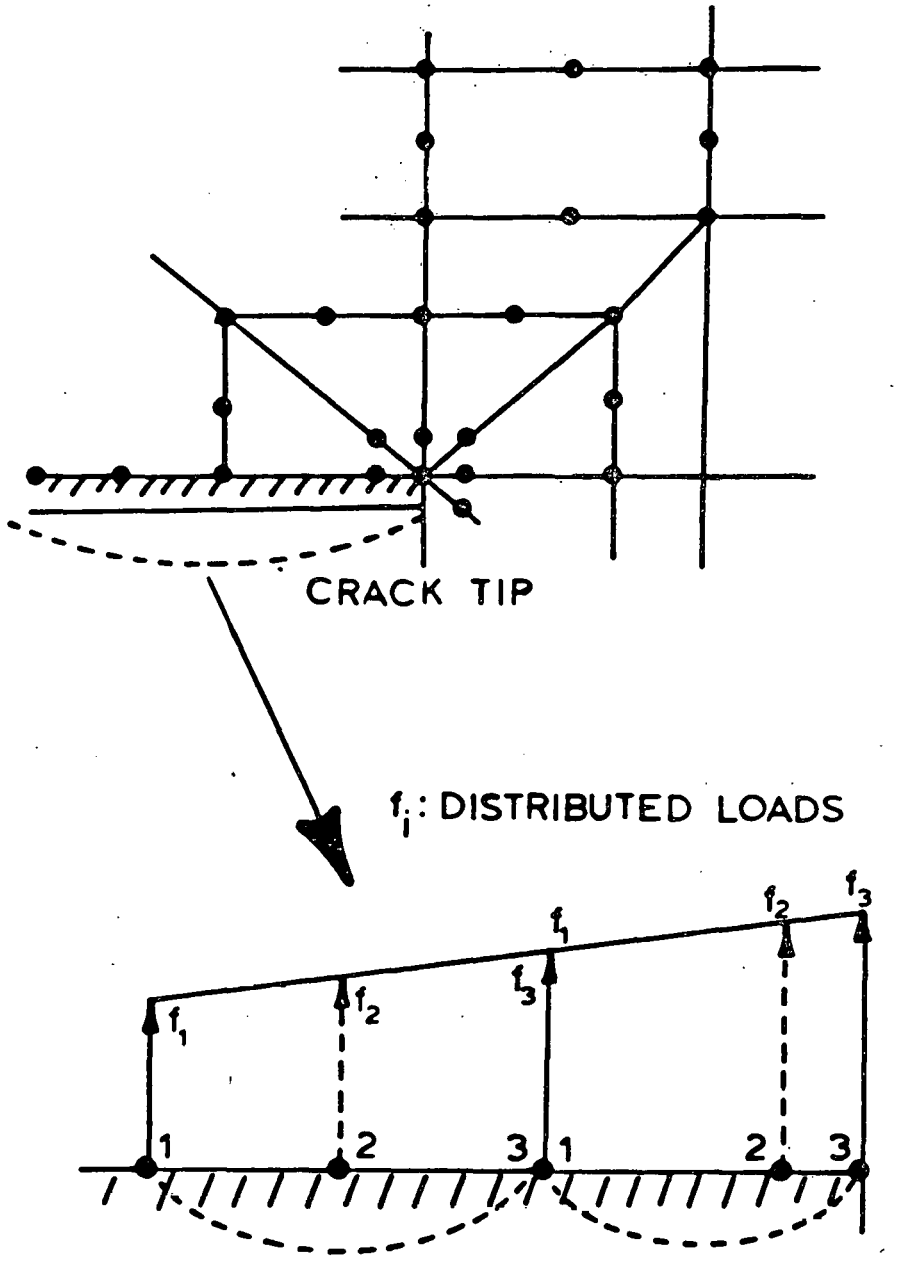

Figure B.2: Crack Tip Singular Element and Distributed load on Crack Surface

Equivalent Nodal Force: $f_i^{eq} = L(af_1 + bf_2 + cf_3)/2$

Equivalent Nodal Force		Coefficient		
		a	b	c
Quadratic isoparametric element	f_1^{eq}	4/15	2/15	-1/15
	f_2^{eq}	2/15	16/15	2/15
	f_3^{eq}	-1/15	2/15	4/15
Crack tip singular element	f_1^{eq}	7/15	4/15	-1/15
	f_2^{eq}	-1/15	16/15	1/15
	f_3^{eq}	-1/15	0	1/15

Table B.1

Equivalent Nodal Force Computation for Quadratic Isoparametric and Degenearte Singular Elements

Appendix C

DETAILED EXPRESSIONS OF ELEMENT MATRICES

The matrix and vector notations adopted in Chapter III are presented here. The stress, strain, and displacement vectors for the plane stress and strain conditions are defined by

$$\boldsymbol{\sigma} = \{\sigma_{xx},\ \sigma_{yy},\ \tau_{xy}\}^T \tag{C.1}$$

$$\boldsymbol{\varepsilon} = \{\varepsilon_{xx},\ \varepsilon_{yy},\ \gamma_{xy}\}^T \tag{C.2}$$

$$\mathbf{U} = \{U_i,\ V_i\}^T \tag{C.3}$$

where U_i and V_i denote nodal displacement in the x and y directions, respectively. For axisymmetric problems,

$$\boldsymbol{\sigma} = \{\sigma_{zz},\ \sigma_{rr},\ \sigma_{\theta\theta},\ \tau_{rz}\}^T \tag{C.4}$$

$$\boldsymbol{\varepsilon} = \{\varepsilon_{zz},\ \varepsilon_{rr},\ \varepsilon_{\theta\theta},\ \gamma_{rz}\}^T \tag{C.5}$$

Based upon the above conventional order of stress and strain vectors, the associated matrices and element equations are as follows;

a) Matrix of material constant ($\boldsymbol{\sigma} = \mathbf{D}_e \boldsymbol{\varepsilon}$, $\boldsymbol{\varepsilon}_c = \bar{\mathbf{C}}\ \mathbf{D}_0^{-1}\boldsymbol{\sigma}$)

Plane stress condition:

$$\mathbf{D}_e = \frac{E}{(1-\nu)} \begin{bmatrix} 1 & \nu & 0 \\ & 1 & 0 \\ \text{symmetric} & & (1-\nu)/2 \end{bmatrix}$$

$$\mathbf{D}_o^{-1} = \begin{bmatrix} 1 & -\nu & 0 \\ & 1 & 0 \\ \text{symmetric} & & 2(1+\nu) \end{bmatrix} \quad \nu = 1/2$$

(C.6)

Plane strain condition:

$$\mathbf{D}_e = \frac{E(1-\nu)}{(1+\nu)(1-2\nu)} \begin{bmatrix} 1 & \nu/(1-\nu) & 0 \\ & 1 & 0 \\ \text{symmetric} & & (1-2\nu)/2(1-\nu) \end{bmatrix}$$

$$\mathbf{D}_o^{-1} = \begin{bmatrix} (1+\nu)(1-\nu) & -\nu(1+\nu) & 0 \\ & (1+\nu)(1-\nu) & 0 \\ \text{symmetric} & & 2(1+\nu) \end{bmatrix} \quad \nu = 1/2$$

(C.7)

Axisymmetric problem:

$$\mathbf{D}_e = \frac{E(1-\nu)}{(1+\nu)(1-2\nu)} \begin{bmatrix} 1 & \nu/(1-\nu) & \nu/(1-\nu) & 0 \\ & 1 & \nu/(1-\nu) & 0 \\ \text{symmetric} & & 1 & 0 \\ & & & (1-2\nu)/2(1-\nu) \end{bmatrix}$$

$$\mathbf{D}_o^{-1} = \begin{bmatrix} 1 & -\nu & -\nu & 0 \\ & 1 & -\nu & 0 \\ & & 1 & 0 \\ \text{symmetric} & & & 2(1+\nu) \end{bmatrix} \quad \nu = 1/2$$

(C.8)

b) Thermal strains (ε_T)

Plane stress condition:

$$\varepsilon_T = \alpha \Delta T \{1, 1, 0\}^T \tag{C.9}$$

For plane strain condition, α is replaced by $(1 + \nu)\alpha$.

Axisymmetric problem:

$$\varepsilon_T = \alpha \Delta T \{1, 1, 1, 0\}^T \tag{C.10}$$

c) Differential operator $\mathbf{B}$ ($\varepsilon = \mathbf{B}\mathbf{U}$)

Plane stress and strain conditions:

$$\mathbf{B} = \begin{bmatrix} N_{i,x} & 0 & N_{i,y} \\ 0 & N_{i,y} & N_{i,x} \end{bmatrix}^T \tag{C.11}$$

Axisymmetric problem:

$$\mathbf{B} = \begin{bmatrix} 0 & N_{i,r} & N_i/r & N_{i,z} \\ N_{i,z} & 0 & 0 & N_{i,r} \end{bmatrix}^T \tag{C.12}$$

Appendix D

COMPUTER CODE TMFC

A concise description of the developed finite element code TMFC is presented. The code is aimed for both research and field applications and has been calibrated against various examples. Although the code TMFC is presently for two-dimensional plane and axisymmetric geometries associated with the uncoupled thermoelastic, thermoviscoelastic, and fracture analyses, it provides a basis for further possible developments so that plasticity, large deformation, and crack propagation with creeping flow can be adopted in the UCC and in-situ waste disposal simulations.

The code TMFC consists of three main processors; namely, pre-processor, main-processor, and post-processor. The working in-core space for each processor is dynamically allocated and the execution of a modularized function is performed by macro instruction. The capabilities of each processor are briefly summarized below.

1. Pre-processor
   a) Generation of nodal points, element connectivity, boundary constraint codes, and material numbers.
   b) Graphical presentation of the generated information.

2. Main-processor
   a) Thermal responses:

1) Steady-state or transient heat conduction equation with two-point recurrence scheme.

2) Heat source/sink term.

3) Upwinding scheme for the convective diffusion equation.

4) Temperature-dependent thermal coefficients.

5) Time-dependent bounadry temperature condition.

6) Constant or variable reference temperature.

b) Thermoelastic responses:

1) Temperature-dependent elastic constants.

2) Two-dimensional failure criteria.

c) Fracture responses:

1) Crack tip singular element with quadratic isoparametric element.

2) Computation of stress intensity factors by use of the displacement method.

d) Thermoviscoelastic responses:

1) Thermorheologically simple material postulate with the generalized creep and temperature shift functions.

2) Incremental solution algorithm with the strain rate expression.

3) Automatic time step size selection.

4) Linear interpolation of the retrieved temperature solutions at each time step.

5) Incorporation of element failure.

3. Post-processor

a) Sorting of output data for thermal and mechanical responses.

b) Graphical presentation of results such as temperature, displacement, stress, and subsidence.

In order to handle large capacity field problems, the required information is retrieved or saved by using external files while the in-core space is mainly used for the computational procedure. In addition, a long-term analysis requires a careful preparation of model and control parameters associated with computer resource capacity.

☆U.S. GOVERNMENT PRINTING OFFICE:1984 -746 -081/ 2604 REGION NO. 4